FRA-74-10
REPORT NO. FRA-ORD&D-75-12

FRACTURE RESISTANCE OF RAILROAD WHEELS

C.S. Carter
R.G. Caton

SEPTEMBER 1974

INTERIM REPORT

Prepared for

U.S. DEPARTMENT OF TRANSPORTATION
FEDERAL RAILROAD ADMINISTRATION
Office of Research, Development and Demonstrations
Washington DC 20590

1. Report No. FRA-ORD&D-75-12	2. Government Accession No.	3. Recipient's Catalog No. PB243638
4. Title and Subtitle FRACTURE RESISTANCE OF RAILROAD WHEELS		5. Report Date September 1974
		6. Performing Organization Code
7. Author(s) C.S. Carter and R.G. Caton		8. Performing Organization Report No. DOT-TSC-FRA-74-10
9. Performing Organization Name and Address Boeing Commerical Airplane Company* P.O. Box 3707 Seattle WA 98124		10. Work Unit No. (TRAIS) RR312/R5323
		11. Contract or Grant No. DOT-TSC-617
		13. Type of Report and Period Covered Interim Report June 6,1973-March 6,1974
12. Sponsoring Agency Name and Address U.S. Department of Transportation Federal Railroad Administration Office of Research, Development & Demonstrations Washington DC 20590		
		14. Sponsoring Agency Code
15. Supplementary Notes *Under contract to:	U.S. Department of Transportation Transportation Systems Center Kendall Square Cambridge MA 02142	

16. Abstract

The effects of manufacturing method, chemical composition, heat treatment, temperature, and loading rate on the plane strain fracture toughness K_{IC} of railroad wheels have been determined. Carbon content of the wheels is shown to be the principal factor which controls their toughness.

One hundred wheels which fractured in service are analyzed by means of fracture mechanics procedures. The locations, configurations, and size of thermal and plate cracks which initiated brittle fracture are reviewed, and estimates made of the stress levels which resulted in failure.

Estimates have been made of the minimum size of crack which could result in the failure of wheels under adverse service conditions. These are discussed with respect to the minimum size of defect which can be reliably detected by NDT.

Included in the report are state-of-the-art reviews on thermal and plate cracking and on the stresses developed in railroad wheels.

17. Key Words Railroad wheels Carbon steels Fracture mechanics Fracture toughness Failure analysis	18. Distribution Statement DOCUMENT IS AVAILABLE TO THE PUBLIC THROUGH THE NATIONAL TECHNICAL INFORMATION SERVICE, SPRINGFIELD, VIRGINIA 22151.
19. Security Classif. (of this report) Unclassified	20. Security Classif. (of this page) Unclassified	21. No. of Pages	22. Price

Form DOT F 1700.7 (8-72)   Reproduction of completed page authorized

PREFACE

Preceding page blank

TABLE OF CONTENTS

TABLE OF CONTENTS—Concluded

LIST OF FIGURES

LIST OF TABLES

1.0 INTRODUCTION

One major cause of train derailments has been the failure of wheels. These often result in costly damage to equipment and pose serious threats to life, as in the case of freight trains hauling hazardous materials, or high speed passenger trains. For example, a broken wheel derailed a freight train in Laurel, Miss. in 1969 (ref. 1). The train included tank cars carrying a liquefied petroleum gas. Most of these cars exploded following the derailment, igniting dwellings and buildings as well as inflicting mechanical damage. Several fatalities and over $3 million worth of damage resulted. With the current trends in greater vehicle capacity and higher speeds, the incidence of wheel failure may further increase unless remedial action is taken.

Primary causes of wheel failures are the development of thermal cracks in the wheel rim and the growth of fatigue cracks in the wheel plate. If incipient cracking is not detected during prescribed inspection intervals and the condition corrected, the cracks will eventually propagate to critical length resulting in a complete brittle fracture of the wheel. However, little information has been reported on the resistance to crack extension and critical crack size in railroad wheel materials. Accordingly, the objectives of this program are to provide data on the fracture toughness and fatigue crack growth characteristics of this critical truck component and the inspection procedures necessary to detect cracks before they have grown to critical size.

To meet these objectives, the program has been divided into two phases. Phase I, the results of which are discussed in this report, has been directed to establishing the fracture toughness properties of wheels and assessing the significance of the results with respect to service performance. Phase II, which will be reported at a later date, is directed to establishing the fatigue crack growth characteristics of wheel plates and assessing the feasibility of defining inspection procedures to prevent plate failures.

The specific tasks conducted in Phase I were:

- Conduct literature surveys to determine the current state of knowledge with respect to thermal cracking and plate failure and to the stresses experienced by wheels in service.

- Review the wheel inspection procedures currently used by wheel manufacturers and major railroads.

- Determine the influence of the wheel manufacturing process, wheel class, loading rate, and temperature on the fracture toughness of wheels.

- Relate the fracture toughness properties to the mechanical properties and metallurgical characteristics of the wheels.

- Document the type and size of cracks which resulted in the service failure of a number of wheels, and estimate the stresses which caused failure.

1

- Conduct fracture mechanics analyses to provide estimates of the relationship between applied stress and the critical crack size which will cause brittle fracture of wheels in service, taking into account the effect of wheel class, crack location, service temperature, and loading rate.

2.0 REVIEW OF THERMAL CRACKING AND PLATE CRACKING
IN RAILROAD WHEELS

2.1 THERMAL CRACKS

Wheels are required to fulfill two main functions in railroad service:

(a)   to act as a wheel which supports the weight of the vehicle, and

(b)   to act as a brakedrum.

In the latter capacity, the wheels (along with the brake shoes) are required to dissipate, as frictional heat, the energy to be absorbed in stopping or controlling the speed of the train. The rate at which heat is developed is directly proportional to the wheel load, to the square of the speed, and to the deceleration.

As a result of heating, the tread tends to expand but is restrained from doing so by the cooler underlying material in the rim. This results in the development of compressive stresses in the tread surface while it is hot. If the stresses developed are sufficiently high, plastic deformation can occur in compression. Plastic deformation is promoted by the reduction in yield strength of the steel which occurs as the temperature is increased. On subsequent cooling, the tendency of the surface layers to contract is restrained by the underlying material, and residual tensile stresses, acting tangentially, are developed. In addition, the heat produced by the action of the brake shoes can lead to metallurgical changes at the tread surface.

The above effects can lead to thermal cracking, which consists of a series of cracks running transversely to the tread, or flange, and spreading radially inwards. These cracks can penetrate to a significant depth and may initiate complete brittle fracture of the wheel. Wheel fractures due to thermal cracking have been experienced in locomotives, passenger cars, and freight cars (refs. 2 and 3). The factors known to affect the development of thermal cracks and subsequent wheel failure are discussed below.

2.1.1 Mechanisms of Thermal Crack Growth

Two distinct mechanisms of cracking have been associated with thermal crack growth (ref. 2):

(1)   fatigue

(2)   cleavage

Thermal cracks can propagate to critical length by either mechanism (figs. 1 and 2) but have also been observed to extend by each mechanism acting alternately (fatigue-cleavage-fatigue) as shown in figure 3 (refs. 3 and 4).

Fatigue-type thermal cracks generally exhibit the characteristic progression marks of fatigue fracture (fig. 1) and extend much more slowly than cleavage type cracks. Wandrisco

3

and Dewez (ref. 2) reported that fatigue-type cracks are usually associated with frequent brakings and relatively low energy dissipation such as occurs in wheels under multiple unit cars or switcher locomotives. They also noted that these cracks often originate near the front edge of the tread, when an overhanging brake shoe condition exists, or at the tip of a flange (fig. 1).

To account for these observations, Wandrisco and Dewez postulated that the fatigue-type cracks grow by thermal fatigue. The theory has been developed by Van Swaay (ref. 5) who noted that thermal cracks are associated with "hot spots." The latter develop because the actual area of contact between the wheel and brake block is relatively small (normally about 0.4 in. diameter) and the heat produced by braking flows into the wheel through small areas. This results in high local temperatures (1500°-2000°F) relative to the bulk temperature of the rim. At hot spots, the normal thermal expansion and contraction is inhibited by the restraint imposed by relatively cold surrounding material. Consequently the hot spot experiences cycles of thermally induced plastic strain each time it passes beneath the brake block where its temperature is again increased. Waldron and Wise (ref. 6) suggest that thermal fatigue cracks extend to a significant extent only when the balance between cracking and removal of damaged material by wear is upset by higher thermal amplitudes. Crack propagation beyond the hot spot region occurs in a similar way but is controlled by the magnitude of the temperature gradients and cyclic thermal strains generated by braking in the bulk of the tread and underlying material.

Cleavage-type thermal cracks have the characteristics of brittle fracture in that they form rapidly and extend by a cleavage mechanism. Evidence obtained from wheels containing this type of defect, which developed in service or braking tests, indicates that these cracks occur as a result of residual tensile stress gradients developed below the tread surface by rapid stop braking (ref. 2). Cleavage-type cracks, about 1 in. deep, have been developed in class C wheels as a result of one severe emergency stop (ref. 2). Cleavage-type cracks form at temperatures close to ambient, this being demonstrated in dynamometer tests conducted by Weaver et al. (ref. 7) where audible cracking occurred below 100°F. Similar observations have been reported in other studies (ref. 8).

There has been considerable controversy regarding the initiation of thermal cracks. In particular, the role of metallurgical changes which can occur at the tread surface as a result of heating has been questioned. It has been argued that the stresses involved in the formation of martensite and its associated brittleness were responsible for cracking (ref. 9). However, it has been clearly shown that the formation of martensite is not a prerequisite (refs. 3, 5, and 10). In fact, Berg and Kucera (ref. 3) have reported that cracks can form in the absence of any detectable metallurgical change although they point out that transformed microstructures of many types, including martensite, are usually associated with thermal crack formation. Unfortunately, the influence of these microstructural changes on thermal cracking resistance has not been investigated, and it is conceivable that a given microstructure could have different effects depending on the mechanism of thermal crack growth.

Other investigators (refs. 2 and 4) have reported that thermal checks can act as initiation sites for both fatigue and cleavage-type thermal cracks. Thermal checks consist of

4

very shallow randomly orientated cracks. They are quite common, being seen on other metallic surfaces subjected to fluctuating heat flow, and are believed to be a mild form of thermal fatigue cracking (ref. 6).

Hirooka et al (ref. 4) studied the rate of thermal crack growth during stop brake tests on wheels which had previously been braked to introduce different residual stresses in the rims (fig. 4). They concluded there was no clear correlation between the residual stress level and the initiation and growth of cracks. Van Swaay (ref. 5) has suggested that compressive stresses developed at the tread surface by wheel/rail contact accelerate the growth of fatigue-type cracks. In fact, he considers that the dynamometer tests conducted to assess thermal cracking resistance are deficient in that mechanical forces on the tread are not simulated. On the other hand, it has been pointed out that such stresses can be beneficial since they prevent the onset of cleavage cracking, provided that the thermal crack depth is less than that of the compressive stress (refs. 5 and 6).

The alternating modes of thermal crack propagation noted earlier can be explained in the following way. A cleavage crack forms when the size of a prior crack, developed by thermal fatigue (or possibly martensite formation), is sufficient to initiate rapid brittle fracture under the action of the residual tensile stresses developed in the tread region by braking. The crack arrests within the rim, at the point where the residual stress is no longer sufficient to maintain propagation. Further crack extension occurs by thermal fatigue during subsequent braking until the crack is of sufficient size to re-initiate cleavage fracture.

2.1.2 Effect of Chemical Composition

Several investigators have studied the effect of chemical composition on thermal cracking susceptibility. There is general agreement that the resistance to cracking decreases as the carbon content is raised, but the effect of other alloying elements has not been firmly established.

Both dynamometer tests (refs. 2, 8, and 11) and service experience (ref. 12) have demonstrated the adverse effects of carbon content. Dynamometer tests conducted by U.S. Steel Corporation showed that reducing the carbon content from 0.7% to 0.5% increased the resistance to cleavage thermal cracks (ref. 2). Other dynamometer tests have shown the thermal cracking resistance is further increased as the carbon content is lowered to 0.4% (ref. 11).

Ravenet and Gauthier (ref. 9) concluded that the major factor influencing thermal cracking behavior was the M_s temperature. This is the temperature at which martensite formation commences after austenitizing and is determined by the chemical composition of the steel. From an examination of service data, they concluded that the minimum M_s temperature for satisfactory resistance to thermal cracking was 545°F. Other investigators (ref. 13) have suggested this temperature should be 750°F. Van Swaay (ref. 5) considers that the susceptibility to thermal cracking increases with total alloy content and the strength level. On the other hand, Lee and Murray (ref. 11) found that additions of up to 2.4% nickel, 1% chromium, 1% silicon, and 0.5% molybdenum both singly and in combination had little effect on cracking susceptibility at the 0.4% carbon level. Addition of grain refining elements increased the resistance to thermal cracking, vanadium having a

greater effect than aluminum (ref. 11). Vacuum casting was also reported to provide greater resistance to thermal cracking than air cast steel from the same heat (ref. 5).

2.1.3 Wheel Failure From Thermal Cracks

Irrespective of their mechanism of growth, thermal cracks can extend to the critical length required to initiate brittle fracture of the wheel under the action of tangential residual tensile stresses in the bulk of the rim. General heating of the rim, and subsequent cooling, are required to develop these stresses. This condition can be produced by brake applications of appreciable duration such as occur in controlling the speed of a train down long grades or when the brakes fail to release properly. This is known as drag braking. Both Wetenkamp (ref. 8) and Eck (ref. 14) have noted that failure often occurs during cooling from a severe drag application.

That brittle fracture can occur under these conditions has been demonstrated by dynamometer tests. Wetenkamp et al. (ref. 8) partially saw-cut through the rim of a number of wheels to simulate a thermal crack, and subjected them to drag braking. Fracture occurred when the tensile stress developed by braking reached a critical level. It was also demonstrated by Hirooka et al. (ref. 4) that brittle fracture occurred when thermal cracks of sufficient size were developed in wheels by repeated rapid stop braking, tensile stresses having been previously developed in the wheel rims by drag braking. Large thermal cracks did not initiate failure when compressive stresses were present in the rim. Hirooka et al. also demonstrated that the critical size of thermal crack and residual tensile stress level could be related in terms of fracture mechanics parameters.

Wetenkamp et al. (ref. 8) have found that increasing the carbon content of the steel or enlarging the plate thickness will decrease the resistance to brittle fracture. Also, for the same wheel design and carbon content, rim-quenched wheels which contained as-manufactured residual compressive stresses in the rim required a greater number of dynamometer drag brakings to cause failure than did fully quenched wheels in which rim tensile stresses were developed during manufacture.

Although the temperature at which the wheel had been tempered during manufacture had little influence on the resistance to failure, except at low tempering temperatures, it did affect the extent to which the crack propagated into the plate (ref. 8). In rim-quenched wheels, the degree of plate cracking decreased as the tempering temperature was increased, whereas the opposite effect was observed with fully quenched wheels. These observations can be attributed to increasing stress relief in the wheel plate as the tempering temperature was raised. Reducing the plate tensile stresses in rim-quenched wheels by tempering would lead to arrest of a crack, whereas reducing the compressive stresses in fully quenched wheels would have the opposite effect.

2.2 PLATE CRACKS

Plate cracks have been found in passenger cars (ref. 15), freight cars (ref. 16), and diesel locomotives (ref. 17). Most failures are reported to occur in the front hub fillet or the

rear rim fillet (ref. 17) although there have been instances of cracking in the rear hub fillet (refs. 1 and 15). Bruner et al. (ref. 17) report that the greatest incidence is at the front hub fillet.

Plate failures can be associated with high radial stresses at these critical locations. It is believed that the high tensile stresses which can be produced in the failure areas as a result of rim heating during drag braking are primarily responsible (refs. 15-18). Lateral loads against the flange can also produce high radial cyclic stresses and act in combination with vertical loading stresses, which are at a maximum in the failure areas. Quantitative data on these stresses, and factors which control their magnitude, are reviewed in section 4.0.

Most wheel breakages at these locations have been attributed to fatigue cracks which have grown to sufficient size to initiate rapid brittle fracture through the plate. Figure 5 illustrates a wheel which fractured as a result of fatigue crack growth at the rear rim fillet. An enlarged view of the origin area is shown in figure 6.

In many instances fatigue cracks have initiated from processing defects such as machining defects, mill scale, and decarburization (ref. 15). However, there have been instances where cracking was not associated with prior defects (ref. 16). These have been explained by means of fatigue analyses which have shown that the stresses which develop under some service conditions exceed the fatigue strength of the wheel material (refs. 16-18).

There have also been reports of brittle fractures initiated directly from surface defects. In the Laurel accident, a class C wheel failed in a brittle manner from a roughly machined area in the back hub fillet, the machining tears being up to 0.035 in. deep (ref. 1). A derailment in Ohio is reported to have occurred in a similar way (ref. 1). A failure in Canada was also believed to have occurred as a result of a brittle fracture initiated from a martensitic surface layer produced by the use of dull tools during manufacture (ref. 1).

To combat the problem of surface defects, specifications for new wheels now require that the surface roughness shall not exceed 500 microinches where corrective machining or grinding has been employed, and shot peening of the plate is mandatory. It should be noted, however, that controlling the surface finish does not preclude the possibility of forming martensite during machining. Furthermore, the depth to which compressive stresses can be introduced by peening is limited, and its benefits may be lost by surface corrosion, or tensile plastic yielding of the plate as a result of braking.

2.3 INCIDENCE OF SERVICE FAILURES

The Wheels, Axles, Bearings, and Lubrication Committee of the Association of American Railroads publishes annual statistics on defective wheels removed from service (ref. 19). These statistics are based on returns made by some of the member railroads of the AAR and thus do not encompass all wheel failures which occur within the United States. Wheel failures reported in the period 1968-1972 are summarized in table 1, the cause of failure being classified according to the Field Manual of the AAR Interchange Rules (Rule

TABLE 1.—SUMMARY OF WHEEL FAILURES REPORTED TO AAR FOR PERIOD 1968–1972 (REF 19)

Date	Number of failures reported	Cause of failure (%)								
		Cracked or broken flange	Cracked or broken rim	Thermal cracks	Cracked or broken plate	Burst hubs	Shattered rim	Tread shelled	Subsurface defect	Other (a)
1968	251 [25% cast, 75% wrought]	4.25	14	17	19.5	0.5	33	0.5	4.25	7
1969	419 [14.3% cast, 85.7% wrought]	6	13.5	3	17	0.75	54	0	2	3.75
1970	354 [25.5% cast, 74.5% wrought]	2.5	24	7	19	1	45	1	1	—
1971	348 [36.2% cast, 63.8% wrought]	4	39	6.5	20	1.5	20	2	7	—
1972	710 [27.3% cast, 72.7% wrought]	2.5	26	10.5	24	0.8	35	0.2	1	—

aReported as various combinations of flange/rim/plate/hub cracked or broken

41, Section F6). It should be emphasized that these wheels were removed from service having one of the defects listed in table 1 and were not necessarily associated with derailments.

Table 1 indicates that thermal cracks were responsible for about 10% of the failures. This may be an underestimate because a significant proportion of all failures were reported to be due to cracked or broken flanges or rims. Some of these may have been associated with thermal cracks, particularly when it is considered that the cause of failure may be diagnosed by field personnel with little experience in failure analysis.

Cracked or broken plates are currently the cause of about a quarter of all the wheel failures reported. Furthermore, the statistics indicate that their incidence is tending to increase.

Information on train accidents resulting from wheel failures is published by the Bureau of Railroad Safety, Department of Transportation (ref. 20). Table 2 summarizes the data available for the period 1969-1971, from which it can be seen that about 100 accidents per year are the result of wheel failure. Unfortunately, the cause of failure is reported in a general way, and it is not possible to establish the number of accidents associated with thermal or plate cracks.

Damage to equipment, track, and roadbed as a result of wheel and axle failures cost, on average, $31,205 per train accident in 1971 (ref. 20). On this basis alone, the financial loss to the railroads due to wheel failures exceeds $3 million per year and does not include the cost of damage to lading or third parties.

TABLE 2.—TRAIN ACCIDENTS RESULTING FROM DEFECTS IN OR FRACTURES OF WHEELS DURING PERIOD 1969-1971 (Ref. 20)

Cause	1969			1970			1971		
	Cast wheel	Wrought wheel	Total	Cast wheel	Wrought wheel	Total	Cast wheel	Wrought wheel	Total
Flange broken	12	6	18	7	6	13	3	4	7
Tread or rim defective	15	23	38	6	16	22	5	11	16
Broken, overheating	2	1	3	2	0	2	1	2	3
Broken, other causes	16	42	58	18	34	52	28	40	68
Broken, other or unknown composition	—	—	2	—	—	9	—	—	6
Total	45	72	119	33	56	98	37	57	100

3.0 FRACTURE MECHANICS CONCEPTS

A fracture mechanics approach is adopted to meet the requirements of this program. Fracture mechanics concepts and their application are discussed in a number of publications (refs. 21, 22, and 23) and are briefly outlined below.

3.1 STRESS INTENSITY FACTOR

Fracture mechanics is concerned with the influence of cracks or sharp flaws on fracture behavior. When a load is applied to a cracked structural member, the overall stress field is disturbed in the vicinity of the crack. The stress is concentrated around the crack tip and is much higher than in the remainder of the member. Fracture mechanics uses elastic theory to describe this elevation of stress at the crack tip.

Using this approach, it can be shown that the stress field around any crack can be uniquely described as a single parameter known as the stress intensity factor and defined as K. The magnitude of K is determined by the loading conditions and geometry of the crack. Although localized plastic yielding occurs at the crack tip, elastic theory can be used to describe the stress field, provided that general yielding does not occur. Equations for K have been derived for most types of cracks experienced in service (refs. 24 and 25) and they can be written in the general form:

$$K = M\sigma(\pi \ell)^{1/2} \tag{1}$$

where

σ = applied stress

ℓ = crack length

M = a factor which is determined by the loading conditions (e.g., tension or bending) and crack shape

In other words, the stress intensity is proportional to the applied stress times the square root of the crack length.

For example, the stress intensity for a through-the-thickness crack in a wide sheet or plate is given by:

$$K = \sigma(\pi 0.5\ell)^{1/2} \tag{2}$$

where

σ = applied stress

ℓ = crack length

11

3.2 FRACTURE TOUGHNESS

As the stress intensity increases, due to an increase in applied stress or crack length, a point is reached at which the crack becomes unstable and rapidly propagates to complete failure. Since the stress distribution near the crack tip, and localized plastic deformation in this region, are completely controlled by the stress intensity factor, fracture occurs when the stress intensity reaches a critical value. This critical value of the stress intensity factor is called the fracture toughness and is designated K_C. Its value for a given material can be established experimentally by introducing a sharp crack into a specimen and measuring the stress and crack length at the point of unstable fracture, provided that the net-section stress at fracture does not exceed the tensile yield strength of the material.

If the thickness of the material is sufficiently large with respect to the crack tip yield zone, a state of plane strain can be developed which provides maximum constraint at the crack tip. This represents the minimum toughness condition in that further increases in thickness do not lead to a reduction in the critical stress intensity. Under these conditions, the critical stress intensity is referred to as the plane strain fracture toughness and is designated K_{IC}. An empirical rule for plane strain conditions to prevail is that the material thickness exceeds $2.5 (K_{IC}/TYS)^2$ where TYS is the tensile yield strength (ref. 26).

The fracture toughness parameter, K_{IC}, is a material property in much the same way as tensile yield strength. It can be influenced by such variables as temperature, microstructure, and tensile strength. Once K_{IC} is established for a wheel material, the conditions of applied elastic stress and crack size which will result in rapid unstable fracture can be established from equation (1) using the appropriate value of M for the desired types of crack and loading conditions. In the case of the through-thickness crack discussed above, the conditions for fracture can be written as:

$$K_{IC} = \sigma(\pi 0.5c)^{1/2} \tag{3}$$

where

c = critical crack length

Assuming a K_{IC} value of 30 ksi in.$^{1/2}$* for a wheel plate, this value can be substituted into equation (3) to determine the relationship between applied stress and the critical size of crack which will cause failure. For example, a 2-in.-long crack will cause failure if the applied stress exceeds 17 ksi. Thus, if the fracture toughness and maximum stress experienced in service are known, the minimum size of crack can be established that must be detected by inspection to avoid brittle fracture.

---

*The dimensions of the stress intensity equations are stress, and length$^{1/2}$. Hence, fracture toughness values are expressed in ksi in.$^{1/2}$ units.

Fast loading rates can significantly reduce the fracture toughness of some steels. The plane strain fracture toughness under these conditions is denoted as K_{Id}, the subscript indicating dynamic loading. This is an important consideration in this program because high loading rates can be experienced in wheel plates as, for example, when the flange contacts special work such as crossings.

It can be seen from the above that in order to establish the critical crack size for wheels, and hence the minimum size of flaw which must be detected by inspection, the following must be established:

- Fracture toughness properties of the wheel materials for the temperatures and loading rates experienced in service

- Nature and magnitude of the stresses experienced by wheels during service

- Configuration of cracks which may develop during service

In addition, the current wheel inspection procedures must be determined to assess their ability to detect cracks before they achieve critical size.

The remainder of this interim report discusses the acquisition and analysis of this information.

4.0 WHEEL STRESSES

This section presents available data on the stresses which can be experienced in wheels. Primary emphasis is placed on the tangential stresses which develop in the rim and radial stresses in the plate, since they are associated with propagation of thermal and plate cracks, respectively. Information on cyclicly applied stresses is included and will be used to analyze fatigue crack growth in wheel plates in a future report.

Stresses introduced into wheels during fabrication and under service conditions are discussed below.

4.1 FABRICATION STRESSES

4.1.1 Heat Treatment

4.1.1.1 Rim-Quenched Wheels

Compressive stresses are introduced into the wheel rim by rim quenching and are balanced by tensile stresses in the plate. Several factors influence the magnitude of the residual stresses developed. These include the design of the wheel (ref. 27) and the mechanical properties at elevated temperatures. The tempering treatment which follows quenching also has a significant effect. Data presented in table 3 shows that the residual stresses decrease as the tempering temperature is increased. In practice, a tempering temperature of 850°-900° F is generally used to meet the specified hardness requirements and to reduce the residual stresses to a level which the manufacturer considers appropriate for service. The rate at which wheels are cooled after tempering is also important, lower stresses being developed by slow cooling (ref. 28).

Results of residual stress measurements made on new wheels by several investigators are summarized in table 3. The radial and tangential stresses reported for various wheels act in the same direction at comparable measurement locations. However, there is considerable variation in the magnitude of the stresses, which presumably results from variations in the design and/or processing of the wheels. Tangential compressive stresses in the rim are within the range of 15 to 45 ksi. Wandrisco and Dewez (ref. 2) have also reported that these stresses are normally in the range 20-25 ksi. It is important to note that the rim stresses shown in table 3 were based on a few measurements made at the rim surface, and do not reflect the stress gradients in the rim. An example of the latter is shown in figure 7.

The highest residual tensile stress recorded in the plate of each wheel (table 3) acts in a radial direction at the front hub and rear rim fillets. From the limited data available, it would appear that radial tensile stresses of 15-35 ksi are typical of these locations, although a value of 58.6 ksi was reported to have been measured at the rear rim fillet in a diesel locomotive wheel (ref. 17).

14

TABLE 3.—RESIDUAL STRESSES IN AS-MANUFACTURED, RIM-QUENCHED WHEELS

Wheel		Radial stress (ksi)						Tangential stress (ksi)				Remarks	Reference
Design	Class	FFN1	FFN2	BFN1	BFN2	FR	BR	FFN1	FFN2	BFN1	BFN2		
B33	ND	-2	+11	+4	-5	ND	ND	0	-1	0	-9	Average for six wheels	16
A40, F36	ND	ND	+20 to +35	+20 to +35	ND	ND	ND	ND	ND	ND	ND	Reported as typical values	17
36-in. dia	C	-10	+35	+1	-15	-20	-45	+2	+15	-3	-10	Reported as typical values	7
European 36-in. dia	0.5% carbon (tempered above 932 F)	-14.2	+12.8	+11.4	-22.7	-22.7	-22.7	0	+1.4	0	-24	One wheel	28
36-in. dia	C (tempered at 900 F)	-15	+16.3	+15	-18.4	-22	-15	ND	ND	ND	ND	Average for five wheels	
36-in. dia	C (tempered at 900 F)	-6	+18	+8	-11	-20	-16	+2	+9	+3	-10	One wheel	8
36-in. dia	C (tempered at 800 F)	-18	+30	+23	-26	-38	-46	+6	+17	+10	-17	One wheel	

ND = Not reported

Diagram labels: BR, BFN1, BFN2, FR, FFN1, FFN2

15
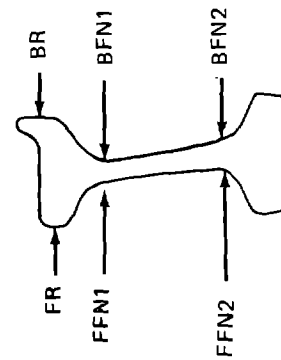
It can be seen from table 3 that in going through the plate thickness there is a reversal of stress from tension to compression. This presumably is the result of bending moments experienced by the plate during heat treatment.

4.1.1.2 Fully Quenched Wheels

Complete quenching of a wheel produces tensile stresses in the rim and compression stresses in the plate—in other words, opposite to what occurs in rim-quenched wheels. The residual quenching stresses are relieved as the tempering temperature increases (ref. 8).

4.1.1.3 Untreated Wheels

The stresses developed in untreated wheels depend primarily on the rate of cooling from the rolling or normalizing temperature. Tangential rim stresses are primarily compressive in nature, measured values on one wheel being in the range +3 to -7 ksi (ref. 8). Similar stresses were recorded in the plate.

4.1.2 Wheel Mounting

Yontar (ref. 15) measured the stresses developed in a 28-in. wheel during press-fit mounting on the axle. Radial tensile stresses of about 2 ksi were developed at the front hub fillet whereas at the rear rim fillet an average compression stress of 6 ksi was measured. Similar stresses were recorded during the mounting of A40 and F36 wheels (ref. 29). Tangential tensile stresses of 10-15 ksi also developed in the hub fillet region and decreased fairly uniformly to a level of about 2 ksi at the rim fillet.

4.2 SERVICE STRESSES

The stresses experienced in wheels during service result primarily from the following conditions (ref. 17):

1) Vertical loads due to equipment and loading. These loads can apply at any point across the wheel tread, fluctuating once in each revolution of the wheel, and may be accelerated by dynamic effects due to track deviations and operating conditions.

2) Lateral loads applied against the front of the flange as a result of curve negotiation, hunting, and nosing; against the rim faces from the action of car retarders; and against the back of the flange by guardrail and special trackwork. These loads occur less frequently than vertical loads but also fluctuate during each revolution of the wheel.

3) Thermal gradient effects, resulting from the conversion of kinetic energy of the train into heat when the brake shoes are applied to the wheel tread. The stresses caused by braking can be considered to be of a steady nature since they do not fluctuate during each wheel revolution.

16

The stresses developed in the above ways act in conjunction with each other and are algebraically additive.

Estimates of the stresses experienced in service have been obtained in the following ways:

- Application of static loads to the wheel tread or rim to simulate vertical and lateral loads

- Heating of the wheel rim to simulate braking

- Computer simulation of service loads and braking conditions

- Direct measurement during service

Available data are reviewed below.

4.2.1 Vertical Loading Stresses

Maximum wheel loads used in design are based on the static gross weight of the vehicle. Dynamic effects can, however, increase the loads experienced by the wheel. Meachan and Ahlbeck (ref. 30) showed by means of a computer study that the rocking of a high-cube hopper car, induced by low rail joints, could increase the static loads by a factor of 2.3. Dynamic load factors of 1.5-1.6 were found for corrugated track. The dynamic load factors also increased with the stiffness of the track.

Bruner et al. (ref. 16) measured the stresses developed in the plate of a B33 wheel subjected to static vertical loads mechanically applied at the center of the tread. This wheel design was selected because at the time work was reported (1966) the greatest amount of freight was hauled in 70-ton cars on B33 wheels. Loads up to 60,000 lb were used, the maximum load providing for a dynamic loading factor of about 2 with respect to the design maximum load. The stress patterns produced by the three loading positions shown in figure 8 can be illustrated by considering the maximum load used (table 4). Of the critical fillet locations BFN1* and FFN2*, higher stresses are developed at FFN2. At this location, the maximum stresses (compressive) occur in the radial direction at the 0° loading position. A compressive stress of 19.1 ksi is developed at 0° and a tensile stress of 4.5 ksi at the 180° loading position. Thus in one wheel revolution, vertical loading stresses fluctuate from -19.1 to +4.5 ksi, a stress range of 23.6 ksi. The highest tensile stress recorded was 8.5 ksi in the radial direction, at the BFN2 location.

Yontar (ref. 15) has measured the stress experienced by 28-in.-diameter reverse dish wheels in rapid transit service. Under normal operation, the stress ranges at the front and

---

*BF and FF denote the front face and back face respectively; N1 and N2 denote the rim fillet and hub fillet respectively (see table 3).

TABLE 4.—SUMMARY OF MAXIMUM STRESSES MEASURED IN STATIC LOAD TESTS

Loading condition	Maximum stresses (ksi)[a]					
	BFN1		FFN2		BFN2	
	0° (b)	180°(b)	0°(b)	180°(b)	0° (b)	180°(b)
B33 wheel (ref. 16)						
60,000-lb vertical load	−16.9	+2.3	−19.1	+4.5	+8.5	−4.8
20,000-lb lateral load on rear rim	−5.9	+5.3	−24.2	+9.7	+29.7	−12.9
20,000-lb lateral load on front rim	+5.2	−5.3	+19.0	−13.5	−30.0	+13.9
F36 wheel (ref. 29)						
60,000-lb vertical load	−4.2	+3.1	−9.0	+3.9	+5.6	−1.8
20,000-lb lateral load on flange front	+2.7	−2.7	+10.0	−3.7	−1.8	+3.8
A40 wheel (ref. 29)						
60,000-lb vertical load	0.77	0.79	−11.7	+4.2	+7.3	−2.8
20,000-lb lateral load on flange front	−3.4	−0.34	+11.6	−4.1	−13.8	+3.8

[a]Underlined values are maximum tensile stresses measured at each location under loading conditions noted.

[b]Loading positions shown in Figure 8

rear hub fillets were 3 ksi and 7 ksi, respectively, and were usually 29% tension and 71% compression. These stresses periodically doubled through dynamic action of the truck.

Because of plate cracking problems experienced in diesel locomotive wheels, the AAR measured the stresses developed in A40 and F36 wheels (ref. 29). Vertical load was applied at two separate loading points on the tread surface to assess the effect of changing the contact point between wheel and rail due to lateral movement of the wheel relative to the rail. With the exception of the BFN1 location, the highest stresses occurred in the radial direction when the load was applied to the outside of the tread. At the BFN1 location, the stress increased as the load position approached the flange. Similar effects have been observed in other loading tests (ref. 31) and as a result of computer simulation (ref. 17). The stress ranges measured in these wheels when a 60,000-lb load was applied were lower than discussed above for the smaller diameter B33 wheel (table 4).

Lovelace (ref. 31) has shown that the stress at the BFN1 location is significantly increased when the tread is worn hollow. For example, in an H36 wheel subjected to a 75,000-lb vertical load, the maximum stress and stress range increased from about 7 ksi in a new wheel to 19 ksi in a worn wheel.

To study the effect of design variations on wheel stress due to vertical loads, Bruner et al. (ref. 17) conducted an extensive computer simulation study on A40 and F36 wheels. Increasing the plate thickness and fillet radii decreased the stress at the BFN1 and FFN2 locations, as did a change from a straight to an S-shaped plate. The stress was approximately inversely proportional to the square of the wheel diameter.

4.2.2 Lateral Loading Stresses

The effect of lateral loads applied to the rim faces was evaluated in some of the studies discussed above. Most investigators used a maximum load of 20,000 lb because such a value (and higher) has been measured in service (ref. 17).

Lateral loads up to 20,000 lb were separately applied to the front and back of a B33 wheel by Bruner et al. (ref. 16). Their results for the 20,000-lb load are shown in table 4. A 20,000-lb load on the front rim face resulted in a tensile stress at FFN1 of 19 ksi at 0° and a compressive stress of 13.5 ksi at the 180° position. This represents a stress range of 32.5 ksi. However, these lateral loading stresses are opposite in sign to the vertical loading stresses at any point (table 4) so the combined vertical and lateral loads at each position result in lower stresses. Similar loading on the back rim results in a 24.2-ksi compressive stress at 0° and 9.7 tension at 180°, resulting in a stress range of 33.9 ksi. Furthermore, these stresses due to loading at the back of the rim are in the same direction as the vertical loading stresses and thus their additive effect can be quite substantial (table 4). Similar conditions prevail at the rear hub fillet where loading on the back rim produced a tensile stress of 29.7 ksi.

The stresses developed in A40 and F36 wheels by the application of a 20,000-lb lateral load were lower than the stresses developed in the B33 wheel (table 4), indicating that wheel design influences the stress distribution.

Bruner et al. (ref. 17) used computer simulation to examine the effect of several wheel design variations on stresses due to lateral loading. Increasing the plate slope, plate thickness, and fillet radii reduced the stress, as did a change in plate shape from a straight to an S-shape.

Measurements (ref. 15) of the stresses experienced by rapid transit car wheels (28-in.-diameter, reverse dish) showed that the range of stress at the rear hub fillet could be as high as 34 ksi when the vehicle traversed special trackwork (switches, etc.).

4.2.3 Stresses Developed During Braking

As discussed earlier, the frictional heat produced by braking results in the development of compressive stress in the rim while it is hot. These stresses are balanced by radial tensile stresses in the plate with the highest stresses at the rim and hub fillets. The method of braking has a significant influence on the distribution of temperature and hence the stresses within the wheel. Although the rate of energy dissipation is much higher in rapid stop braking than drag braking, the extended duration of the latter is such that the wheel is heated to a considerable depth below the tread.

19

Eck and Novak (ref. 32) used computer simulation to determine the temperature field generated in a worn 36-in. cast wheel under simulated drag braking (fig. 9). The thermal fields penetrated deeper into the wheel structure than those produced by a 2-minute emergency braking from 60 mph (fig. 10). It should be noted that although the temperatures and thermal gradients at the tread surface can be much higher in service, thus indicating a limitation of the computer simulation, the method is reported to be considerably more accurate within the bulk of the wheel (ref. 3). The temperatures developed by drag braking the rim and hub fillets were estimated to be of the order of 400° F and 150°F, respectively. Similar temperatures were measured at these locations during drag braking on a descending gradient (ref. 29).

As a consequence of the temperature distribution generated by drag braking, the stresses developed in the plate fillet regions of the wheel are considerably higher than those produced under emergency braking conditions. An octahedral shear stress pattern corresponding to the temperature distribution in the worn wheel after 20 minutes of cyclic drag braking is shown in figure 11. In the hub fillet area, the maximum stress is approximately an order of magnitude higher than that developed under the emergency brake application depicted in figure 12.

Bruner et al. have also used computer simulation to compare the radial stresses developed in the plate by drag and emergency braking (ref. 17). Their results, shown in table 5, are similar to those reported by Eck and Novak (figs. 11 and 12) in that much higher stresses are developed at the critical fillet locations by drag braking. The magnitude of the stresses developed during drag braking increased with heating time, and as Eck (ref. 14) has noted, plate fracture usually occurs during or near the end of the drag application.

TABLE 5.—COMPARISON OF PLATE FILLET STRESSES DEVELOPED DURING DRAG AND EMERGENCY BRAKING USING COMPUTER SIMULATION (AFTER BRUNER ET AL., REF. 17)

Braking conditions	A40 wheel		F36 wheel	
	BFN1 (ksi)	FFN2 (ksi)	BFN1 (ksi)	FFN2 (ksi)
Rapid stop	+21	+32	+4	+5
Drag braking (50,000 Btu/hr A40 wheel; 20,000 Btu/hr F36 wheel)	+35	+52	+22	+26

That high fillet stresses can develop in this way has been confirmed experimentally. Heating the tread of A40 and F36 wheels to 400°F to simulate drag braking produced radial stresses which exceeded yield point magnitude in the critical BFN1 and FFN2 fillet regions (ref. 29). In similar tests on a B33 wheel, radial tension stresses of 38 ksi and 42.6 ksi were measured at the BFN2 location.

20

It can be seen from the above that stresses which can result from brake heating are much higher than those from either vertical or lateral loading.

Computer simulations have been performed to assess the effect of design variations on the stresses experienced by the fillets during drag braking (refs: 17 and 33). Although there is general agreement that increasing the rim thickness and fillet radii reduces the stress, there is conflicting evidence on the plate thickness and on changing the plate shape. Wetenkamp (ref. 33) has suggested that the effect of a design change depends on the magnitude of the thermal load applied to the wheel.

The position at which the brake shoe rides on the tread surface is reported to affect the stress magnitude (ref. 17). The stress at BFN1 increases as the shoe moves across the tread from the outside corner to the flange. Conversely, the stresses at FFN2 decrease when the shoe moves in the same way. Bruner et al. (ref. 18) noted that this may explain why most plate failures occur at the front hub fillet, since a misaligned brake shoe rides more easily towards the front of the tread than towards the flange side.

On the basis of an experimental study of the effect of tread heating, Yontar (ref. 15) concluded that the stress developed at a given location in the plate could be linearly related to the temperature gradient across the wheel face (fig. 13), but pointed out that this was applicable only in the case of linear gradients.

4.2.3.1 Residual Stresses Resulting From Braking

The residual stresses which result from braking are primarily a function of the thermal gradient developed. This is determined by the thermal loads experienced by the wheel and their rate of dissipation. Other factors believed to affect the magnitude of the residual stresses include the following (refs. 2 and 4):

- Elevated temperature strength of the wheel steel

- Volumetric changes associated with microstructural transformation changes

- Stress relaxation at elevated temperatures

- The Bauschinger effect

- Initial residual stresses

- Wheel design

Residual stresses in a new wheel and a wheel removed from service in Europe are compared in figure 14 (ref. 13). It can be seen that tensile stresses of about 30 ksi have developed in the rim during service and are balanced by compressive stresses in the plate. Available information on the stresses which can develop at these locations are reviewed below.

Plate Stresses—Only limited information is available on the residual stresses developed in the plate. Wetenkamp et al. (ref. 8) have shown that residual tensile stresses introduced during manufacture decrease as the number of drag brakings increase, and that compressive stresses can be developed in this way. Compressive stresses as high as 70 ksi in the radial direction and 53 ksi in the tangential direction were measured (ref. 8) on the front face of the plate following drag testing of a rim-quenched wheel. Lower compressive stresses were present at the back face and these reversed to tensile stresses of about 44 ksi close to the hub fillet. Measurements on a wheel removed from service in Europe (fig. 14) indicate residual compressive tangential stresses as high as 42 ksi in the plate.

Yontar (ref. 15) measured the residual stresses in the plate of rim-quenched wheels removed from rapid transit service which involved frequent stops from a maximum speed of 55-60 mph. Although the residual tensile stresses were lower than those in new wheels, a complete reversal to compressive stress had not occurred.

Rim Stresses—Wetenkamp et al. (ref. 8) have experimentally demonstrated that drag braking can change the residual stress distribution across the rim from one that is predominantly compression (as manufactured) to one that is predominantly tension (fig. 15). Figure 15 also illustrates that the stress gradients within the rim are rather complex and that a single measurement on the outside of the rim does not adequately characterize the rim stresses.

The same investigators have also shown that the magnitude of the residual tensile stresses increases with the number of drag brakings (with constant testing conditions) up to a maximum level. Furthermore, they demonstrated that the compressive rim stresses developed in rim-quenched wheels by heat treatment retard the buildup of tensile stresses, whereas the tensile stresses present in fully quenched wheels had the opposite effect. Consequently, fewer drag tests are required to attain a given tensile stress level in a fully quenched wheel than a rim-quenched wheel. These effects are illustrated schematically in figure 16.

Hirooka et al. (ref. 4) have conducted a rather extensive study to determine the factors which influence the distribution of residual stresses in wheels subjected to drag braking. Rim-treated wheels (0.60%-0.75% carbon) were dynamometer tested with a single, composition type, brake block applied to the tread. Each wheel was rotated at 50 mph and a constant braking force was applied for 50 seconds, and released for 10 seconds, in every minute. It was found that the maximum temperature and temperature distribution in the wheel become constant after about 60 minutes' testing. Accordingly, the residual stresses were measured when this steady state condition had been achieved and the wheel cooled to ambient temperature.

Plate profile was found to have a significant effect. Two wheels, A and B, having the plate configurations shown in figure 17, were tested. Maximum tensile stress developed in the A wheel was 17 ksi, the stress decreasing with increasing distance from the tread surface (fig. 18). In contrast, the maximum stress in the B wheel was more than twice as high, and as shown in figure 18, the stress decreased with increasing distance from the front rim corner. Plates with an S-shape and lower stiffness were found to have lower residual stresses compared to straight plates.

Hirooka et al. (ref. 4) also found that the maximum stress increased with increasing brake force (fig. 19). It was shown that the maximum temperature reached at a given rim location increased with the braking force and could be linearly related to the residual stress (fig. 20). The investigators caution, however, that this apparent correlation requires further verification. In particular, the correlation does not account for a buildup of residual stress with increasing number of drag cycles as was observed by Wetenkamp et al. (ref. 8).

From the above data, it would appear that tensile residual stresses up to about 50 ksi can be developed within the rim by drag braking, and may be about 60 ksi close to the tread surface.

Information regarding the residual rim stresses developed by rapid stop braking is sparse. Rapid stop braking tests from 115 mph were conducted by Weaver et al. (ref. 7) on class C wheels. A single surface measurement on the rear side of the rim indicated that the initial compressive stress of 40 ksi was reduced to 23 ksi after 37 stops with composition brake shoes, and to 9 ksi following 36 stops with metal shoes. Unfortunately, the stresses within the rim were not determined, but the fact that audible detection of rapid thermal crack propagation (and arrest) following the 36 stops with metal brake shoes was reported is indicative of a steep tensile stress gradient below the tread surface. Wandrisco and Dewez (ref. 2) measured the residual stresses developed below the tread surface after a single brake application from 115 mph. Figure 21 shows that the tensile stresses near the tread were close to or exceeded yield-point magnitude and increased with the strength level of the steel.

4.3 COMBINED STRESSES

It was noted in section 4.2.2 that the plate fillet stresses due to vertical loading and lateral loading on the rear rim are additive, since they act in the same direction. Table 4 shows that tensile stresses of 38.2 ksi could be developed in this way at the BFN2 location in a B33 wheel. In rim-treated wheels, these stresses would be counteracted by compressive stresses developed during heat treatment (table 3). On the other hand, they would be increased if residual tensile stresses had been developed at this location by drag braking (sec. 4.2.3.1), and under these circumstances the combined stresses could approach yield-point magnitude.

The same combination of vertical and lateral loading on the B33 wheel produced lower tensile stresses at the BFN1 and FFN2 locations, the values being 7.6 and 14.2 ksi, respectively. Nevertheless, as shown in table 3, tensile residual stresses as high as 35 ksi can exist at these locations in rim-treated wheels, and even higher tensile stresses can be developed during drag braking. Consequently, the combined stresses can reach the yield strength of the plate material.

In addition, worn treads, higher lateral loads, and some design features could raise the loading stresses to higher levels than estimated above.

From the above considerations, it would appear imperative to estimate the critical crack size in the fillet regions as that which will cause failure at the material yield strength. As will be shown later, this is substantiated by service experience.

These combined stresses can also promote the initiation of fatigue cracks. Bruner et al. (refs. 16 and 17) have shown that the stress range and mean stress which can be developed are sufficient to exceed the unnotched fatigue strength of the wheel material. Their effect on the rate of propagation of fatigue cracks will be assessed in a future report.

5.0 WHEEL INSPECTION

The inspection methods and criteria currently used for the detection of cracks or defects in new wheels and those in service are discussed in this section.

5.1 NEW WHEELS

Inspection procedures for new wheels are given in AAR Specifications M107 and M208 for wrought and cast wheels, respectively. The requirements for the detection of cracks and defects are the same in both specifications.

Wheel rims are ultrasonically inspected after heat treatment to detect internal discontinuities. Flat bottom holes of specified size and location in a wheel or portion of a rim are used as a reference standard. Flaw indications equal to or larger than the reference discontinuity are cause for rejection.

Wet magnetic particle inspection of wheel plates is required after final machining. It is specified that the magnetizing current shall be large enough to induce magnetic fields of sufficient intensity to disclose surface discontinuities exceeding 0.015 in. in depth and 0.25 in. in length, and the inspection must be performed to detect discontinuities whose axes may be in any direction. However, the specification is nonspecific in rejection criteria, the following being required: "Interpretation of magnetic particle discontinuity indications is based upon their location, size, direction and shape. Experience with service performance and destructive testing shall be used for evaluation." Discontinuities may be removed by machining or grinding, but must be followed by magnetic particle inspection.

5.2 IN-SERVICE INSPECTION

The AAR Interchange Rules (Rule 41) and the AAR Wheel and Axle Manual (Section 3C) describe and illustrate the types of defects which require the wheel to be removed from service. Thermal cracking in any stage of development is cause for the immediate removal of the wheel from service. Wheels with plate cracks must also be removed, the manual noting that it is important that they be detected in the early stages. Wheels which show evidence of overheating in service from stuck or dragging brakes must be removed from service and scrapped. This is because of the high residual tensile stresses which may have developed in the rim.

The AAR rules do not specify the inspection techniques to be used or the frequency of inspection. To obtain information on current practice, several major railroads were contacted by letter. They were asked if they would provide information on the inspection techniques used and the inspection intervals for wheels on locomotives, freight cars, and passenger cars. A summary of the replies is given in table 6. Visual inspection is principally used, with magnetic particle or penetrant being employed under special circumstances by some railroads.

25

TABLE 6.—SUMMARY OF WHEEL INSPECTION PROCEDURES

Railroad	Inspection procedures		
	Method	Frequency	Remarks
A	Visual	At originating terminals and intermediate inspection points on line of road	Passenger and freight cars
	Visual using bright light	Each trip if possible	Locomotives—special attention to tread and rim (for thermal cracks)
B	Visual	Each time dispatched from an originating terminal and when car is on repair track; if wheels are removed due to defective journal or axle then given an inspection in shop.	Freight cars
		Each time locomotive serviced and each time wheels gaged every 30 days	Locomotives
C	Visual	At repair yard	Locomotives, freight, passenger cars
		In shop for wheel tread turning	Locomotives
D	Visual	Train yard inspection any time conditions permit. More often in areas where thermal cracks are a problem.	Freight, passenger cars
	Magnetic particle inspection (dry)	Sometimes	Particularly locomotives
E	Visual	Daily	Locomotives
	Penetrant	If above reveals possible cracks	
	Visual	On conditioning or repair tracks	Freight cars
F	Visual	Freight train classification yards, repair track	Freight
		Station time	Passenger
		Monthly and between dispatchments	Locomotives

6.0 TEST PROCEDURES

6.1 SELECTION OF WHEELS FOR TESTING

Railroad wheels are manufactured by either rolling of forged preforms or by casting. It was recently estimated that over 7 million cast wheels are in service with class I railroads, which represents about half of all wheels used in AAR interchange service (ref. 34).

The AAR specifications M107 and M208 cover wrought and cast wheels, respectively. They provide for four different classes of wheels—U, A, B, and C—to be selected according to the loads and braking anticipated in service (table 7). The four classes differ in specified carbon content and hardness requirements for the rim (table 7). To achieve the required hardness, class A, B, and C wheels must be austenitized, rim quenched, and tempered. This treatment also results in normalizing and tempering of the unquenched plate and hub regions. Specification M107 allows entire wheel quenching and tempering of wrought wheels to classes A, B, and C which are designated AE, BE, and CE, respectively. Cast wheels are not fully quenched. While specification M208 allows the use of high carbon class UI material, wheels of this class are no longer manufactured because of their susceptibility to thermal cracking.

All classes, except A (and AE), are used for freight cars. Class U is primarily used for this application because of its lower cost, and grade C is essentially restricted to high-capacity freight cars (100 or 125 tons). Classes A and B are normally used for diesel locomotives and passenger cars to minimize thermal cracking problems.

Thus, to adequately characterize the fracture toughness properties of railroad wheels in the rim and plate regions, the effect of manufacturing method, carbon content, and heat treatment have to be taken into account. Accordingly, the following wheels were selected for testing. (The number code given each wheel for identification is shown in parentheses.)

Wrought		Cast
Class U	(Wheel 3)	Class U (Wheel 1)
Class A	(Wheel 4)	Class C (Wheel 2)
Class C	(Wheel 5)	
Class U - used	(Wheel 6)	
Class CE	(Wheel 7)	

Wheels to AAR design R33 (multiwear) were selected because of the wide use of 33-in.-diameter wheels for freight cars. A different size would not be expected to influence the test results. The multiwear rim provides a sufficient depth for removal of K_{IC} specimens of the required size.

TABLE 7.—CHEMICAL COMPOSITION AND HARDNESS SPECIFIED FOR RAILROAD WHEELS

Class	Intended service	Rim hardness (BHN) Min	Rim hardness (BHN) Max	Carbon[a] content (%)
U	General service where an untreated wheel is satisfactory	—	—	0.65-0.80
A	High-speed service with severe braking conditions but moderate wheel loads	255	321	0.57 max.
B	High-speed service with severe braking and heavier wheel loads	277	341	0.57-0.67
C	(1) Service with light braking conditions and high wheel loads (2) Service with heavier braking conditions where off-tread brakes are employed	321	363	0.67-0.77
[b]U1	—	—	—	0.95-1.20

[a]The following are required for all wheel classes: 0.60-0.85 Mn, 0.05 max P,
0.05 max S, 0.15 min Si.

[b]Cast only

New wheels have been used for the basic evaluation. These were selected because initial fatigue damage is essentially a surface phenomenon. Once a crack is initiated, the fatigue damage experienced by a component is concentrated in a local region at the crack tip. Hence, the fracture toughness is not generally considered to be affected by prior fatigue cycling (by service loading) of the bulk material. To demonstrate the validity of this contention, one used wheel was used. A wheel which had worn to the AAR minimum thickness limit was used to ensure it had experienced extensive service usage.

Identities of the wheels obtained, and details of the heat treatment, where known, are given in table 8.

TABLE 8.—WHEEL IDENTIFICATION AND HEAT TREATMENT

Wheel Number	Wheel Class	Manufacturer's identification	Heat treatment details (reported by manufacturer)
1	U, cast	3-73 GS 49506 CR 33	Normalized at 1700° F for 45 min—programmed cool to avoid residual stresses
2	C, cast	12-72 GS 09171 C CR 33	Normalized at 1700° F for 45 min—rim quenched to provide Brinell hardness in tread of 321-363; tempered at 900° F for 2 hr; controlled temperature gradients to minimize residual stresses
3	U, wrought	12-71 G 54761 R33	Untreated
4	A, wrought	4-69 Ⓔ 36384 A R33	No details supplied
5	C, wrought	2-73 G 53307 C R33	Rim toughened
6	U, wrought used	2 28 56 ⚓ S 277 Z 4464 AAR IW	Untreated
7	CE, wrought	7-73 ⚓S ⚓7646 CE R33	No details supplied

28

The procedures adopted to characterize the fracture toughness and tensile properties of the rim and plate regions, together with their metallurgical characteristics, are described below.

6.2 SPECIMEN LOCATIONS

Fracture toughness tensile specimens were removed from the wheels at the locations shown in figure 22 and according to the schedule given in table 9. Crack orientations with respect to the wheel were radial for the rim specimens and tangential for the plate specimens, both as shown in figure 23, and thus corresponded to the direction of brittle crack propagation experienced in service. The used wheel was a special case since, due to the amount of wear, K_{IC} rim specimens had to be rotated 90° so that the crack was still radial but the propagation direction was from the front to the rear rim faces. Other investigators (ref. 10) found that differences in crack orientation do not have any effect on the fracture toughness of wheels.

TABLE 9.—TEST SPECIMENS REMOVED FROM EACH WHEEL

Wheel		Specimens fabricated						
		Rim			Plate			
Number	Class	Fracture toughness K_{IC}	Tensile	Charpy	Fracture toughness		Tensile	Charpy
					K_{IC}	K_{Id}		
1	U, cast	7	1	2	4	4	1	2
2	C, cast	7	1	2	2	–	1	–
3	U, wrought	7	1	2	5·	4	1	2
4	A, wrought	7	1	1	5	4	1	2
5	C, wrought	7	1	2	5	4	1	2
6	U, wrought (used)	5	1	–	5	–	1	–
7	CE, wrought	2	1	–	5	4	1	2

6.3 SPECIMEN TYPES

The tensile specimens used are shown in figure 24. These were nominally 1 in. gauge length and 0.25 in. diameter in the test section. Charpy specimens were standard 0.394 in. square, V-notch type and are shown in figure 25. The dynamic fracture toughness was evaluated using fatigue precracked standard Charpy specimens; the nominal dimensions of these specimens are also given in figure 25. The specimen sizes for fracture toughness K_{IC} evaluation were nominally 1 in. by 2 in. by 8.2 in. in the rim and 0.75 in. by 2 in. by 8.2 in. in the plate. Owing to wheel geometry considerations, it was not possible in all cases to adhere to these dimensions. Figure 26 gives the actual specimen sizes tested for each wheel.

6.4 SELECTION OF TEST TEMPERATURES

To ascertain the lowest temperature a wheel can reasonably be expected to experience in service in the United States (including Alaska), a survey was undertaken correlating weather records with localities having railroads. Information from the U.S. Department of Commerce (ref. 35) was correlated with major railroad locations identified from the Rand McNally Railroad Atlas of the United States. The data extracted was the mean normal minimum for January together with the lowest temperature ever recorded. The records covered the period 1931 to 1960. Results of this survey are given in appendix A, table A1. It was concluded that testing at -40° F would be adequate to cover the lowest temperature reasonably expected.

Testing at -40° F was performed on the K_{IC} and K_{Id} fracture toughness specimens. All Charpy and tensile tests were conducted at room temperature. The K_{IC} and K_{Id} specimens were tested at temperatures up to 300° F to assess the effects of the elevated temperatures experienced during braking.

6.5 TEST METHODS

6.5.1 Tensile Testing

Tensile specimens were tested on a 30-kip capacity Tinius Olsen tensile test machine. Strain rate to the 0.2% offset yield strength was 0.005 in. per inch per minute and thereafter 0.05 in. per inch per minute to failure. Tests were performed at room temperature.

6.5.2 Charpy Testing

Standard 0.394-in.-square Charpy V-notch impact test specimens were tested in a 240 ft-lb capacity Wiedemann impact test machine. Tests were performed at room temperature.

6.5.3 K_{IC} Testing

K_{IC} specimens were fatigue precracked and tested in three-point bending to conform to ASTM E399-72 (Standard Method of Test for Plane-Strain Fracture Toughness of Metallic Materials). Tests were conducted at temperatures in the range of -40° to 300° F. Because of difficulties in meeting ASTM E399-72 requirements, plate specimens were not tested above 70° F. Temperatures below 70° F (room temperature) were obtained by enclosing the specimen in a cooling box. Cooling was regulated by using liquid nitrogen. Elevated temperatures (above 70° F) were obtained by exposing the specimens to radiant heaters. Temperatures were monitored by thermocouples attached to the specimen.

30

6.5.4 K_{Id} Testing

Plane strain dynamic fracture toughness data (K_{Id}) were obtained by testing precracked standard 0.394-in.-square Charpy-V-notch specimens in a computerized impact testing system. Data were obtained at a hammer velocity of 17 fps. Tests were conducted at -40° F, 75° F, 150° F, and 300° F.

6.5.5 Metallographic Analysis and Hardness Survey

Macrosections were taken from two locations within each wheel to evaluate the rim and the plate. These are identified as GF2 and GF5 for each wheel, respectively. The GF5 locations were polished and etched in 50% aqueous solution of hydrochloric acid at a temperature of 180°F. All sections were photographed to document the macrostructure in the rim and plate of each wheel.

Three Brinell hardness impressions were made in the rim of each wheel as required by the M107 and M208 specifications. In addition, hardness traverses were made 0.1 in. apart in the GF5 section and 0.2 in. apart in the GF2 section at the locations shown in figure 27. Hardnesses were measured on the Rockwell C scale for all wheels except the class A. Due to its lower hardness, the class A wheel was measured on the Rockwell B scale. All values were then converted to Brinell hardness.

Microsections were taken from X, Y, and Z locations shown in figure 27. Typical microstructures were photographed before and after etching in 2% Nital.

Inclusion ratings were performed on each wheel per ASTM E45-63 (Recommended Practice for Determining the Inclusion Content of Steel).

An assessment of both the percentage pearlite and pearlite colony size was made. The percentage of pearlite in a microstructure was determined by a point counting technique. In this method, a grid was superimposed on a projection of the microstructure. Counts were actually made of ferrite grains falling at grid intersections. These data were then statistically analyzed to give percentage ferrite (and hence percentage pearlite) in the microstructure. The relative percentages were obtained within 99% confidence limits. The technique is fully described in reference 36. Pearlite colony size was assessed using the linear intercept method whereby the number of colony boundaries intercepted in a given length is counted.

6.5.6 Chemical Analysis

A chemical analysis was performed on each wheel and compared to the supplier's test certificates.

6.5.7 Fractography

Selected fracture faces of the broken fracture toughness specimens were examined both visually and also by means of the scanning electron miscroscope.

7.0 RESULTS

7.1 TENSILE PROPERTIES

The room temperature tensile properties of the rim and plate of each wheel are reported in table 10. Yield and tensile strengths of the class A and C rims were considerably higher than in the plate as a result of rim quenching. There was little difference between these regions in the untreated class U and fully quenched class CE wheels. Ductility, as measured by reduction of area, was similar in the rim and plate of each wheel, except the wrought class C, which was lower in the plate.

With the exception of the tensile specimens from the wrought class A wheel, the fracture modes were initially fibrous, changing to cleavage as failure progressed. Percentage fibrosity varied from less than 1% up to 25% and varied in its location from the center to the edge of the cross section. Figure 28 shows a typical tensile fracture. The tensile fracture from the wrought class A wheel was typically a ductile, cup-cone fracture, 100% fibrous with no cleavage evident.

TABLE 10.—RESULTS OF TENSILE TESTING AT ROOM TEMPERATURE

Wheel		Specimen		UTS (ksi)	TYS (ksi)	Elongation (%)	Reduction in area (%)
Number	Class	Number	Location				
1	U, cast	W1-S1-R	Rim	110.6	54.5	8	11.5
		W1-S2-P	Plate	108.3	51.8	8	11.3
2	C, cast	W2-S1-R	Rim	144.8	93.4	8	16.1
		W2-S2-P	Plate	115.2	60.3	8	18.8
3	U, wrought	W3-S1-R	Rim	109.1	59.4	9	14.5
		W3-S2-P	Plate	109.3	58.6	9	18.1
4	A, wrought	W4-S1-R	Rim	104.1	65.6	16	37.7
		W4-S2-P	Plate	89.6	47.2	14	35.0
5	C, wrought	W5-S1-R	Rim	135.5	86.6	11	32.6
		W5-S2-P	Plate	107.8	52.3	10	21.4
6	U, wrought (used)	W6-S1-R	Rim	120.7	64.7	9	16.1
		W6-S2-P	Plate	121.5	67.7	10	15.7
7	CE, wrought	W7-S1-R	Rim	168.4	108.1	9	29.9
		W7-S2-P	Plate	153.7	90.0	11	28.4

33

7.2 CHARPY IMPACT

Room temperature Charpy impact values are given in table 11. Values were less than 5 ft-lb for the rim and plate regions of all wheels except in the case of the class A wheel, for which 6 to 8 ft-lb was recorded. All the fractures with the exception of the class A wheel were essentially 100% cleavage. Both rim and plate fractures from the class A wheel showed approximately 10% fibrous shear.

TABLE 11.—RESULTS OF ROOM TEMPERATURE CHARPY TESTS

Wheel		Specimen		Charpy value (ft-lb)
Number	Class	Number	Location	
1	U, cast	W1-1A-CR W1-1B-CR	Rim	<1 2.5
		W1-2A-CP W1-2B-CP	Plate	2.0 3.0
2	C, cast	W2-1A-CR W2-1B-CR	Rim	3.5 4.0
3	U, wrought	W3-1A-CR W3-1B-CR	Rim	4.0 3.5
		W3-2A-CP W3-2B-CP	Plate	3.0 3.0
4	A, wrought	W4-1A-CR	Rim	6.5
		W4-2A-CP W4-2B-CP	Plate	8.0 8.0
5	C, wrought	W5-1A-CR W5-1B-CR	Rim	3.0 2.5
		W5-2A-CP W5-2B-CP	Plate	2.5 2.5
7	CE, wrought	W7-2A-CP W7-2A-CP	Plate	2.0 2.5

7.3 FRACTURE TOUGHNESS, K_{IC}

In essence, the fracture toughness tests conducted to ASTM E399-72 consist of loading a precracked specimen to failure. The specimen is instrumented to obtain a curve of load versus crack-opening displacement at the mouth of the notch. After completion of the test, a 5% offset secant line is constructed on the load displacement curve and the load corresponding to the point of intersection of the secant line with the curve (which represents a 2% crack extension) is designated P_Q. The stress intensity corresponding to P_Q is calculated, and designated as K_Q. If the following criteria are fulfilled, then K_Q is equal to the plane strain fracture toughness K_{IC}:

1) Specimen thickness $> 2.5 \dfrac{K_Q^{\,2}}{TYS}$

2) Crack length $\qquad$ $> 2.5 \dfrac{K_Q}{TYS}^2$

3) $\dfrac{P_{max}}{P_Q}$ $\qquad$ $\leqslant 1.10$

where P_{max} is the maximum load recorded in the test. Items 1 and 2 are required to ensure that plane strain conditions are operative at the crack tip. Item 3 was recently introduced as a result of experimental work which had shown that items 1 and 2 were insufficient to guarantee a valid K_{IC} in some materials.

Results of the fracture toughness tests conducted in this program are given in table 12. Some of the tests did not fulfill the above requirements for a valid K_{IC} test, and the reasons are indicated in table 12. In a number of instances, the thickness and crack length requirements were fulfilled but the P_{max}/P_Q requirement was not complied with. However, in several of the tests conducted on wheels 1, 6, and 7, the K_Q value was comparable to valid K_{IC} values even though the P_{max}/P_Q significantly exceeded 1.10. This suggests that the load requirement is too restrictive for wheel materials.

The fracture toughness results obtained are plotted as a function of test temperature in figures 29, 30, and 31. Class U wheels are shown as a single plot, as are class C results. Class A values are plotted separately. It can be seen that there is no significant difference between the toughness of the rim and plate regions of each wheel. Furthermore, K_{IC} is only slightly sensitive to temperature within the range -40° to 70° F in each wheel. The effect of higher temperatures cannot be adequately assessed because few valid K_{IC} values were obtained at 150° and 300°F. Nevertheless, there is an upward trend in the data, above room temperature, which is particularly noticeable in the class C wheels (fig. 30). Valid measurements of K_{IC} could not be obtained for the class A wheel, presumably because of its relatively high toughness and low yield strength.

The only results not conforming to the general trend are the 70° F and 150° F tests of the wrought class C wheel (wheel 5) rim. These values are approximately 20 ksi in.$^{1/2}$ higher than the highest of the other values plotted (using a mean of 58 ksi in.$^{1/2}$ for the room temperature value of wheel 5). It is known that residual compressive stresses are introduced into the rim by heat treatment. If these stresses were present, they would tend to resist crack opening of the K_{IC} specimen. Using the difference of 20 ksi in.$^{1/2}$ as a measure of the effort needed to overcome this resistance, a compressive residual stress of approximately 30 ksi was calculated (ref. 37).

Measurements of residual stress in one specimen (No. W5-K6) revealed an actual residual compressive stress of 29.1 ksi acting normal to the crack plane.

These results are in agreement with the range of residual compressive stresses, reported in the literature for new wheels, of 15 to 45 ksi (sec. 4.1.1).

TABLE 12.—RESULTS OF FRACTURE TOUGHNESS (K_IC) TESTING

Wheel		Specimen		Test temperature (°F)	Specimen dimensions (in.)[a]			Load, P_Q (lb)	K_Q (ksi in.$^{1/2}$)	$\dfrac{P_{max}}{P_Q}$	Conforms to ASTM E-399-72 W and a requirements	Remarks
Number	Class	Location	Number		Width (B)	Thickness (W)	Crack length (a)					
1	U, cast	Rim	1-9AK	-40	1.005	2.004	1.06	4560	37.5	1.21	No	
			1-1BK	-40	1.007	2.008	1.04	4290	33.8	1.02	Yes	$K_Q = K_{IC}$
			1-7K	0	1.001	1.988	1.02	3880	30.8	1.18	Yes	
			1-1AK	70	1.001	2.004	1.05	4400	35.7	1.10	Yes	$K_Q = K_{IC}$
			1-8K	70	1.001	1.998	1.01	5010	38.5	1.34	No	
			1-9BK	150	1.007	2.004	1.05	5490	44.3	1.09	No	
			1-6K	300	1.004	2.006	1.05	5460	44.1	1.69	No	$K_Q = K_{IC}$
		Plate	1-7KP	-40	0.752	1.702	0.94	2080	26.9	1.10	Yes	Load curve not obtained
			1-6KP	70	–	–	–	–	–	–	–	
			1-8KP	70	0.758	1.712	0.84*	3920	48.6*	1.00	No	*Did not satisfy ASTM E-399-72 crack criteria
			1-9KP	70	0.746	1.704	0.96	2950	40.0	1.11	No	
2	C, cast	Rim	2-1BK	-40	1.008	1.993	1.03	3840	30.5	1.09	Yes	$K_Q = K_{IC}$
			2-8K	0	0.999	1.999	1.02	4280	33.4	1.06	Yes	$K_Q = K_{IC}$
			2-6K	70	1.004	1.990	1.00	4950	37.8	1.07	Yes	$K_Q = K_{IC}$
			2-1AK	70	0.993	1.994	0.87*	5650	35.5*	1.24	No	*Did not satisfy ASTM E-399-72 crack criteria
			2-9AK	70	0.998	1.993	1.07	4460	38.3	1.10	Yes	$K_Q = K_{IC}$
		Plate	2-9BK	150	1.007	2.000	1.04	5730	45.8	1.10	Yes	$KQ = K_{IC}$
			2-7K	300	1.003	1.999	1.03	7820	61.8	1.34	Yes	
			2-9KP	-40	0.747	1.709	0.93	2330	29.3	1.02	Yes	$K_Q = K_{IC}$
			2-1KP	70	0.754	1.708	0.83*	5040	45.8*	1.00	No	*Did not meet ASTM E-399-12 crack criteria

TABLE 12.—CONTINUED

| Wheel Number | Class | Specimen Location | Specimen Number | Test temperature (°F) | Specimen dimensions (in)[a] | | | Load, P_Q (lb) | K_Q (ksi in $^{1/2}$) | $\dfrac{P_{max}}{P_Q}$ | Conforms to ASTM E-399-72 W and a requirements | Remarks |
					Width (B)	Thickness (W)	Crack length (a)					
3	U,wrought	Rim	3-1BK	-40	1.007	1.997	0.99	4100	29.4	1.40	Yes	
			3-7K	0	1.008	2.005	0.96	5750	40.1	1.00	No	
			3-9AK	0	1.003	2.004	0.97	4010	28.6	1.57	Yes	
			3-1AK	70	1.008	1.999	1.03	4790	39.1	1.22	Yes	
			3-8K	70	0.998	2.002	1.01	5210	39.9	1.46	No	
			3-9BK	150	1.008	2.005	1.02	5260	40.3	1.35	No	
			3-6K	300	1.002	2.003	1.08	5150	44.0	1.83	No	
		Plate	3-9KP	-40	0.753	1.709	0.92	2640	32.3	1.01	Yes	$K_Q = K_{Ic}$
			3-6KP	-40	0.748	1.709	0.90	2990	35.4	1.10	No	
			3-8KP	0	0.749	1.709	0.91	2530	30.5	1.39	Yes	
			3-7KP	70	0.753	1.709	0.92	3820	46.7	1.14	No	
			3-1KP	70	0.759	1.709	1.12*	3070	46.5*	1.21	No	*Did not meet ASTM E-399-72 crack criteria
4	A,wrought	Rim	4-1BK	-40	1.003	1.998	1.06	6400	53.3	1.00	No	
			4-7K	0	1.001	1.992	1.00	7830	59.7	1.03	No	
			4-9AK	0	0.996	1.995	1.03	6050	48.5	1.00	No	
			4-1AK	70	1.001	1.997	1.04	7080	57.2	1.00	No	
			4-8K	70	1.006	1.993	1.01	7440	57.3	1.33	No	
			4-9BK	150	1.004	2.001	1.10	5870	52.0	1.59	No	
			4-6K	300	1.007	2.005	1.06	6920	56.7	1.46	No	
		Plate	4-9KP	-40	0.752	1.993	0.96	5010	47.6	1.08	No	
			4-6KP	-40	0.754	1.994	1.05	4260	46.7	1.00	No	
			4-7KP	0	0.754	2.005	0.97	5390	51.0	1.16	No	
			4-8KP	70	0.758	2.005	1.01	4220	42.3	1.86	No	
			4-1KP	70	0.753	1.994	1.02	3890	40.6	1.72	No	

TABLE 12.—CONCLUDED

Wheel Number	Class	Location	Specimen Number	Test temperature (°F)	Width (B)	Thickness (W)	Crack length (a)	Load, P_Q (lb)	K_Q (ksi in.½)	$\frac{P_{max}}{P_Q}$	Conforms to ASTM E-399-72 W and a requirements	Remarks
5	C,wrought	Rim	5-1BK	-40	0.990	1.996	1.03	4500	36.2	1.00	Yes	$K_Q = K_{Ic}$
			5-9AK	0	1.006	1.998	0.96	5130	36.2	1.09	Yes	$K_Q = K_{Ic}$
			5-1AK	70	0.996	1.992	0.85*	10,300	62.8*	1.00	No	*Did not satisfy ASTM E-399-72 crack criteria
			5-6K	70	1.008	2.002	1.13	6820	63.4	1.00	No	
			5-7K	70	1.009	2.007	1.18	5310	53.5	1.00	Yes	$K_Q = K_{Ic}$
			5-9BK	150	0.999	1.998	1.00	8830	66.8	1.13	No	
			5-8K	300	1.006	1.996	1.00	8810	66.4	1.72	No	
		Plate	5-6KP	-40	0.754	1.703	0.92	2280	28.2	1.23	Yes	
			5-7KP	-40	0.758	1.703	0.93	2230	28.0	1.25	Yes	
			5-8KP	0	0.753	1.704	0.96	2020	27.1	1.25	Yes	
			5-1KP	70	0.752	1.704	0.94	2760	35.6	1.19	No	
			5-9KP	70	0.752	1.707	0.95	2420	31.6	1.41	No	
6	U,wrought, used	Rim	6-1BK	-40	0.695	1.683	0.90	1900	24.1	1.24	Yes	
			6-9AK	0	0.695	1.686	0.92	2120	29.4	1.10	Yes	$K_Q = K_{Ic}$
			6-1AK	70	0.695	1.683	0.81*	3180	35.8*	1.16	No	*Did not satisfy ASTM E-999-72 crack criteria
			6-8K	70	0.701	1.686	0.91	2220	29.9	1.58	No	
			6-9BK	150	0.702	1.686	0.88	2900	36.7	1.32	No	
		Plate	6-9KP	-40	0.705	1.709	0.93	2200	29.3	1.10	Yes	$K_Q = K_{Ic}$
			6-6KP	-40	0.501	1.004	0.58	815	22.5	1.41	Yes	
			6-1KP	70	0.707	1.701	0.91	2460	31.9	1.40	Yes	
			6-8KP	70	0.701	1.694	0.89	2940	37.5	1.06	Yes	$K_Q = K_{Ic}$
7	CE,wrought	Rim	7-1BK	-40	1.004	1.988	1.03	3710	30.1	1.21	Yes	$K_Q = K_{Ic}$
			7-1AK	70	1.004	1.995	0.99	5530	35.0	1.10	Yes	$K_Q = K_{Ic}$
		Plate	7-6KP	-40	0.756	2.004	0.95	3290	30.1	1.10	Yes	$K_Q = K_{Ic}$
			7-9KP	-40	0.755	2.000	0.96	3060	28.7	1.09	Yes	$K_Q = K_{Ic}$
			7-8KP	0	0.753	2.004	1.00	3830	38.1	1.00	Yes	$K_Q = K_{Ic}$
			7-1KP	70	0.755	2.004	0.96	3680	34.3	1.21	Yes	
			7-7KP	70	0.756	2.004	0.97	3770	35.6	1.10	Yes	$K_Q = K_{Ic}$

aSpecimen dimensions identified according to ASTM E-399-72.

Immediately the question may be raised about the influence of compressive stresses on the K_{IC} values of the other rim-treated wheels. However, a comparison of the data between the plate and the rim for these wheels reveals comparable K_{IC} values, thus indicating that any residual stress system in these specimens had little or no effect.

7.4 DYNAMIC FRACTURE TOUGHNESS K_{Id}

Values of K_{Id} were calculated from a load/deflection curve in a similar manner to K_{IC}. However, there is no specification to control specimen geometries, testing procedures, etc. and the degree of control obtained in K_{IC} testing by ASTM E399-72 is not available. The values obtained are given in table 13 and the results are plotted in figure 32. It can be seen that the results obtained show similar trends to the K_{IC} data, toughness increasing with increasing temperature.

TABLE 13.—DYNAMIC FRACTURE TOUGHNESS (K_{Id}) VALUES

Wheel		K_{Id} (ksi in.$^{1/2}$)[a]			
Number	Class	-40° F	75° F	150° F	300° F
1	U, cast	—	21.0 (W1-S2A)	—	59.2 (W1-S2D)
3	U, wrought	31.6 (W3-2A)	32.1 (W3-2B)	43.4 (W3-2C)	63.1 (W3-2D)
4	A, wrought	—	36.5 (W4-S2B)	58.6 (W4-S2C)	63.4 (W4-S2D)
5	C, wrought	—	21.5 (W5-S2B)	36.1 (W5-S2C)	—
7	CE, wrought	—	36.6 (W7-2B)	42.2 (W7-2C)	87.5 (W7-2D)

[a]Specimen numbers in parenthesis

7.5 HARDNESS

The results of the Brinell hardness tests on the wheel treads are given in table 14. In all cases where a hardness range was specified, the results obtained were the minimum acceptable.

Figures 33 through 39 show the results of the hardness traverses across the wheel section. Since these numbers are converted from a Rockwell number, direct comparison of the values obtained with an actual Brinell test may be misleading. In any event, the values obtained are not representative of the specification requirement, since hardness must be taken on the wheel surface. The hardness values provide a quantitative evaluation of differences existing within the wheel due to processing effects.

TABLE 14.—COMPARISON OF BRINELL HARDNESSES OBTAINED BY BOEING
WITH SPECIFICATION REQUIREMENTS

Wheel		BHN	Specification requirement
Number	Class	(Boeing)	
1	U, cast	235	Not required
2	C, cast	321	321-363
3	U, wrought	241	Not required
4	A, wrought	255	255-321
5	C, wrought	321	321-363
6	U, wrought (used)	285	Not required
7	CE, wrought	321	321-363

Considering the class A wheel, it can be seen that of the two sections evaluated, the hardness was comparable for both. As indicated by the tensile results, the plate hardness was appreciably lower than that of the rim.

The wrought class U wheel had uniform hardness in comparable areas of the sections evaluated. However, the cast class U showed a higher tread hardness in the GF5 compared to the GF2 location. The used, wrought class U wheel was particularly inhomogenous, varying measurably in the two locations evaluated at the tread, plate, and flange.

Both the cast and wrought class C wheels displayed remarkable uniformity of hardness in the sections evaluated. The fully heat-treated wrought class CE, however, showed differences in hardness of the tread, flange, and plate between the GF2 and GF5 locations.

Similar to the class A wheel, the cast class C and the wrought class C wheels showed a greater hardness in the rim than in the plate, as would be expected of rim quenching. The wrought class CE did not exhibit this rim/plate hardness difference, again as to be expected in a fully quenched wheel.

7.6 METALLOGRAPHY

Macrosections of each wheel, taken from the GF5 location, are shown in figures 40 through 46. The cast class U and C wheels show typical cast dendritic structure. The wrought class A wheel shows evidence of retention of the cast structure in the center of the rim, indicating incomplete breakdown during working. The remainder of the wheels (i.e., wrought classes U, C, and CE) show a fine structure indicating complete breakdown of any prior cast structure.

No evidence of thermal damage was seen on the tread surface of the used, wrought class U wheel (fig. 45).

40

Microsections taken from the X, Y, and Z locations (shown in fig. 27) were examined for inclusion content. These were estimated per ASTM E45, Method A, and the results are given in table 15. Ratings for both the cast U and cast C wheels are given for comparison, although strictly speaking this method is not applicable to cast structures. Inclusions appeared to be predominantly of the class D type, that is globular oxides. The analysis shows the used wheel (wrought class U) had the greatest inclusion content. The wrought classes A and C wheels were the cleanest, with the minimum of inclusions, and the cast classes U and C and the wrought classes U and CE wheels were intermediate in cleanliness, having similar ratings. In the cast class C wheel, however, the inclusions were light as opposed to heavy in the other wheels.

Typical microstructures for both the rim and plate are shown in figures 47 through 53. Except for the class A wheel, the microstructures of all wheels at the tread, rim center, and plate were similar in that they were essentially fully pearlitic and contained less than 1% ferrite (table 16). In the class A wheel, the ferrite content was considerably higher in the plate than in the tread region, which in turn was slightly lower than at the rim center. These observations are due to the different cooling rates experienced at these locations during rim quenching, ferrite formation being suppressed by faster cooling rates.

Examination of the pearlite revealed variations in the colony size (table 17). The smallest colonies were in the rims of the heat-treated wheels, the colony size being slightly larger in the unquenched plate. The largest colony size was in the wrought class U wheel (wheel 3) and is attributed to the absence of a normalizing treatment after rolling.

Also reported in table 17 is the prior austenite grain size for each wheel. All wheels were in the range ASTM 6-8. It can be seen that the pearlite colony size bears little or no relationship to the prior austenite grain size.

7.7 CHEMICAL ANALYSIS

The results of the chemical analysis for each wheel are given in table 18. The carbon content of all wheels, except the class A, was within the range 0.70%-0.75%. Manganese content of all wheels was 0.6%-0.7%. According to the Boeing analysis, the silicon content was marginally below the specification requirements for the wrought classes U, A, and C. The manufacturer's analysis indicated that the silicon content was acceptable. It is unlikely that the lower silicon content within the limits determined would have any measurable effect on the toughness or mechanical properties.

7.8 FRACTOGRAPHY

Optical and low-power examination of the fractures obtained from the K_{IC} specimens was made to compare the fracture morphology between wheels and to assess the effect of test temperature. All specimens tested at room and lower temperatures exhibited essentially 100% cleavage fracture. A qualitative assessment of the rim specimen fractures at this temperature showed that the wrought class U wheel (No. 3) had the largest cleavage facets. This wheel also has the largest pearlite colony size (table 17). The next largest facets

41

TABLE 15.—INCLUSION RATINGS PER ASTM E45, METHOD A

Wheel		Inclusion rating[a]
Number	Class	
1	U, cast	D2H
2	C, cast	D2L
3	U, wrought	D2H
4	A, wrought	D1H
5	C, wrought	D1H
6	U, wrought (used)	D3H
7	CE, wrought	D2H

[a]H indicates heavy
L indicates light

TABLE 16.—PERCENTAGE FERRITE MEASURED IN LOCATIONS MICROSECTIONED FOR EACH WHEEL

Wheel		Percentage ferrite (99% confidence)		
		Rim location		
Number	Class	Tread (X)	Center (Y)	Plate location (Z)
1	U, cast			
2	C, cast			
3	U, wrought	<1	<1	<1
4	C, wrought			
5	U, wrought (used)			
7	CE, wrought			
4	A, wrought	9.5	15.9	28.6

X, Y, and Z indicate microsection locations shown in Figure 27

42

TABLE 17.–PEARLITE COLONY SIZES AND PRIOR AUSTENITE GRAIN SIZES
DETERMINED FOR RIM AND PLATE LOCATION OF WHEELS

Wheel		Rim				Plate	
Number	Class	Pearlite colony (size (in. x 10^{-3})		Prior Austenite grain size (ASTM)		Pearlite colony size (in. x 10^{-3})	Prior Austenite grain size (ASTM)
		Tread	Center	Tread	Center		
1	U, cast	1.81	2.24	7	7	2.44	6
2	C, cast	1.38	1.81	6-7	6-7	2.09	6
3	U, wrought	4.45	4.37	6	6	4.49	7
4	A, wrought	1.06	1.14	8	8	1.38	8
5	C, wrought	1.30	1.65	6	6	1.85	6
6	U, wrought– used	1.65	2.09	8	8	1.85	7
7	CE, wrought	1.06	1.22	7	7	1.14	8

occurred on the used wheel, which was also a wrought class U. The remainder of the fractures rated in order of coarseness are the cast class U; the cast class C, wrought class C, and wrought class CE; and finally the wrought class A. These ratings relate extremely well to the pearlite colony sizes obtained for the rim centers of each wheel. There was no correlation with the prior austenite grain size.

The effect of the temperature of testing on the fracture appearance for the rim and plate specimens is summarized in table 19. Figures 54 through 60 document the fracture appearance with respect to temperature for each wheel rim. The wrought class A wheel exhibited slight shear lip development at room temeprature, with the transition to 100% fibrous fracture occurring between 150° F and 300° F. The cast class U, both wrought class U rims, and the cast and wrought class C were 100% cleavage at room temperature and below. At 150° F these wheels began to show 1% to 5% shear lip formation. At 300° F only the cast class U and cast class C had changed to essentially 100% fibrous. The wrought class U tested had 50%/50% mixed cleavage/fibrous fracture modes at 300° F and the wrought class C exhibited 70% fibrous fracture at this temperature. The wrought class CE was tested only at -40° F and 70° F and showed 100% cleavage at both temperatures. All plate fractures tested at temperatures from -40° F to 70° F showed 100% cleavage as the fracture mode.

Fractures from the K_{IC} test specimens tested at 70° F were observed with the scanning electron microscope. They were viewed in the center of the fractured ligament and all showed 100% cleavage. Fractographs are shown in figures 61 through 68. Figure 65 shows the fracture of the class A wheel tested at 300°F. As can be seen, the topography is 100% ductile, fracture having occurred by microvoid coalescence. The size of the cleavage facets in each fracture could be ranked in the same order as the size of the pearlite colony sizes measured for each wheel.

TABLE 18.—COMPARISON OF CHEMICAL ANALYSES MADE BY BOEING AND THE WHEEL MANUFACTURER[a]

Wheel		Boeing analysis					Supplier analysis					Specification requirement				
Number	Class	C	Mn	Si	P	S	C	Mn	Si	P	S	C	Mn	Si (min)	P (max)	S (max)
1	U. cast	0.70	0.62	0.23	0.020	0.038	0.73	0.73	0.40	0.024	0.032	0.65 to 0.80	0.60 to 0.85	0.15	0.05	0.05
2	C, cast	0.71	0.62	0.21	0.012	0.031	0.72	0.69	0.37	0.013	0.025	0.67 to 0.77	0.60 to 0.85	0.15	0.05	0.05
3	U, wrought	0.71	0.70	0.14	0.014	0.012	0.70	0.73	0.23	0.016	0.014	0.65 to 0.80	0.60 to 0.85	0.15	0.05	0.05
4	A, wrought	0.53	0.60	0.13	0.010	0.026	0.53	0.67	0.22	0.010	0.021	0.57-max	0.60 to 0.85	0.15	0.05	0.05
5	C, wrought	0.70	0.64	0.11	0.006	0.020	0.70	0.73	0.22	0.007	0.017	0.67 to 0.77	0.60 to 0.85	0.15	0.05	0.05
6	U, wrought (used)	0.73	0.61	0.16	0.032	0.040	—	—	—	—	—	0.65 to 0.80	0.60 to 0.85	0.15	0.05	0.05
7	CE, wrought	0.75	0.67	0.23	0.021	0.050	0.72	0.71	0.30	0.014	0.037	0.67 to 0.77	0.60 to 0.85	0.15	0.05	0.05

[a]Values are reported in weight percent

TABLE 19.—ESTIMATE OF RELATIVE PERCENTAGES OF CLEAVAGE AND FIBROUS FRACTURE MODES EXHIBITED BY K_{IC} FRACTURES

| Wheel | | Relative percent cleavage/fibrous of fracture face[a] | | | | | | | |
| Number | Class | Rim | | | | | Plate | | |
		-40°F	0°F	70°F	150°F	300°F	-40°F	0°F	70°F
1	U, cast	100% C	100% C	100% C	>95% C <5% F	100% F	100% C	100% C	100% C
2	C, cast	100% C	100% C	100% C	>99% C <1% F	<1% C >99% F	100% C	100% C	100% C
3	U, wrought	100% C	100% C	100% C	>95% C <5% F	50% C 50% F	100% C	100% C	100% C
4	A, wrought	100% C	100% C	>95% C <5% F	30% C 70% F	100% F	100% C	100% C	90% C 10% F
5	C, wrought	100% C	100% C	100% C	>99% C <1% F	30% C 70% F	100% C	100% C	100% C
6	U, wrought (used)	100% C	100% C	100% C	>99% C <1% F	—		100% C	100% C
7	CE, wrought	100% C	—	100% C	—	—	100% C	100% C	100% C

[a] C = cleavage   F = fibrous

45

8.0 DISCUSSION

Mechanical properties of the wrought wheels tested in this program are compared in table 20 with values reported by other investigators for wheels of similar class. While there is general agreement between the sets of data, the yield and tensile strengths of the class A and C test wheels were somewhat lower. This is consistent with the hardness values of these wheels which were equal to the lower limit required by the AAR specification (table 16).

TABLE 20.—COMPARISON OF WROUGHT WHEEL TENSILE PROPERTIES

Class	Location	Yield strength (ksi)	Tensile strength (ksi)	Reference
A	Rim	71-78 (65.6)	120-128 (104)	2 and 8
	Plate	54 (47)	97-107 (89.6)	8 and 15
B	Rim	85-88	144-145	2 and 8
	Plate	50	117	8
C	Rim	88-127 (86.6)	156-178 (135.5)	2, 8, and 15
	Plate	47-66 (52.3)	117-128 (107.8)	8 and 15
CE	Rim	88 (108.1)	147 (168.4)	8
	Plate	89 (90.0)	149 (153.7)	8
U	Rim	50-55 (59.4/64.7)	121-126 (109/120.7)	8
	Plate	50-56 (58.6/67.7)	122-127 (109.3/121.5)	8

(   ) = Boeing data

Yield and tensile properties of the class U and class C wheels were similar for both wrought and cast wheels (table 10). The only difference in mechanical properties was a lower reduction of area in the rim of the cast class C wheel.

Fracture toughness properties below 150°F were also uninfluenced by the method of fabrication. Figures 29 and 30 indicate comparable fracture toughness in the rim and plate of class U and class C wheels in wrought and cast forms. However, the fracture mode transition temperature of the cast class U rim was lower than that of the wrought. This can be attributed to the practice of normalizing class U wheels by the manufacturers of cast wheels.

Carbon content had an adverse effect on the fracture toughness. This is illustrated in figure 69, which shows the Boeing results, and data reported by British Railways. It can be seen that there is good agreement among the data obtained by both sources and that the toughness falls quite markedly as the carbon content is raised from 0.5% to 0.75%.

The fracture toughness values for the rim and plate regions were similar for untreated class U wheels. While rim quenching significantly increased the yield and tensile strengths of the rim relative to the plate, there was no effect on the fracture toughness. The relationship between yield strength and fracture toughness at a carbon level of 0.70-0.75% is shown in figure 70. The toughness of these fully pearlitic steels is invariant over the wide range of yield strength developed by heat treatment.

These observations can be rationalized on the basis of work reported by Gladman et al. (ref. 38). They conducted an extensive study of the structure-property relationships in ferrite-pearlite high carbon steels. In fully pearlitic steels, the fracture toughness (20 ft-lb Charpy impact transition temperature) was found to improve with decreasing pearlite colony size and carbide plate thickness; however, toughness was impaired by decreasing the interlamellar spacing of the pearlite. On the other hand, the only microstructural variable affecting the yield strength was the interlamellar spacing of the pearlite, which was inversely related to yield strength. As can be seen from table 17, rim quenching only slightly reduced the pearlite colony size relative to the plate. Consequently it appears that quenching of the rim results in a reduction in both the interlamellar spacing and carbide plate thickness, the net effect of these structure changes being to maintain the toughness at a constant level while increasing the yield strength.

Gladman et al. (ref. 38) have also shown that in ferrite-pearlite steels, a significant feature affecting yield strength and toughness is the percentage of free ferrite (and its associated grain size). Increasing the ferrite content has lowered the yield strength but improved toughness. The effect of carbon on fracture toughness can be thus explained since the proportion of free ferrite is inversely related to the carbon content.

The effect of loading rate on fracture toughness also appears to depend on the microstructure. At a carbon level of about 0.7%, where the microstructure is predominantly pearlitic, the toughness may or may not be reduced by dynamic loading. For example, in the fully heat-treated class CE plate the value of K_{Id} is equal to the K_{IC}, whereas in the cast class U and wrought class C there is a difference of about 10-15 ksi in.$^{1/2}$. Similarly, British workers (ref. 39) have reported that the toughness of rail steel, which has a predominantly pearlitic microstructure, is insensitive to loading rate, but Stone (private communication) found a difference about 10 ksi in.$^{1/2}$ in similar material. It would seem probable that the interlamellar spacing is the microstructural feature which dominates the response to dynamic loading, although this has not been verified.

At carbon levels of about 0.5 and lower, it appears that the toughness is definitely reduced by dynamic loading. The data obtained from the class A wheel indicate this, and Castagna et al. (ref. 13) reported dramatic reductions in the toughness of 0.45C grain refined steel when the loading rate increased. This can be associated with the free ferrite content of these steels and the fact that the toughness of low carbon ferritic steels is significantly reduced by dynamic loading (ref. 23).

9.0 ANALYSIS OF WHEELS FRACTURED IN SERVICE

A fractures mechanics analysis of wheels fractured in service is presented in this section. There were three main objectives:

1) Ascertain the location, configuration, and size of thermal cracks and plate cracks which initiated brittle fracture of the wheel.

2) Estimate the stresses which resulted in brittle fracture, using the fracture toughness values reported in section 8.0.

3) Compare these stresses with the values experienced in service (sec. 4.0).

In addition, information was sought on the modes of crack extension and factors influencing the initiation of cracks.

Information on wheels that fractured in service has been obtained from reports of failure analyses conducted by a major U.S. railroad serving the Midwest and Western states. One hundred wheels fractured in service as a result of either thermal or plate cracks during the period 1969 to mid-1973 have been reviewed and the following information documented for each wheel:

● Design

● Method of manufacture

● Class (and chemical analysis when reported)

● Age at failure, assuming wheel entered service in year of manufacture

● Rim thickness at failure

● Month in which failure occurred

● Sketch of fractured wheel showing initiation site and crack path

● Sketch and dimensions of crack which initiated brittle fracture

● Factors which may have contributed to failure

In most instances the dimensions of the crack which initiated brittle fracture were included in the failure analysis report, but there were a few cases where estimates had to be made from a photograph of the fracture face. The crack size could not be established for some wheels because the fracture faces were not exposed or were damaged. The above information (where available) is documented for each wheel in appendix B and is discussed below.

48

Of the hundred wheel fractures documented, 95 were removed from freight cars and 5 from diesel locomotives. Most were one-wear 33 in. diameter, and the wheel classes were distributed as below:

Class U	57
Class U1	20
Class A	2
Class B	9
Class C	6
Class Unknown	6

9.1 CRACK LOCATIONS

The locations of the cracks which initiated brittle fracture could be divided into five categories:

1. Tread

2. Flange

3. Rear rim

4. Front hub fillet

5. Rear rim fillet

Thermal cracks developed at locations 1-3, and fatigue cracks at locations 4 and 5.

Details of the individual wheel fractures are tabulated in appendix B according to these categories (tables B1-B5). In addition, one wheel fractured as a result of a fatigue crack which developed at the front rim fillet (table B6). This was an unusual case, but the wheel was 57 years old.

Table 21 summarizes the number of wheel failures in each category according to the method of manufacture and wheel class. The vulnerability of the high carbon content class U1 wheels to thermal cracking is evident, when the relatively small number in service is taken into account. Development of thermal cracks at the flange was a major cause of failure in class U wheels. This was reported to be due to faulty brake shoe contact against the flange. Several failures resulting from thermal cracks at the rear rim were associated with car retarder shoe action.

TABLE 21.—SUMMARY OF FAILED WHEELS

Failure initiation site	Class											Total failed
	U		U1	A		B		C		Grade unknown		
	Wrought	Cast	Cast	Wrought	Cast	Wrought	Cast	Wrought	Cast	Wrought	Cast	
Tread surface	4	—	16	1	—	4	—	2	—	—	—	27
Flange	8	21	3	1	—	—	—	—	—	—	—	33
Rear rim	3	1	1	—	—	2	—	—	—	—	—	7
Front hub fillet	13	2	—	—	—	—	—	—	—	6	—	21
Rear rim fillet	5	—	—	—	—	2	—	4	—	—	—	11
Front rim fillet	—	—	—	—	—	1	—	—	—	—	—	1
Total	33	24	20	2	—	9	—	6	—	6	—	100

50

The fatigue cracks initiated at the plate fillets were generally associated with processing defects such as rolled-in mill scale, porosity, and rough machine marks. Plate fractures initiated at the front hub fillet occurred about twice as frequently as those at the rear rim fillet, which is in accordance with observations made by other investigators (ref. 17).

9.2 SIZE AND CONFIGURATION OF CRITICAL CRACKS

The critical crack sizes which initiated brittle fracture of the wheels are summarized in figures 71-75 for the five crack locations. Figure 71 shows that of the cracks initiated at the tread surface, half developed as corner cracks bordering the tread and front rim faces. These cracks were usually attributed to a brake shoe overhanging the front rim. The depth of crack (at the front rim face) relative to the length (at the tread) was predominantly within the range 0.5-1. In one instance, the crack grew through the rim thickness prior to failure. The remaining surface cracks had a semicircular or semielliptical shape, initiating at various positions along the tread surface, the specific point presumably being determined by the distribution of thermal loads along the tread. The depth/length of these cracks varied considerably, class U1 wheels tending to have the higher values. Except for some class U1 and diesel locomotive wheels, the critical crack lengths were generally in the range of 1-3 in. One class B wheel on a diesel locomotive fractured from a corner crack only 0.31 in. long.

Critical sizes of thermal cracks in the flange are shown in figure 72. These cracks usually initiated close to the apex of the flange, with a configuration corresponding to a corner crack. Figure 72 indicates that the depth/length of these cracks was within the range 0.5-1. While most of the fractures which initiated at the flange involved cracks of this type, several wheels failed as a result of thermal cracks which had extended through the flange thickness. Most wheels, which were predominantly class U, had critical crack lengths (at the flange surface) in the range 0.5-1 in., the smallest being 0.19 in. long (fig. 73).

Of the seven wheel fractures resulting from thermal cracks at the rear rim (fig. 74), six were initiated by surface cracks of essentially semicircular shape. One failure was initiated by a corner crack bounded by the rear rim face and underside of the rim. The critical length of these cracks was on the order of 1 in.

On the basis of the above observations, three types of configurations can be associated with thermal cracks:

- Surface cracks

- Corner cracks

- Through-thickness edge cracks

The critical fatigue crack sizes which initiated brittle fracture of the plate are shown in figures 75 and 76 for the front hub and rear rim fillets, respectively. Two types of crack configuration can be identified:

- Surface cracks

- Through-thickness cracks

The depth/length of the surface cracks was about 0.33 for most fractured wheelplates. The majority of these cracks at the front hub fillet were less than 0.25 in. deep, the smallest being 0.06 in., whereas those at the rear rim tended to be slightly larger. Of the wheels which failed from the rear rim fillet, only those which were rim quenched fractured before the fatigue crack had extended through the plate thickness.

The six wheels which fractured from through-the-thickness plate cracks had critical crack lengths exceeding 10 in. This indicates that large cracks can escape detection with current inspection procedures.

9.3 MODE OF CRACK PROPAGATION

Where closeup photographs of the thermal cracks were provided in the failure analysis reports, it was sometimes possible to assess the mode of crack propagation. These observations are included in appendix B (tables B1-B3), and are summarized below.

Both cleavage and fatigue-type thermal cracks were observed, the latter usually exhibiting well-defined "beach marks" in the later stages of growth. Cleavage cracks were mainly observed at the tread of class U and U1 wheels. Fatigue-type thermal cracks were frequently observed at the flange and rear rim, primarily in class U wheels. Three of these thermal cracks grew initially by thermal fatigue but subsequently extended by cleavage.

It is difficult to make any firm comments regarding the mode of crack growth in the class A and B wheels because of the few examples reviewed. Nevertheless, the available data indicate that all the cracks grew by thermal fatigue at the three crack locations, although in one class B wheel a tread thermal crack subsequently propagated by cleavage.

As far as could be ascertained, the fatigue cracks in the plates showed characteristic growth markings.

The regions of rapid fracture in the broken wheels invariably showed the characteristics of brittle fracture, viz. flat fracture with vestiges of shear lip development. Figures 1-3 and 5-6 are typical examples. They correspond to the fractures obtained in the K_{IC} specimens tested below the fracture mode transition temperature.

In the case of the fractures initiated from fatigue cracks at the back rim fillet, the observations are, perhaps, somewhat surprising. As noted previously, the tensile stresses developed at this location during drag braking are associated with a significant temperature rise (for example, 400° F for yield-point-magnitude stresses). Consequently, some evidence of ductility might be expected if failure resulted from thermally induced stresses. The absence of ductility suggests that thermal stresses alone are not responsible for failure, and that residual stresses developed by rim quenching and/or stresses from lateral loading also play a significant role.

9.4 FAILURE TEMPERATURE

Insufficient information was given in the failure reports to firmly establish the temperature at which the individual wheels failed. To obtain some indication as to whether failures were more prevalent at lower temperatures, the incidence of failure was examined with respect to the month in which fracture occurred. As shown in figure 77, there is no significant increase in the number of failures which occurred during the winter months. Essentially the same number of thermal crack and plate failures occurred between April and September as in the colder months of October to March.

These observations are consistent with the fracture toughness results, which were only slightly sensitive to temperature over the range normally encountered in service.
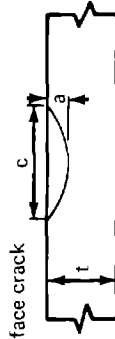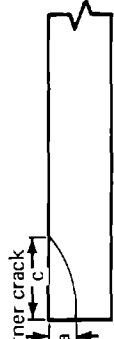
9.5 ESTIMATION OF FAILURE STRESS

As shown in section 9.2, the configurations of cracks initiating brittle fracture in the rim or plate can be grouped into four categories. Stress intensity equations have been developed for these cracks and are given in table 22 (ref. 24, 40, 41, and 42). They are written in terms of the critical stress intensity factor K_{IC} and thus describe the conditions for brittle fracture. Equations (4) and (5) for the surface crack and corner crack, respectively, contain a flaw-shape parameter Q. The value of Q depends on the shape of the crack and the ratio of the applied stress to tensile yield strength, and can be determined from figure 78.

To determine the failure stresses for the fractured wheels, the fracture toughness must be known. In the case of thermally cracked wheels, brittle fracture is believed to occur as a result of residual tensile stresses. The failure conditions can therefore be determined from the K_{IC} value. On the other hand, it is not clear if plate failures are caused by steadily applied thermal and residual stresses, dynamically applied stresses, or a combination of these. It was decided to use the K_{Id} value instead of K_{IC} to allow for any dynamic loading. Based on the previous observation that the failures occurred below the fracture mode transition temperature, the average toughness for 0°-70° F was used (sec. 7.0 and 8.0). The values are listed in table 23. Average yield strength values, used to calculate the flaw-shape parameter Q, are also given in table 23.

These data and the individual critical crack sizes were used to estimate the failure stresses from the appropriate equation listed in table 22. Results are given in appendix B (tables B1-B6) and are summarized in figures 79 and 80. Figure 79 summarizes, in histogram form, the estimates of the residual tensile stresses which initiated wheel failure from thermal cracks. Most failures occurred at stress levels within the range 20-40 ksi, which is well below the yield strength of the rim materials. A few failures which initiated at the tread and rear rim resulted from stresses between 41 and 50 ksi. The highest failure stress was 54 ksi, which occurred in the flange of a class U wheel. These stresses are in good agreement with the residual stresses which have been reported to exist within the rim after drag braking tests (sec. 4.2.3.1).

TABLE 22.—STRESS INTENSITY SOLUTIONS FOR CRACK CONFIGURATIONS EXPERIENCED IN FAILED WHEELS

Crack configuration	Stress intensity solution criteria for brittle fracture	Remarks
Surface crack	$K_{Ic} = 1.1\, \sigma \left(\dfrac{\pi a}{Q}\right)^{1/2}$ (4) (ref. 38)	Solution assumes a/t < 0.5; for deeper cracks, correction factors as required (ref. 39).
Corner crack	$K_{Ic} = (1.12)^2\, \sigma \left(\dfrac{\pi a}{Q}\right)^{1/2}$ (5) (ref. 40)	As above
Through-thickness edge crack	$K_{Ic} = 1.12\, \sigma\, (\pi c)^{1/2}$ (6) (ref. 24)	Solution assumes crack length is small relative to width ℓ; for large c/ℓ, correction factors are required (ref. 24)
Through-thickness crack	$K_{Ic} = \sigma \left(\pi \dfrac{c}{2}\right)^{1/2}$ (7) (ref. 24)	As above

σ = Failure stress

Q = Factor that depends on crack shape and ratio of failure stress/yield strength (fig. M8)

a = Critical crack depth

c = Critical crack length

54

Class	Rim		Plate[a]	
	K_{Ic} (ksi in.$^{1/2}$)	Yield strength (ksi)	K_{Id} (ksi in.$^{1/2}$)	Yield strength (ksi)
A	45	70	NR	NR
B	38	87	NR	NR
C	35	95	30	55
U	35	55	30	55
U1	[b]25	70	NR	NR

[a]NR = not required

[b]Estimated from K_{Id} data reported by D. H. Stone, AAR (private communication)

The histogram for the stresses which caused failure of wheels from thermal cracks at the tread is quite wide and flat and appears to be uninfluenced by the wheel material. Presumably, wide differences in the braking conditions experienced by the individual wheels are responsible for the histogram shape.

A large number of failures initiated at the flange were associated with stresses of 26-30 ksi. This suggests that such stresses may be typical of the conditions developed by a brake block rubbing on the flange at normal freight train speeds.

In most instances the brittle crack, once initiated (by the thermal crack), spread rapidly through both the rim and plate. It appears, therefore, that when the stress developed around a thermal crack is high enough to initiate brittle fracture, the stress gradient in the remainder of the rim is usually sufficient to maintain crack propagation.

A review of the data given in appendix B (tables B1-B3) indicates there is no correlation between the failure stress level and the service life. High stresses existed after a relatively short service life, whereas in some old wheels the stresses were quite low. This can be associated with differences in the braking conditions experienced by the individual wheels.

Estimates of the stress which caused failure of the plate are summarized in figure 80. The radial stresses exceeded 40 ksi in most of the failures which initiated at the front hub fillet. In three instances, failure occurred at stress levels within the range corresponding to the plate yield strength (50-65 ksi). As discussed in section 4.3, stresses of yield strength magnitude can be developed in the front hub fillet as a result of thermal loads or combined mechanical, residual, and thermal stresses. Yield strength magnitude stresses were not recorded for the rear rim fillet, but the sample size was very small. The highest stress which caused failure at this location was 47 ksi.

9.6 BRITTLE CRACK PATHS

Brittle cracks which initiated from thermal cracks followed either of two distinct paths. In one case, the crack extended radially to the hub bore. In the other case, the crack extended radially through the rim but bifurcated in the plate close to the rim fillet, the two cracks formed extending in a tangential direction.

Table 24 summarizes the crack paths according to wheel class. Bifurcation was most apparent in untreated class U wheels, but also occurred in some rim-treated wheels. Cracks in untreated class U1 wheels were primarily nonbifurcated, as were those in the few class A and B wheels. Consequently, there is no obvious correlation between the crack path and the fracture toughness or heat treatment of the wheel material. In addition, there does not appear to be any correlation between the tangential stress in the rim which initiated failure and the crack path. While rapidly moving brittle cracks have an inherent tendency to bifurcate (ref. 43), it is suggested that the crack path is determined primarily by the relative magnitudes of the radial and tangential stresses within the plate, high radial stresses tending to promote bifurcation.

TABLE 24.—INCIDENCE OF BRITTLE CRACK BIFURCATION IN WHEEL PLATES

Class	Number of wheels with bifurcated cracks	Number of wheels with non bifurcated cracks
U	[a]29	8
U1	2	18
A	–	2
B	2	4
C	2	–

[a]In six wheels, the crack deflected to propagate in the tangential direction but did not bifurcate.

Appendix tables B1 and B2 show that in a number of instances, brittle cracks which initiated at the plate fillets were arrested at the rim. This can be associated with the compressive residual stresses developed in the rim during manufacture. In about one third of the plate failures, the brittle crack extended rapidly through both the plate and rim. These are noted as "one stage brittle fractures" in tables B4 and B5. This type of failure was observed in class U wheels in which the rim compressive stresses, and hence degree of fail-safety, are quite low. Several rim-treated wheels also failed in the same way, and this must be attributed to the relief of the residual compressive stresses by braking.

10.0 SIGNIFICANCE OF RESULTS WITH RESPECT TO SERVICE

In this section, the fracture toughness data is used to determine the relationship between the applied stress and critical crack length which will result in brittle fracture of the wheel. The minimum sizes are established for flaws which can cause failure under adverse service conditions. Current inspection procedures are reviewed with respect to those findings. Class U1 wheels are omitted since they are being eliminated from service.

10.1 THERMAL CRACKS

It was concluded earlier (sec. 9.2) that the configuration of a thermal crack usually corresponds to either a corner crack or a surface crack. To establish the conditions under which failure will occur, the following crack shapes are assumed to exist:

1) The ratio of the depth of the corner crack to its length is within the range 0.6-1.0.

2) The ratio of the depth of the surface crack to its length is within the range 0.3-0.5.

These are selected for two reasons. First, for a given crack length and applied stress, the maximum stress intensification is developed in each case by a crack with the shape indicated. Second, cracks having these shapes are frequently experienced in service (sec. 9.2).

Cracks located at the side of the flange may grow through the flange thickness prior to failure; consequently, through-thickness edge cracks must also be considered in the analysis. In this case, however, it appears that through-thickness penetration does not occur until the crack length is approximately 0.3 in. (sec. 9.2).

For cracks having the shapes indicated above, the fracture criteria given in table 22 can be written in the following way:

Surface Crack

$$K_{IC} = 0.9\sigma \ c^{1/2} \tag{8}$$

Corner Crack

$$K_{IC} = 1.45\sigma \ c^{1/2} \tag{9}$$

Through-Thickness Edge Crack

$$K_{IC} = 1.98\sigma \ c^{1/2} \tag{10}$$

where σ is the applied stress and c the critical crack length. Equations (8) and (9) are given in terms of crack length rather than crack depth, as used in table 22, because length is a more meaningful parameter to railroad personnel.

Comparison of equations (8) and (9) shows that for a given applied stress and K_{IC} the critical length of the corner crack is smaller than the surface crack by a factor of 2.6, and thus represents the more hazardous condition.

The relationship between the applied stress and critical crack length has been calculated for these three crack configurations, using the lowest values of K_{IC} likely to be experienced in service. Based on the data given in sections 7.0 and 8.0, the K_{IC} values are:

Class A	40 ksi in.$^{1/2}$
Class B	30 ksi in.$^{1/2}$
Class C	25 ksi in.$^{1/2}$
Class U	25 ksi in.$^{1/2}$

Results are shown in figures 81, 82, and 83 for the different classes of wheel material. They illustrate the decrease in critical crack size with increasing stress level, and the effects of crack configuration and material fracture toughness on the critical crack size. The curves for the through-thickness flange crack are shown only for crack lengths exceeding 0.3 in. for the reasons discussed above.

To estimate the minimum size of crack which must be detected by inspection, the most severe stress conditions likely to be encountered in service must be known. On the basis of results of drag tests (sec. 4.2.3.1) and analysis of service failures (sec. 9.5), it is suggested that a 55-ksi tensile stress is a representative value for the peak of the stress gradients necessary to propagate a crack through the rim. It is recognized that the braking conditions experienced by freight cars, passenger cars, and locomotives are different, but in the absence of pertinent information this peak stress is assumed to be applicable to all vehicles. While much higher stresses can be locally introduced at the tread surface by stop braking (fig. 21), the stress gradient developed is insufficient to propagate the crack completely through the rim. Cleavage-type thermal cracks may, however, form as a result of these local stresses, as discussed later.

The critical crack length at the 55-ksi stress level is shown in table 25. It can be seen that the minimum length which must be detected is 0.1 in. since corner cracks of this size could result in fracture of class U and C wheels. The critical lengths of corner cracks in class A and B wheels, while slightly larger, are less than 0.25 in. The critical length of surface cracks, for example in the center of the tread or rear rim face, is of course larger, being within the range 0.25-0.65 in. for all wheel materials.

58

TABLE 25.—CRITICAL SIZE OF THERMAL CRACKS AT AN APPLIED STRESS OF 55 KSI

Class	Critical crack length (in.)	
	Corner crack	Surface crack
A	0.25	0.65
B	0.14	0.36
C	0.10	0.26
U	0.10	0.26

The question which must now be answered is whether cracks of this size can be detected in service. Cracks of 0.1-0.25 in. in length might be observed with careful visual inspection during depot examination, but could also be quite easily missed. In other words, the level of confidence which can be placed on visually detecting such cracks is low.

Nondestructive testing (NDT) techniques are also limited in their ability to detect small cracks. Packman et al. (ref. 44) evaluated the sensitivity of several NDT techniques, sensitivity being defined as the ratio of the number of cracks detected to the actual number of cracks present. Results of their studies, which were conducted on high strength steel cylinders containing fatigue surface cracks of various size, are shown in figure 84. It can be seen that the sensitivity decreases with decreasing crack size. Shear wave ultrasonic inspection was 100% sensitive for cracks exceeding 0.2 in. in length but was only 50% sensitive for 0.1-in.-long cracks. The minimum crack sizes that could be detected with 100% sensitivity by magnetic particle and penetrant were 0.3 and 0.35 in., respectively.

Consequently, these data indicate that the 0.1-0.2 in. long corner cracks which could cause wheel failure in all but class A wheels cannot be reliably detected by any of these inspection procedures.

Ultrasonics should be effective in detecting surface cracks of critical size in all wheel materials. Similarly, magnetic particle and penetrant should be effective in detecting critical surface cracks in class A and B wheels but not in class C or U wheels. In these instances, however, the minimum detectable flaw size is very close to the critical flaw size. Frequent inspection would therefore be required to ensure that a crack which is below detectable size does not grow to critical size prior to detection. Ultrasonic testing procedures aimed specifically at detecting cracks in wheels have been developed. However, it has not been established whether the crack detection sensitivity of these methods is better (or worse) than that of the shear wave technique.

Figures 81-83 indicate that at low tensile stress levels large flaws (e.g., 2 in. long) will not cause failure. This explains why severely thermally cracked wheels can sometimes be removed from service before wheel failure has occurred. It can also be inferred from these figures that small cracks can be safely tolerated at low stress levels. However, there is no assurance that these small cracks will not propagate rapidly to critical length, or the rim

stresses increase to the failure level, as a result of braking loads imposed during the next journey. Consequently, there is no alternative but to remove thermally cracked wheels from service as required by AAR rules.

The rate at which thermal cracks grow must be known in order to specify inspection intervals. Unfortunately, insufficient information is available for this to be done in the case of fatigue-type thermal cracks. It can be said, however, that the growth rate will depend on the material, the nature of the thermal cycles, and crack tip stress intensity. These, in turn, will be controlled by the magnitude, duration, and frequency of the braking loads experienced by the wheel.

In the case of cleavage-type thermal cracks, it was noted previously (sec. 2.1.1) that they are arrested brittle fractures, and as such, grow in a fraction of a second. This type of crack will be formed when the local residual tensile stress at the tread, and size of a surface crack which has formed previously by thermal fatigue, are sufficient for the stress intensity at the crack tip to reach K_{IC}. Figure 21 shows that stresses of yield strength magnitude can be reached at the tread surface under severe stop braking. The critical surface crack lengths at this stress level have been calculated from equation (8) using the K_{IC} values given earlier in this section and are shown in table 26. They are of the same order of size as the corner cracks which can initiate complete failure of the wheel. Thus, cleavage-type thermal cracks can form instantaneously from nondetectable cracks under some braking conditions. Depending on the residual stress gradients within the bulk of the rim, such cracks may result in spontaneous brittle fracture of the wheel.

TABLE 26.–CRITICAL LENGTH OF SURFACE CRACKS FOR FRACTURE AT STRESSES EQUAL TO YIELD STRENGTH

Class	Typical yield strength of rim (ksi)	Critical crack length (in.)
A	70	0.40
B	87	0.15
C	95	0.09
U	55	0.25

All the above discussion is applicable to fully heat treated wheels of equivalent class.

10.2 PLATE CRACKS

Brittle fracture of the wheel plate can result from the growth of fatigue cracks in the hub or plate fillets. As noted in section 9.5, service failures occur from either small surface cracks which have not penetrated the plate thickness, or large through-the-thickness cracks.

Data presented in section 9.5 showed that depth/length of surface cracks experienced in service is about 1/3. For this crack shape, the relationship between applied stress and critical crack length (c) is given by equation (8):

$$K_{IC} = 0.9\sigma\, c^{1/2}$$

It should be noted that this equation is applicable only to cracks which do not penetrate deeper than about half the plate thickness.

For through-the-thickness cracks, the failure criteria can be estimated from equation (3):

$$K_{IC} = 1.25\sigma\, c^{1/2} \tag{11}$$

As previously discussed, there is some uncertainty as to whether K_{IC} or K_{Id} should be used to determine the critical crack length. To provide the most conservative estimate, it has been assumed that dynamic loading plays a dominant role in initiating brittle fracture of the plate, and K_{Id} has accordingly been used.

From the data given in sections 8.0 and 9.0, the following values for K_{Id} are considered to be representative of the lowest values likely to be experienced in service:

Class A	35 ksi in.$^{1/2}$
Class B	25 ksi in.$^{1/2}$
Class C	20 ksi in.$^{1/2}$
Class U	20 ksi in.$^{1/2}$

The above values were used to determine the relationships between applied stress and critical crack length. Results are shown in figures 85 and 86 for the surface crack and through-thickness crack cases, respectively. Figure 86 should be used for cracks longer than 2 in. because they could be on the verge of breaking through the thickness.

It was shown earlier that stresses of yield strength magnitude can be experienced in the rim fillets (secs. 4.3 and 9.5). Accordingly, the minimum crack size which will cause failure must be determined at this stress level. The typical yield strength of the plate in rim-treated or untreated wheels is about 55 ksi, and the critical crack lengths corresponding to this stress level in figure 85 are:

Class A	0.50 in.
Class B	0.25 in.
Class C	0.16 in.
Class U	0.16 in.

61

Cracks of this size will not be detected by visual inspection, and in view of the limitations of NDT techniques, only the class A and B wheels could be inspected by ultrasonics with a high level of confidence of finding potentially critical cracks.

In fact, it has been shown that cracks up to 8-10 in. long can be missed during visual walk-around inspection of structures (ref. 45). Indeed it was noted in section 9.2 that plate cracks exceeding 10 in. long have escaped detection in service. Figure 86 indicates that the stresses required to initiate failure in the presence of cracks of this order of size are extremely low, being about 5 ksi for freight car wheels. Stresses of this magnitude are quite easily developed in service by lateral loading or moderate drag braking. It must be concluded, therefore, that the wheels are very vulnerable to failure by the time a fatigue crack has grown to a size where there is some possibility of visually detecting it.

One other type of defect must be considered with respect to plate failure. It was noted in section 2.2 that machining tears and other surface defects have been reported to act as initiation sites for brittle fracture. Assuming that these defects have sharp tips, the conditions for brittle fracture are given by equation (4) (table 22). For stresses of yield-strength magnitude (i.e., 55 ksi), and long, shallow flaws (depth/length <0.1), the flaw-shape parameter Q has a value of 0.79 (fig. 77). Using the K_{Id} values given above, the critical flaw depths at 55 ksi are:

Class A	0.084 in.
Class B	0.043 in.
Class C	0.028 in.
Class U	0.028 in.

These small critical defect depths illustrate the necessity to control the finish of the wheel plates. It is pertinent to note that failure of the class C wheel in the Laurel accident can be explained on the basis of the above, since machining tears up to 0.035 in. deep were present at the hub fillet.

While figures 85 and 86 are applicable to fully heat-treated wheels, it is not clear if significantly higher maximum stress levels can be experienced because of their higher yield strength relative to rim-treated wheels.

Data on the rate of growth of fatigue cracks in plate materials are currently being obtained by Boeing. This information and analysis of its significance with respect to service will be given in a future report.

11.0 CONCLUSIONS

The results of this study have shown that the fracture toughness K_{IC} of railroad wheels is controlled primarily by their carbon content. Classes U, C, and CE wheels have the lowest toughness and class A the highest. Similar fracture toughness values were recorded for cast and wrought materials of the same class. There was no significant difference in the toughness of the rim and plate regions of wheels which were untreated, rim treated, and fully quenched.

The fracture toughness was essentially constant over the range of temperature which can be encountered in service. Impact loading reduced the toughness of some wheels but had little effect on others. This effect of loading rate may depend on the microstructural characteristics of the wheel material.

Review of a number of wheels which had fractured in service as a result of thermal crack formation showed that in most cases the critical length of tread cracks was 1-3 in., and 0.5-1 in. for flange cracks. The stresses which caused these failures are considerably less than the yield strength of the material, and they are consistent with the residual tangential stresses which can develop in service as a result of drag braking. In some instances, however, much smaller cracks initiated brittle failure of the wheel. It has been estimated that in the presence of residual tensile stresses of 55 ksi, which could be developed by severe drag braking, the critical crack length is 0.1 in. for class U and class C (or CE) wheels, and less than 0.25 in. for the class A and class B wheels.

An analysis of wheels which fractured from fatigue cracks at the plate fillets showed that stresses of yield-strength magnitude can be developed at these critical locations. Under these circumstances, the critical crack length for plate failure is estimated to be 0.16 in. for class U and class C wheels, and 0.25 and 0.50 for classes B and A, respectively. Furthermore, machining tears, or other surface discontinuities, which exceed 0.028 in. in depth could result in wheel failure.

Available data indicate that cracks less than 0.2 in. in length cannot be detected with 100% confidence by nondestructive testing. It must be concluded therefore that under some service conditions wheel failure can occur from cracks which cannot be reliably detected by currently available NDT techniques.

REFERENCES

1. *Railroad Accident Report: Southern Railway Company Train 154 Derailment With Fire and Explosion, January 25, 1969,* National Technical Information Service report PB 190208, 1969.

2. J. M. Wandrisco and F. J. Dewez, "Service Defects in Treads of Railroad Wheels During Service," ASME paper 60-RR-1, 1960.

3. N. A. Berg and W. J. Kucera, "A Review of Thermal Damage in Railroad Wheels," paper presented at Air Brake Association Annual Meeting, Chicago, 1970.

4. T. Hirooka et al., "Residual Stresses in the Rim of a Railroad Solid Wheel Due to on Tread Drag Braking and Their Effect on Wheel Failure," *Proc. Fourth International Wheelset Congress,* Paris, 1972, p. 91.

5. J. L. van Swaay, "The Mechanism of Thermal Cracking in Railway Wheels," *Proc. Third International Wheelset Congress,* Sheffield, 1969.

6. G. W. J. Waldron and S. Wise, "Service Failures and Their Implications for British Railways," *The Metallurgist and Materials Technologist,* vol. 5, January 1973, p. 15.

7. G. R. Weaver et al., "Investigation of the Thermal Capacity of Railroad Wheels Using COBRA Brake Shoes," *Trans. ASME,* 92, B, 1970, p. 366.

8. H. R. Wetenkamp, O. M. Sidebottom, and H. R. Schrader, "The Effect of Brake Shoe Action on Thermal Cracking and on Failure of Wrought Steel Railway Car Axles," University of Illinois, Experimental Engineering Station Bulletin 387, 1950.

9. P. Ravenet and P. Gauthier, "The SNCF's Decision in Favor of Solid Wheels of Non Alloy Surface Treated Steel," *Proc. First International Wheelset Congress,* Bergamo, 1963, p. 229.

10. P. Fox and G. Hewitt, "Wheel and Tyre Development of British Railways," *Proc. Fourth International Wheelset Congress,* Paris, 2, 1972, p. 67.

11. J. B. Lee and J. D. Murray, "Experimental Work on Segments—Improved Steels for Wheels and Tyres," *Proc. Fourth International Wheelset Congress,* Paris, 1, 1972, p. 37.

12. P. M. Gardner and A. T. Westbrook, "Some Metallurgical Factors Associated With the Thermal Cracking and Shelling Encountered With Wrought Steel Wheels," *Proc. Third International Wheelset Congress,* Sheffield, 1969.

13. M. Castagna et al., "Contribution of Fracture Mechanics to the Search for Optimal Quality in Monobloc Wheels," *Proc. Fourth International Wheelset Congress,* Paris, 3, 1972, p. 108.

14. B. J. Eck, "The Effect of Residual Stresses on Wheel Failure," unpublished report, The Griffin Wheel Company.

15. M. Yontar, "A Modern Approach to Evaluating Operating Plate Stresses in 28 Inch Reversed Disk Wrought Steel Wheels on Transit Cars," *Proc. Third International Congress on Wheelsets,* Sheffield, 1969.

16. J. P. Bruner, G. N. Benjamin, and D. M. Bench, "Analysis of Residual, Thermal, and Loading Stresses in a B33 Wheel and Their Relationship to Fatigue Damage," *Trans. ASME,* 89, B, 1967, p. 249.

17. J. P. Bruner et al., "Effect of Design Variation on Service Stresses in Railroad Wheels," *Trans. ASME,* 90, B. 1968, p. 187 (discussion p. 746).

18. J. P. Bruner et al., "Effect of Operating Conditions on Wrought Steel Wheel Performance," *Proc. Third International Wheelset Congress,* 1969.

19. *Report of the Wheels, Axles, Bearings and Lubrication,* Mechanical Division, Association of American Railroads (published annually).

20. *Accident Bulletin, Summary and Analysis of Accidents on Railroads in the United States.* Federal Railroad Administration, Department of Transportation (published annually).

21. *Fracture Toughness Testing and Its Applications,* ASTM, STP 381, 1965.

22. R. A. Davis and W. E. Quist, "Fracture Toughness," *Materials in Design Engineering,* Nov. 1965, p. 91.

23. A. S. Tetleman and A. J. McEvily, *Fracture of Structural Materials,* John Wiley & Sons, Inc., 1967.

24. P. C. Paris and G. C. Sih, *"Stress Analysis of Cracks"* in *Fracture Toughness Testing and Its Applications,* ASTM, STP 381, 1965, p. 30.

25. H. Tada, P. C. Paris, and G. R. Irwin, *The Stress Analysis of Cracks Handbook,* Del Research Corporation, 1973.

26. W. F. Brown and J. E. Strawley, "Plane Strain Toughness Testing of High Strength Metallic Materials," ASTM, STP 410, 1966.

27. W. Bröhl and N. Brinkman, "Quenching and Tempering Treads of Solid Wheels: Significance in Rail Traffic," *Proc. Third International Wheelset Congress,* Sheffield, 1969.

28. J. LeClerc and C. Camut, "Tests on Rim Treated Wrought Wheels, Residual Stresses and Microstructures of New Wheels," *Proc. Third International Wheelset Congress,* Sheffield, 1969.

29. *Investigation of Service Stresses Imposed on Wheels Under Diesel Locomotives,* Association of American Railroads report MR-235, 1955.

30. H. C. Meacham and D. R. Ahlbeck, "A Computer Study of Dynamic Loads Caused by Vehicle Track Interaction," *Trans. ASME,* 91, B, 1969, p. 808.

31. W. S. Lovelace, "Study of Rim Stresses Resulting from Static Loads on Different 36 Inch Railroad Wheel Designs," ASME paper 71-RR-4, 1971.

32. G. E. Novak and B. J. Eck, "Asymmetrical Wheel Stresses Caused by Thermal and Mechanical Service Loads," ASME paper 72-WA/RT-13, 1972.

33. H. R. Wetenkamp, *Theoretical Thermal Stresses Developed in Railway Car Wheels by the Drag Test,* University of Illinois, T and Am report 336, 1970.

34. G. E. Novak, B. J. Eck, and A. W. Farrell, "Cast Steel Wheels—Present and Future," *Proc. Third International Congress on Wheelsets,* Sheffield, 1969.

35. *NOAA Climatological Data, National Summary,* Dept. of Commerce, 21, 13, 1970.

36. T. Gladman and J. H. Woodhead, "The Accuracy of Point Counting in Metallographic Investigation," *J. Iron and Steel Inst.,* 194, 1960, p. 189.

37. J. Kies et al., "Fracture Testing of Weldments" in *Fracture Toughness Testing and Its Application,* ASTM, STP 381, 1965, p. 328.

38. T. Gladman, I. D. McIvor, and F. B. Pickering, "Some Aspects of the Structure-Property Relationship in High Carbon Ferrite-Pearlite Steels," *J. Iron and Steel Inst.,* 210, 1972, p. 916.

39. D. F. Cannon, E. F. Walker, and R. R. Barr, "The Fracture Toughness of Rail Steels," paper presented at Iron and Steel Institute Meeting on Rail Steels, London, 1972.

40. C. F. Tiffany and J. N. Masters, "Applied Fracture Mechanics" in *Fracture Toughness Testing and Its Applications,* ASTM, STP 381, 1965, p. 249.

41. R. C. Shah and A. S. Kobayashi, "On the Surface Flaw Problem," *Proc. of the ComCAM Symposium on the Surface Flaw,* ASME, 1973.

42. A. F. Liu, "Stress Intensity Factor for a Corner Flaw," *Eng. Fract. Mech.,* 4, 1972, p. 175.

43. A. B. J. Clark and G. R. Irwin, "Crack Propagation Behavior," *Exp. Mech.,* 23, 1966, p. 321.

44. P. F. Packman et al., "The Applicability of a Fracture Mechanics—Non Destructive Design Criterion for Aerospace Structures," *Metals Eng. Quarterly,* Aug. 1969, p. 52.

45. J. C. Eckvall et al., "Preliminary Design of Aircraft Structure to Meet Structural Integrity Requirements," AIAA paper 73-374, 1973.
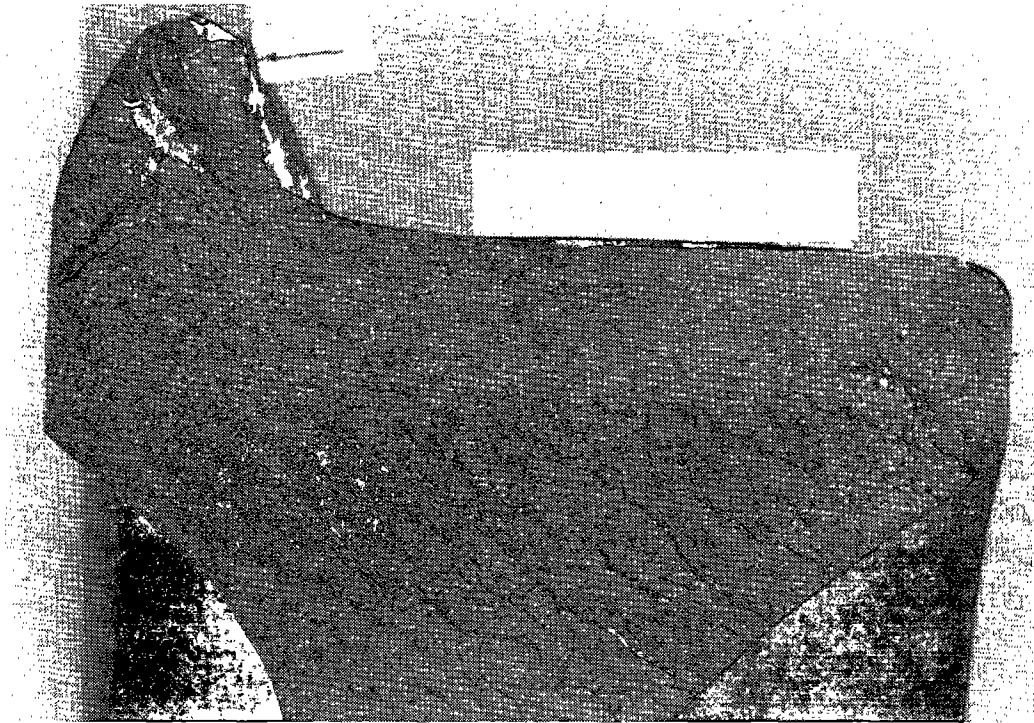
FIGURE 1.—THERMAL CRACK GROWTH BY A FATIGUE
MECHANISM IN A CLASS-U WHEEL
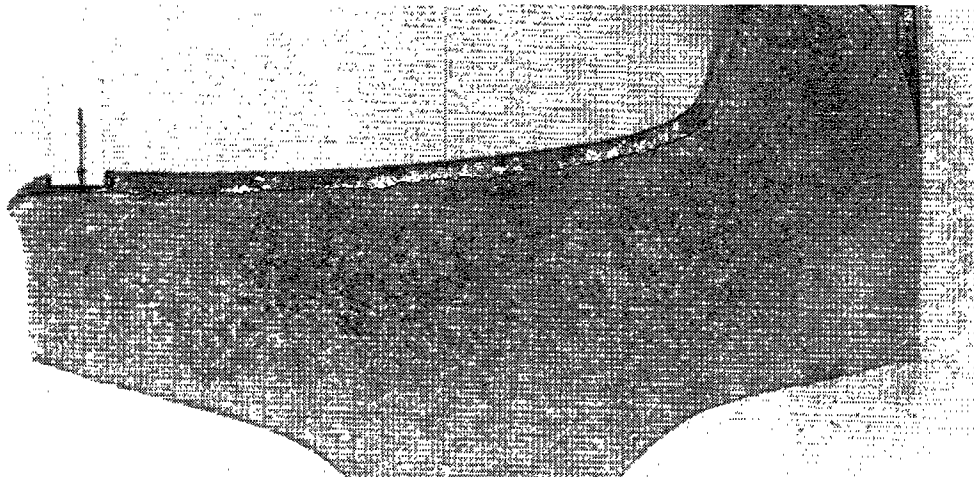
FIGURE 2.—THERMAL CRACK GROWTH BY A CLEAVAGE
MECHANISM IN A CLASS-U WHEEL

FIGURE 3.—THERMAL CRACK GROWTH BY ALTERNATE CLEAVAGE AND THERMAL FATIGUE MECHANISMS IN A CLASS-U1 WHEEL
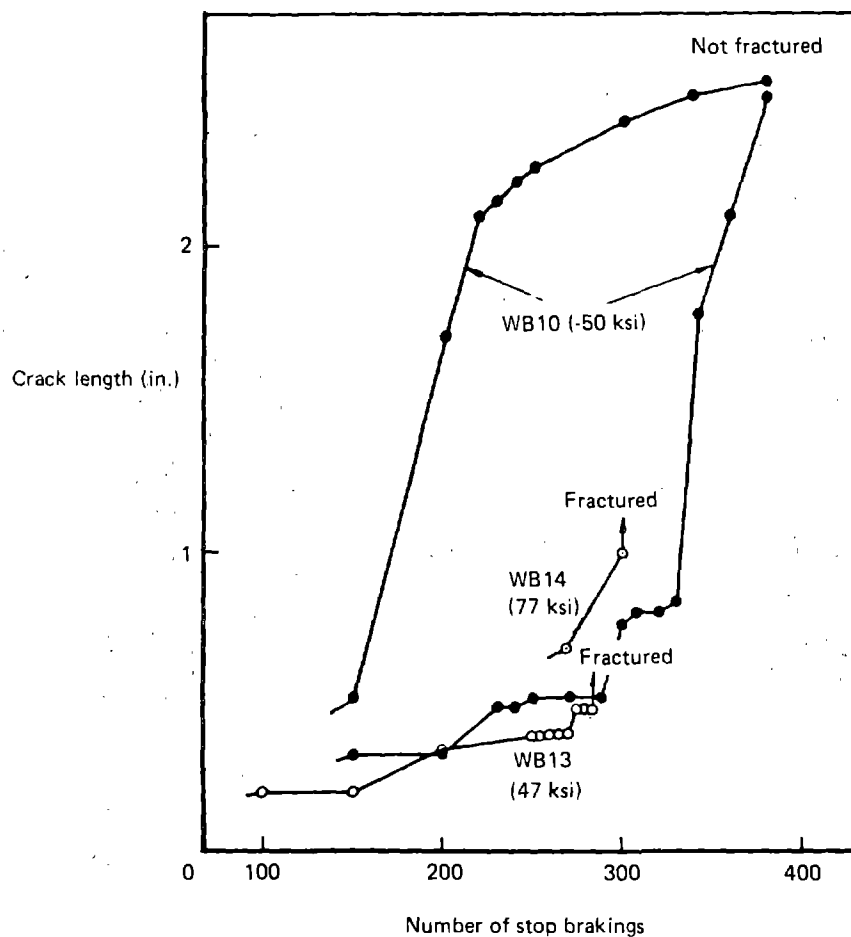
FIGURE 4.—EFFECT OF NUMBER OF STOP BRAKINGS ON THERMAL CRACK
GROWTH IN THREE WHEELS WHICH HAD BEEN PREVIOUSLY
DRAG BRAKED TO PRODUCE THE RESIDUAL STRESSES SHOWN
IN PARENTHESES (RESIDUAL STRESS MEASURED ON FRONT
RIM 0.4 IN. BELOW TREAD CORNER).
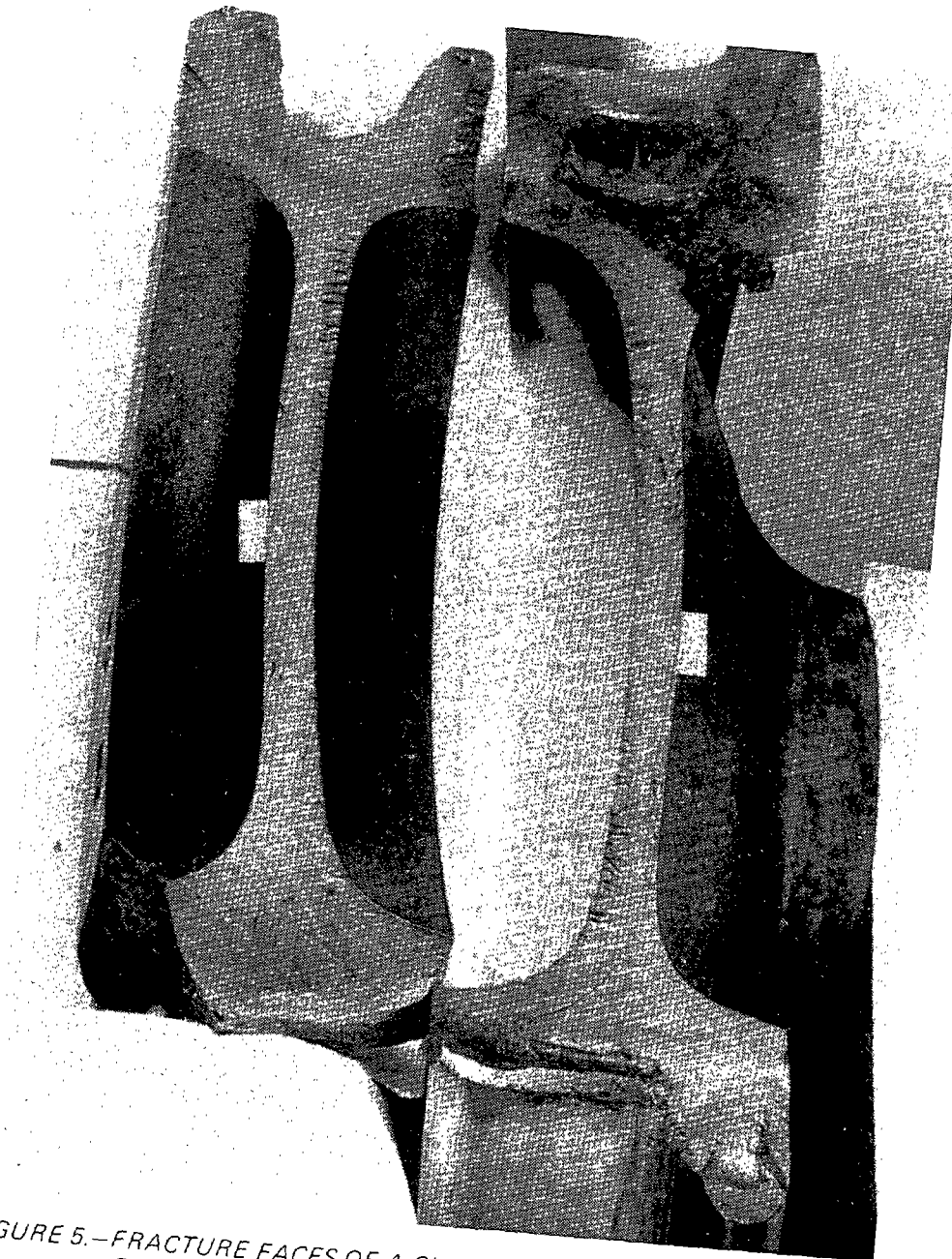
FIGURE 5.—FRACTURE FACES OF A CLASS-C WHEEL THAT FAILED FROM A
FATIGUE CRACK AT THE BACK RIM FILLET
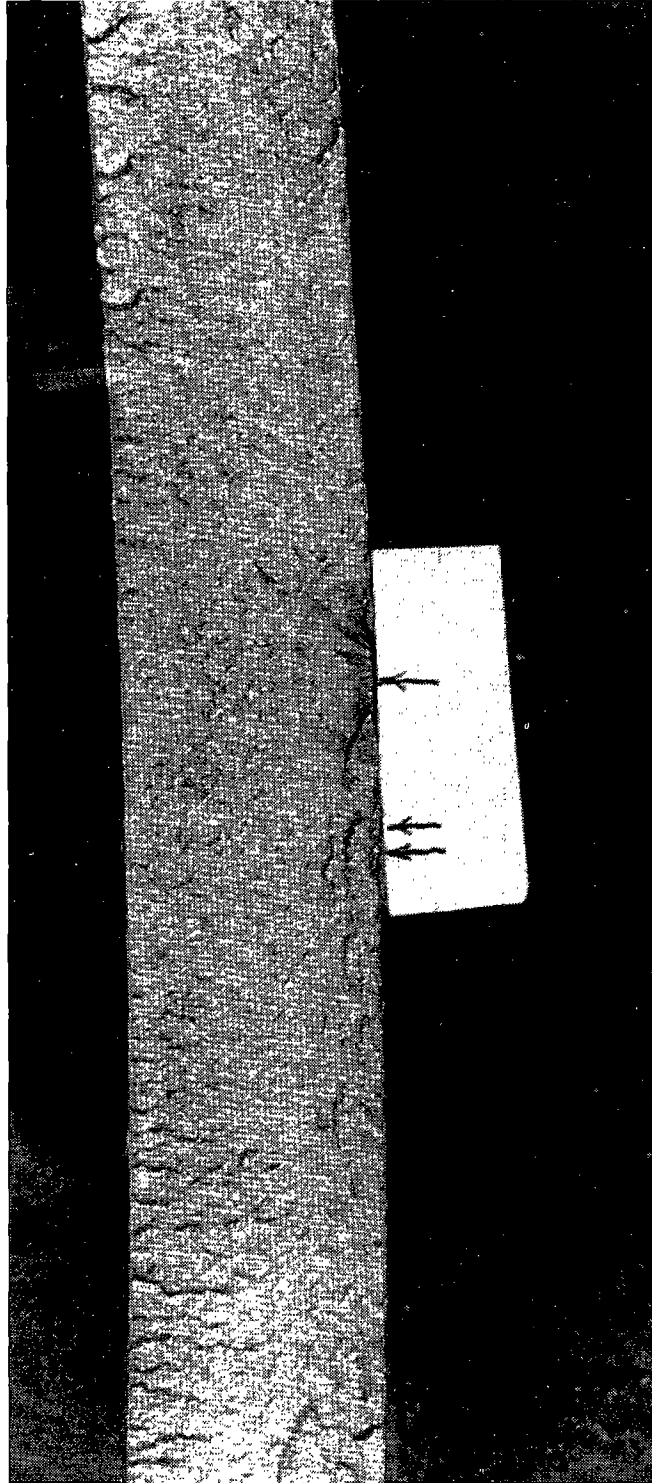
FIGURE 6.—CLOSEUP VIEW OF FATIGUE ORIGIN AREA SHOWN IN FIGURE 5
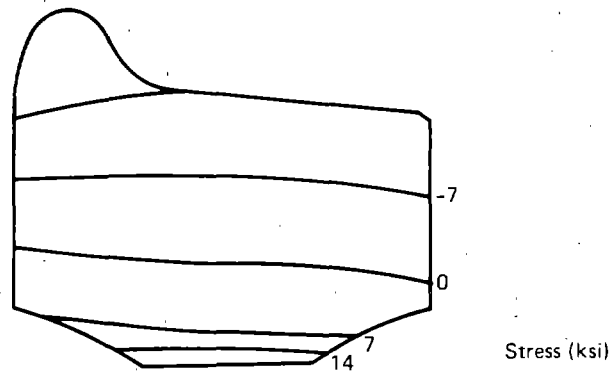
FIGURE 7.—STRESS DISTRIBUTION IN THE RIM OF A RIM-TREATED WHEEL CONTAINING
0.6%—0.75% CARBON (AFTER HIROOKA ET AL., REF. 4)
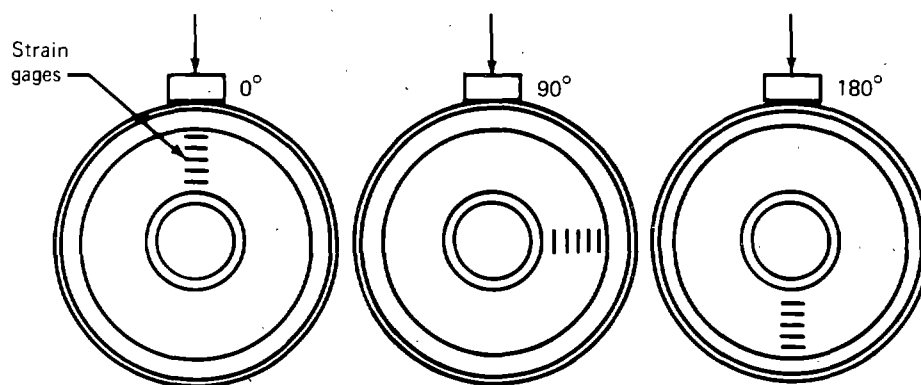
FIGURE 8.—VERTICAL LOADING POSITIONS FOR B33 WHEEL
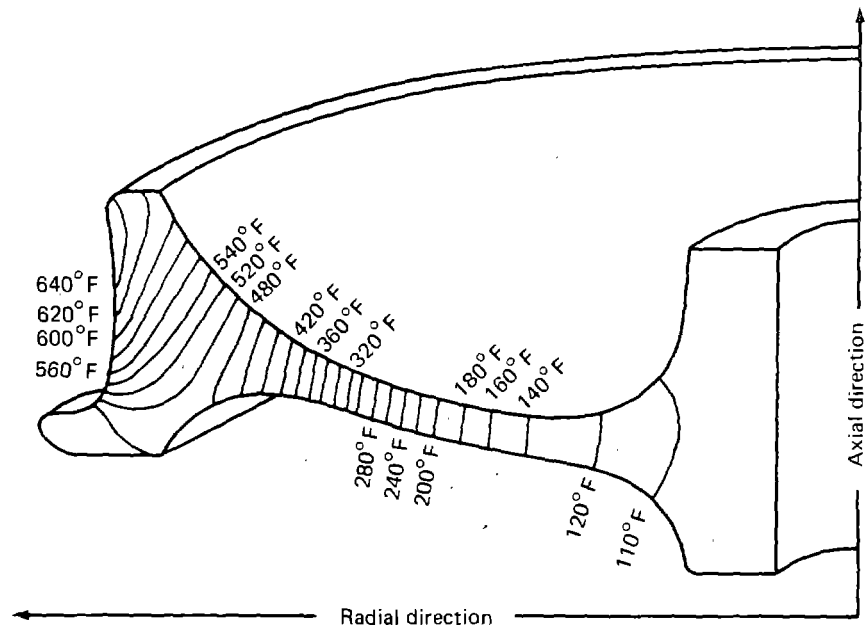
FIGURE 9.—TEMPERATURE DISTRIBUTION IN A WORN 36-IN. WHEEL AFTER 20 MIN OF
CYCLIC DRAG BRAKE APPLICATION; TRAIN VELOCITY: 21 MPH (AFTER
NOVAK AND ECK, REF. 32)
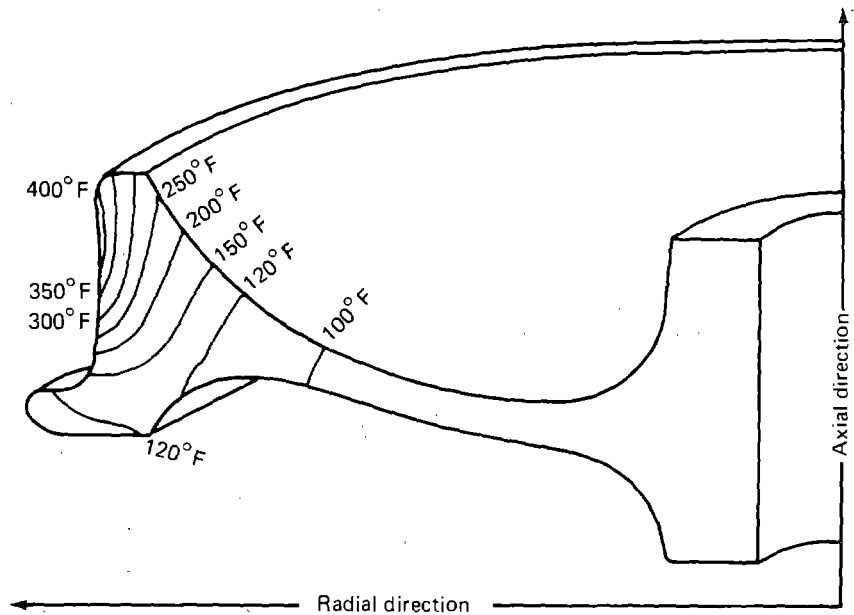
FIGURE 10.—TEMPERATURE DISTRIBUTION IN A WORN 36-IN. WHEEL 65 SEC AFTER
BRAKE APPLICATION; INITIAL TRAIN SPEED: 60 MPH; STOPPING TIME:
2 MIN (AFTER NOVAK AND ECK, REF. 32)
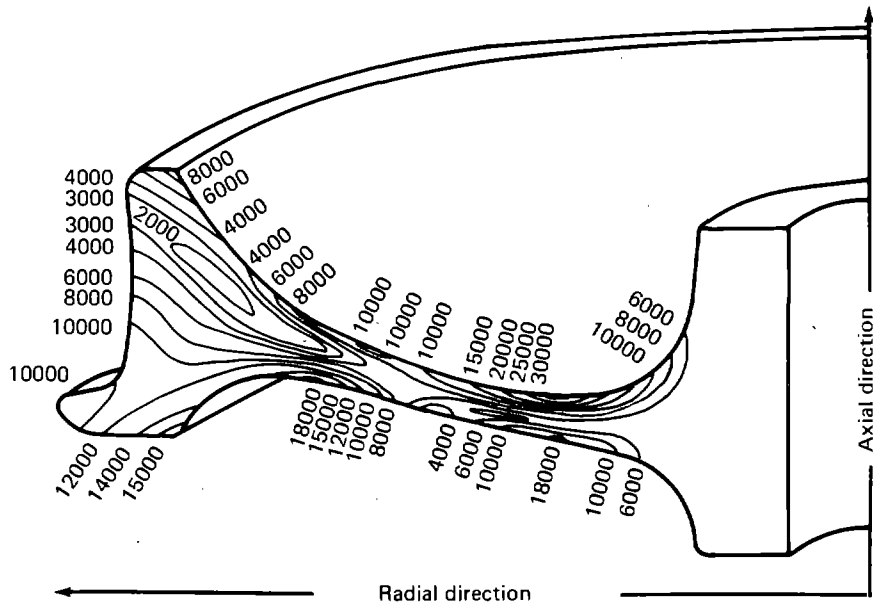
FIGURE 11.—ISOBAR MAP OF OCTAHEDRAL SHEAR STRESSES (SII) AFTER 20 MIN OF CYCLIC DRAG BRAKE APPLICATION; TRAIN VELOCITY: 21 MPH (AFTER NOVAK AND ECK, REF. 32)
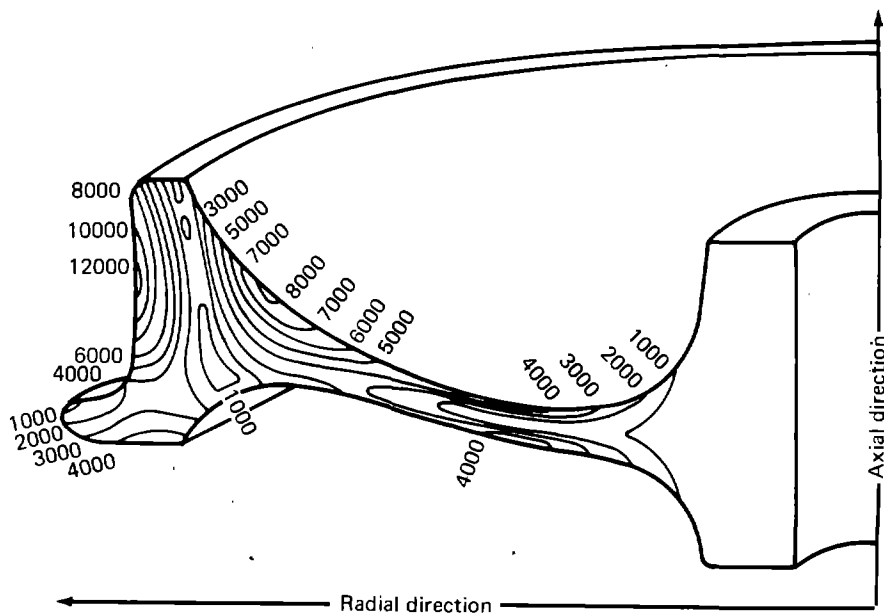
FIGURE 12.—ISOBAR MAP OF OCTAHEDRAL SHEAR STRESSES (PSI) AFTER 65 SEC OF EMERGENCY BRAKE APPLICATION (AFTER NOVAK AND ECK, REF. 32)

76
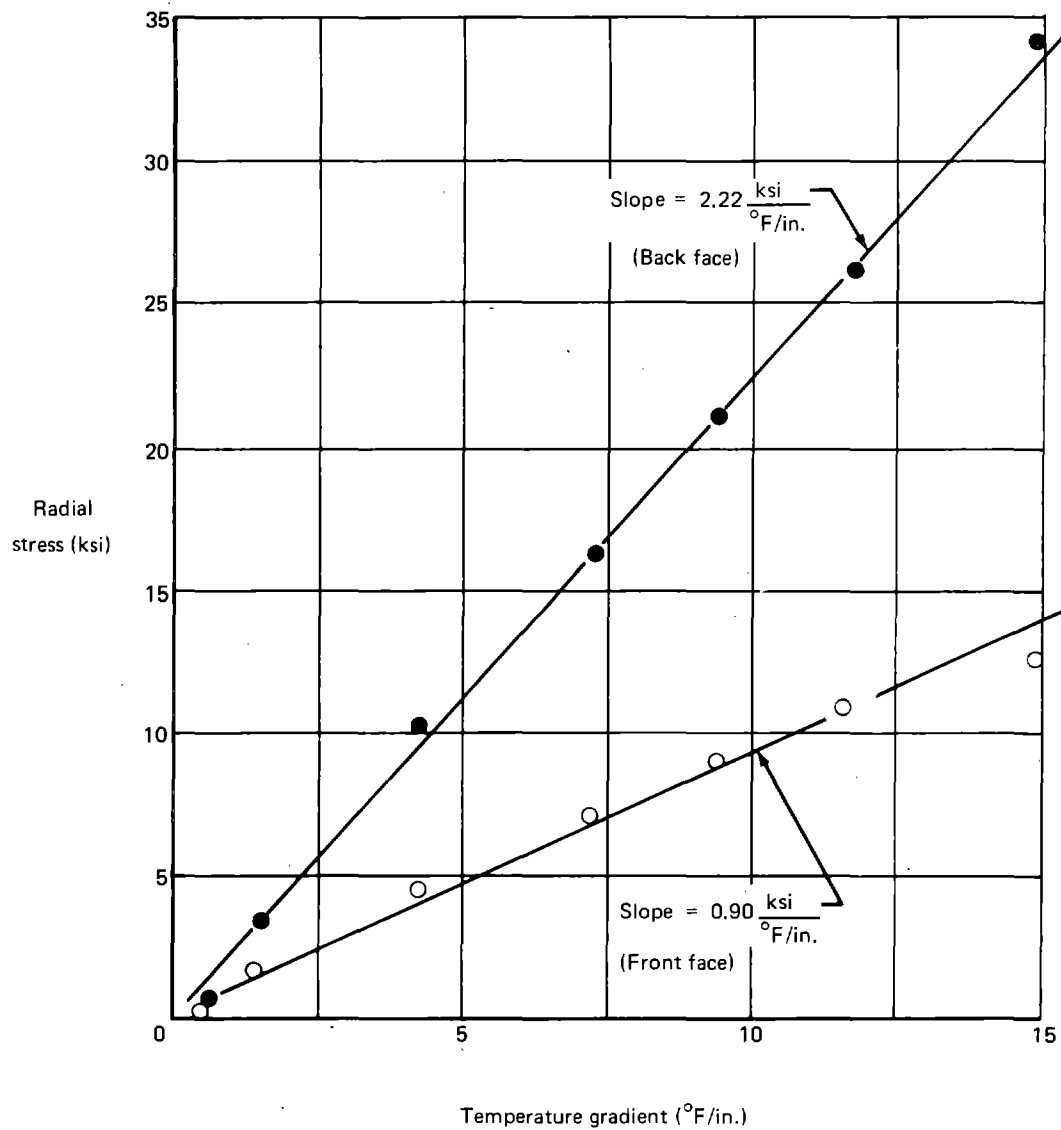
FIGURE 13.—RELATIONSHIP BETWEEN WHEEL HUB FILLET THERMAL STRESS AND
TREAD-TO-HUB TEMPERATURE GRADIENT (AFTER YONTAR, REF. 15)

USED WHEEL

Compression (ksi) Tension
-42.6 -28.4 -14.2 0 +14.2 +28.4

Compression (ksi) Tension
-28.4 -14.2 0 +14.2 +28.6

NEW WHEEL

Compression (ksi) Tension
-28.6 -14.6 0 +14.6 +28.6

Compression (ksi) Tension
-28.6 -14.6 0 +14.6 +28.6
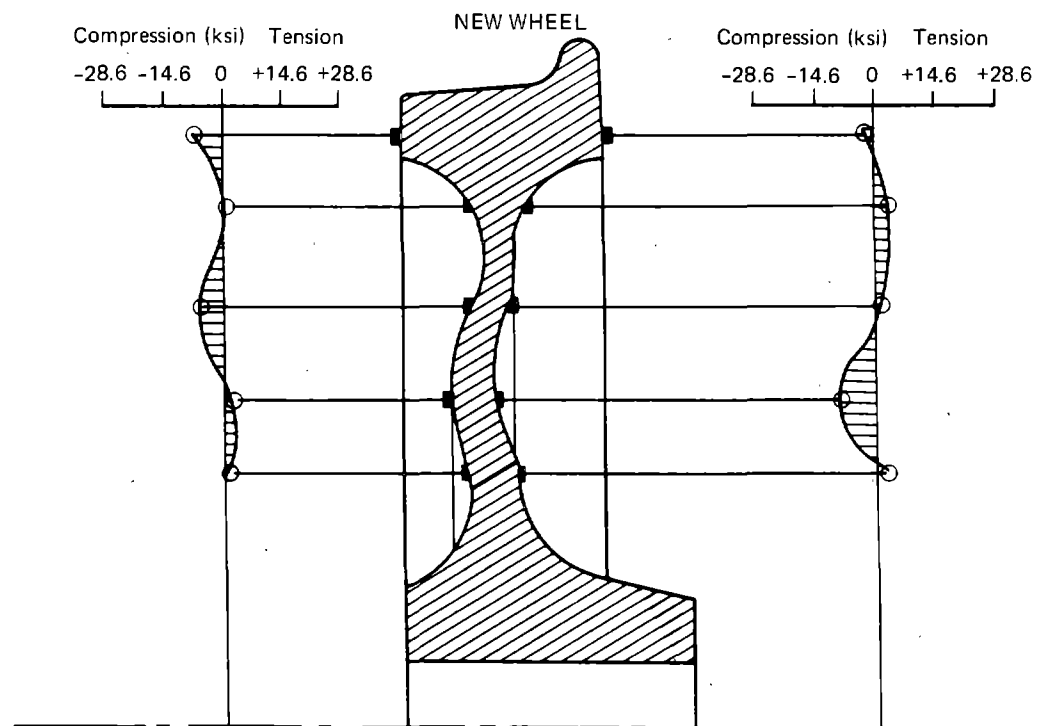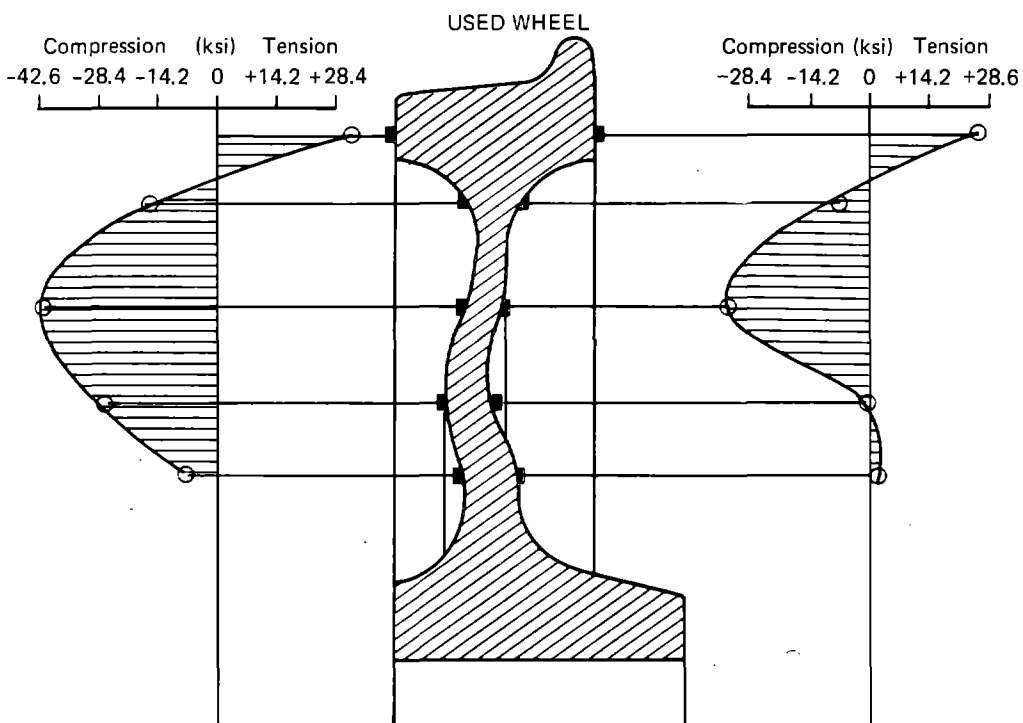
FIGURE 14.—COMPARISON OF RESIDUAL STRESSES IN NEW AND USED WHEELS
(AFTER CASTAGNA ET AL., REF. 13)
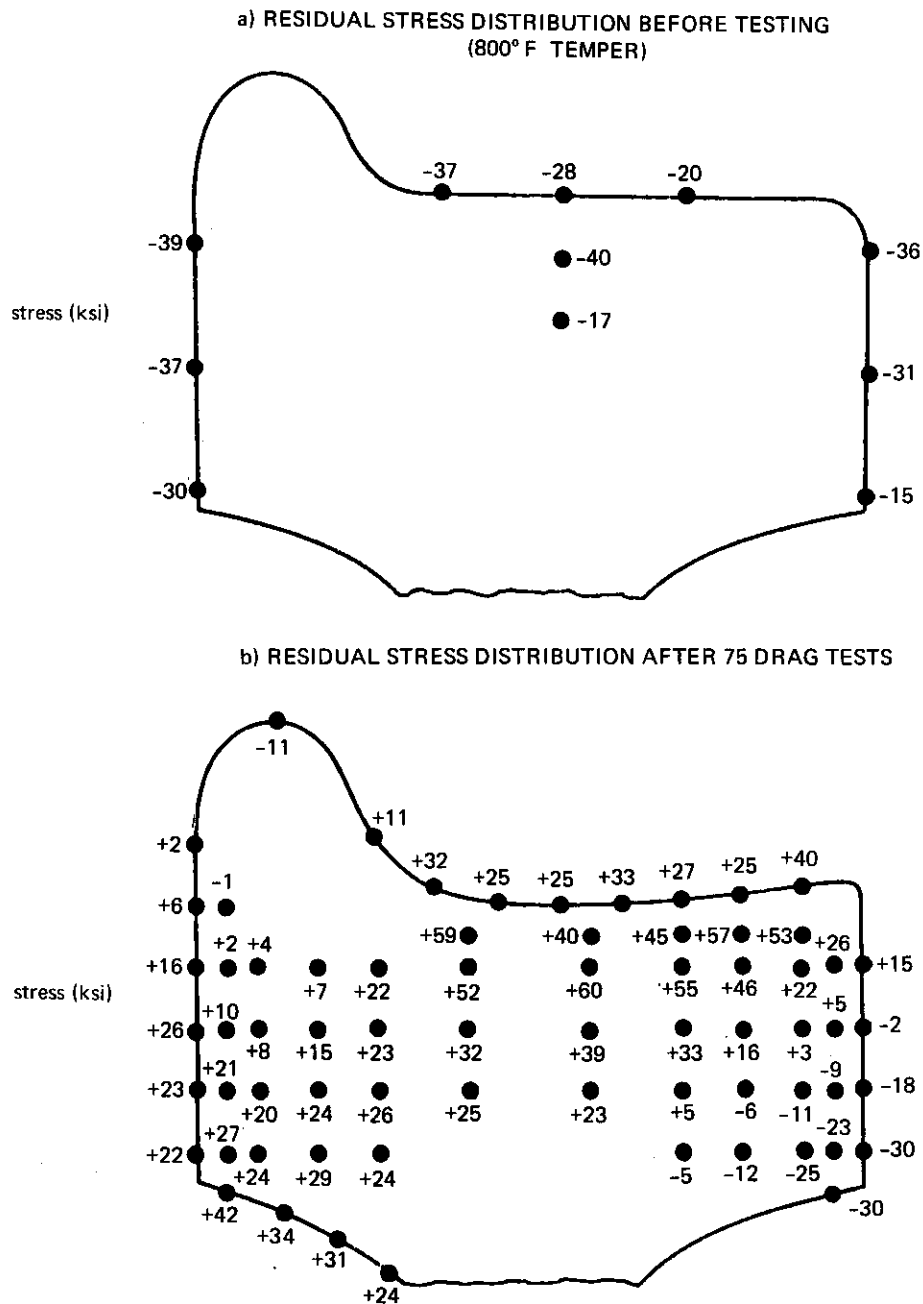
FIGURE 15.—EFFECT OF DRAG TESTING ON RESIDUAL TANGENTIAL STRESS
DISTRIBUTION IN RIM OF RIM-QUENCHED WHEELS (CLASS C)
(AFTER WETENKAMP ET AL., REF. 8)
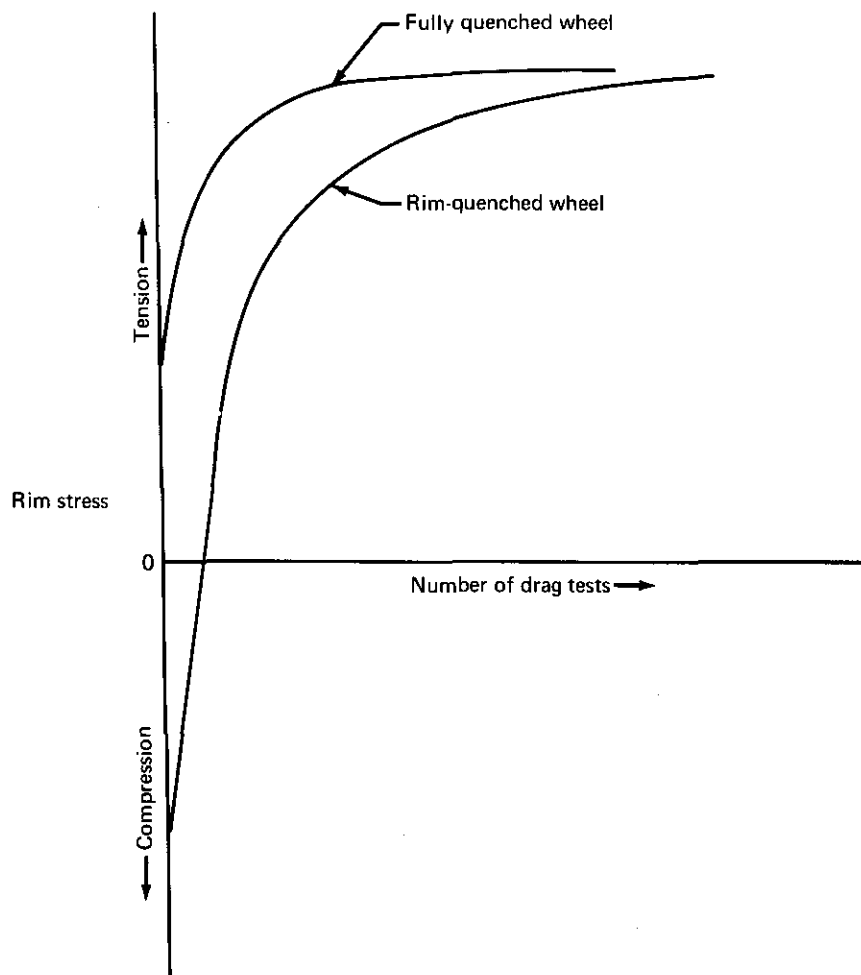
FIGURE 16.—SCHEMATIC REPRESENTATION OF BUILDUP OF RESIDUAL STRESS IN
RIM BY DRAG BRAKING

A-TYPE WHEEL

B-TYPE WHEEL

Unit: mm
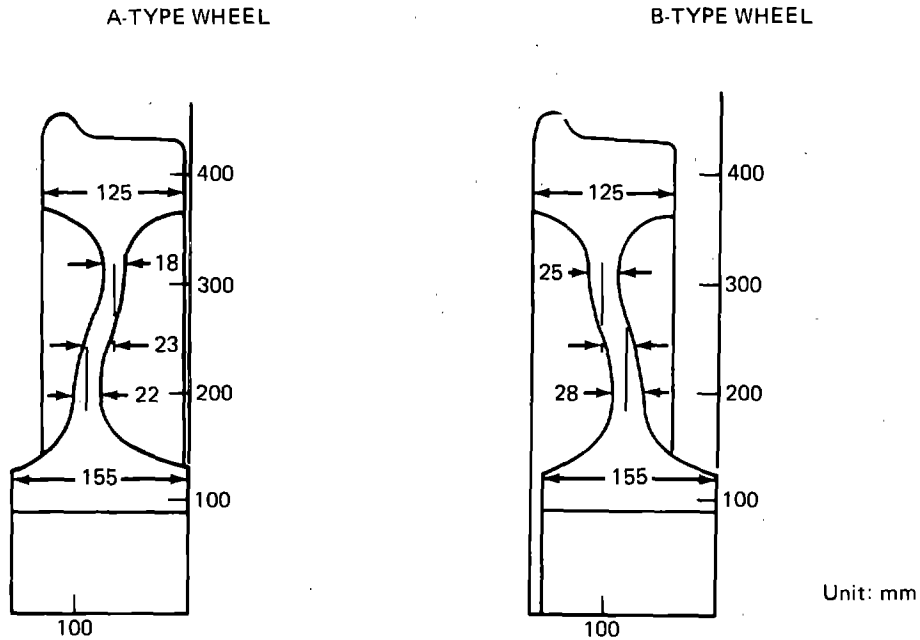
FIGURE 17.—CONFIGURATION OF WHEELS TESTED BY HIROOKA ET AL. (REF. 4)

A-TYPE WHEEL

B-TYPE WHEEL
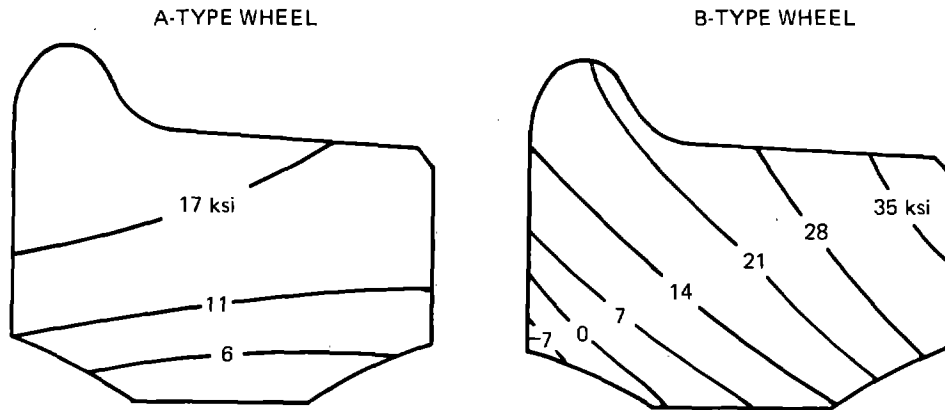
FIGURE 18.—RESIDUAL TANGENTIAL STRESSES DEVELOPED IN A AND B WHEELS BY
DRAG BRAKING (TESTS CONDUCTED AT 50 MPH WITH 660 LB BRAKING
PRESSURE APPLIED FOR 50 SEC AND RELEASED FOR 10 SEC IN EACH
MINUTE; TESTS CONTINUED UNTIL TEMPERATURE REACHED A MAXIMUM)
(AFTER HIROOKA ET AL., REF. 4)

81

a) AS MANUFACTURED   b) 330 LB   c) 440 LB

d) 550 LB   e) 770 LB

Stress—ksi

B-type wheels—fig. 17
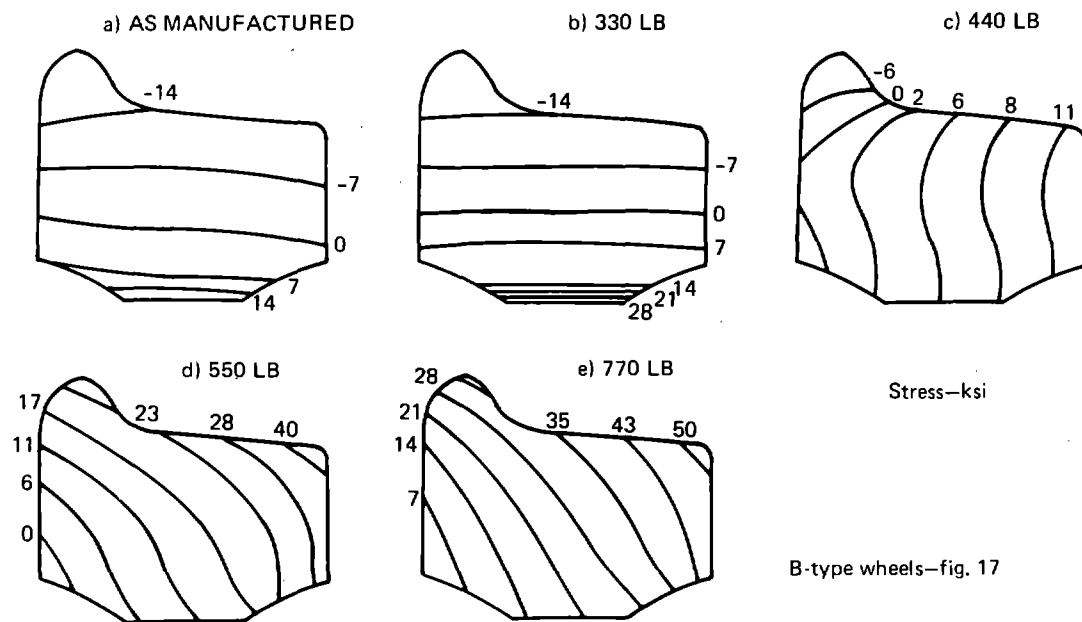
FIGURE 19.—EFFECT OF DRAG BRAKING WITH VARIOUS BRAKING FORCES ON
RESIDUAL TANGENTIAL STRESS DISTRIBUTION IN THE RIM (AFTER
HIROOKA ET AL., REF. 4)
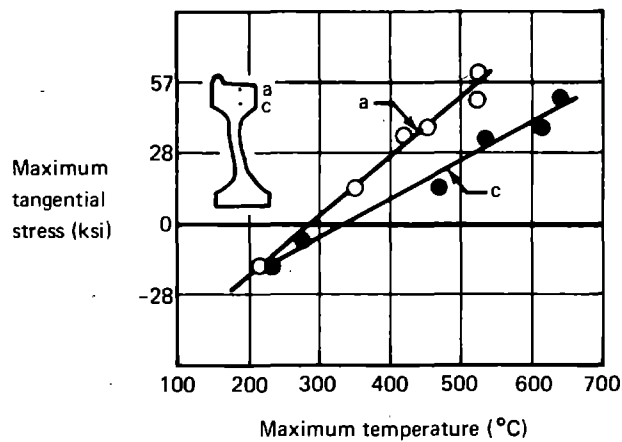
FIGURE 20.—APPARENT CORRELATION BETWEEN MAXIMUM TEMPERATURE ACHIEVED
BY DRAG BRAKING AND MAXIMUM RESIDUAL STRESS DEVELOPED IN RIM
(AFTER HIROOKA ET AL., REF. 4)

82
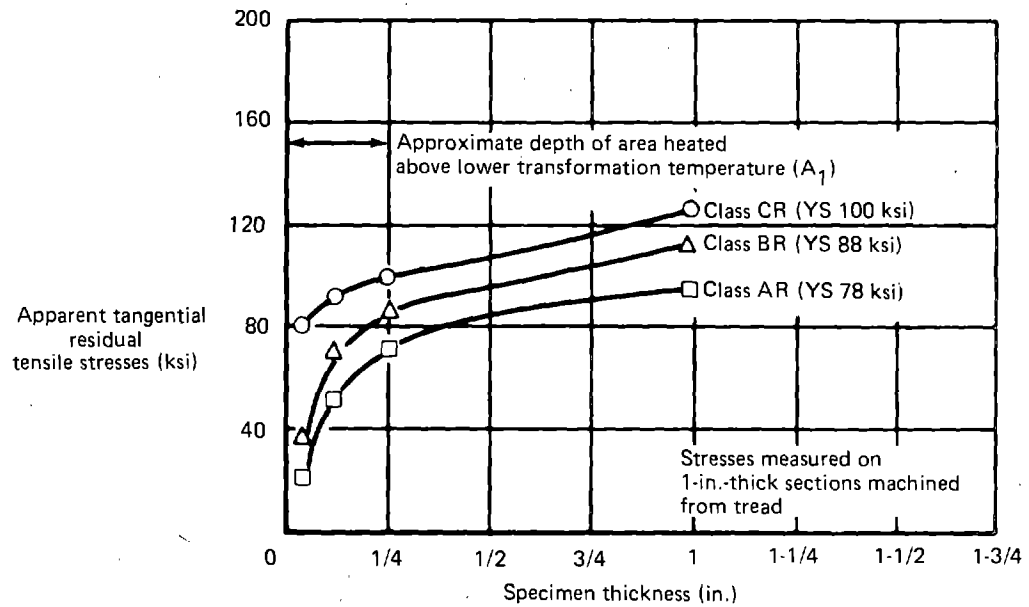
FIGURE 21.—APPARENT TANGENTIAL RESIDUAL TENSILE STRESSES AT TREAD SURFACES
OF VARIOUS CLASSES OF WHEELS AFTER A SINGLE BRAKE APPLICATION
FROM 115 MPH (AFTER WANDRISCO AND DEWEZ REF. 2)

Note: Numbers in triangles are segment identification
         K is rim fracture toughness
         KP   is plate fracture toughness
         C   is rim Charpy—T is rim tensile
         CP   is plate Charpy—TP is plate tensile
         KD   is plate dynamic fracture toughness
         GF   is macro section

Segments 3, 4, and 5
Preserved for
fatigue specimens
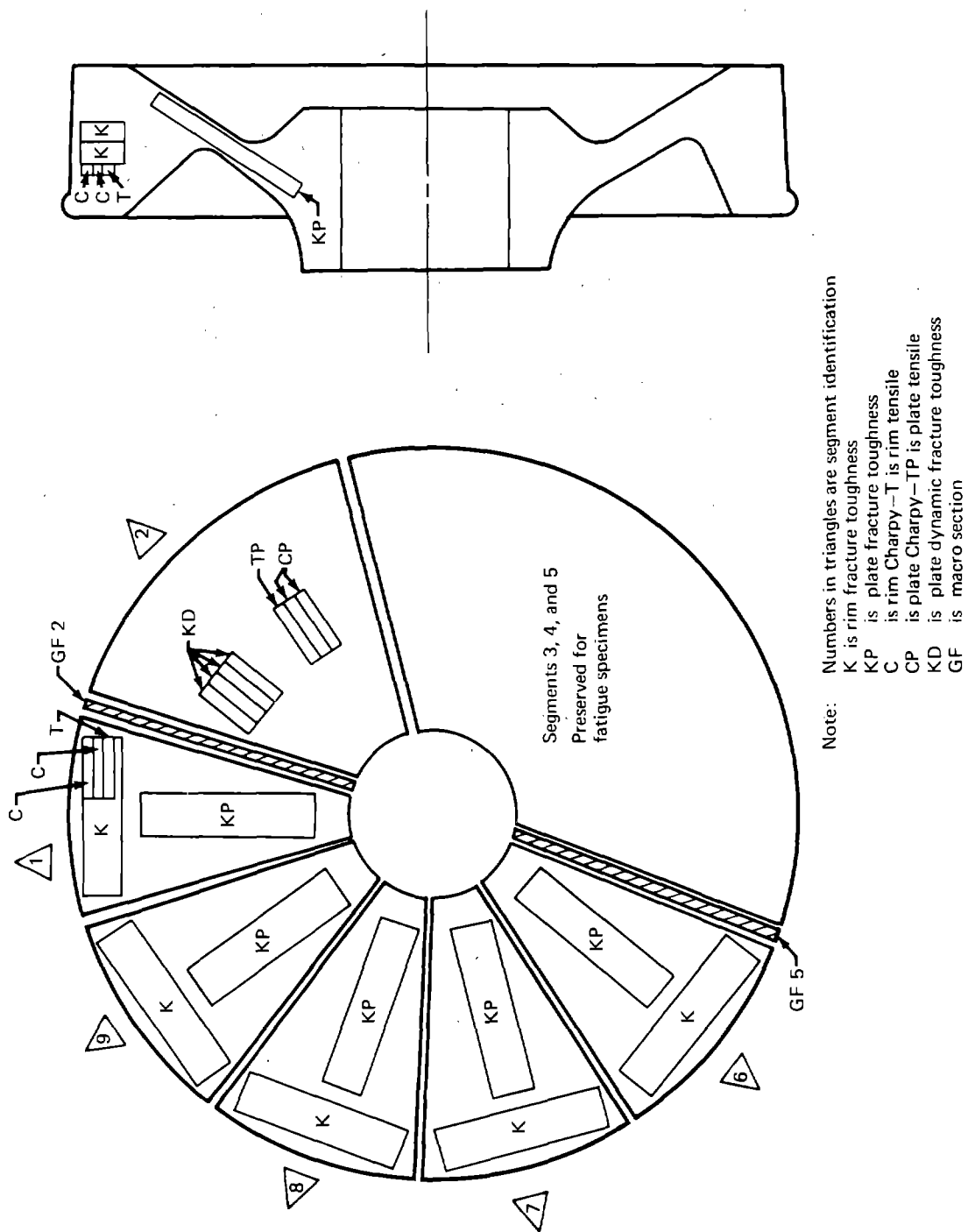
FIGURE 22.—LOCATION OF SPECIMENS WITHIN WHEEL

84

Crack plane

Axis of rotation

Indicates direction of crack propagation
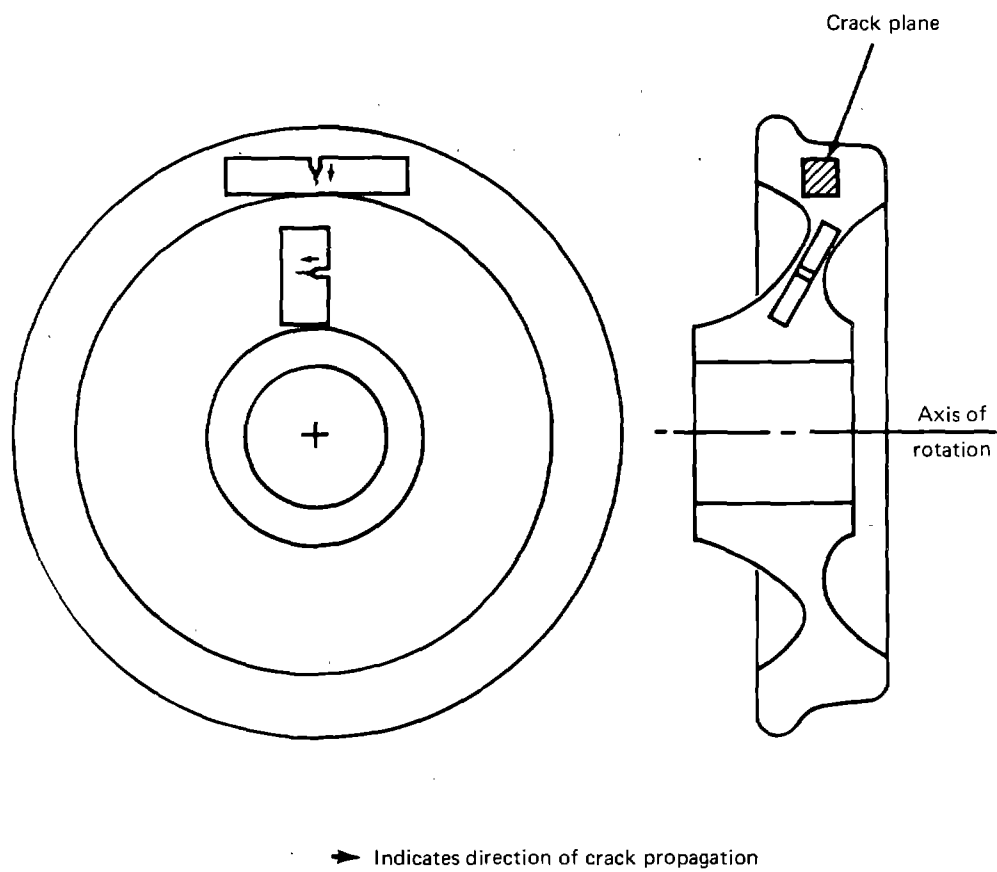
FIGURE 23.—ORIENTATION OF SPECIMENS WITH RESPECT TO THE WHEEL

0.38 DIA

1/2 - 20 NF - 3 thread

32

A

0.50

1.25

0.50 R

3.00
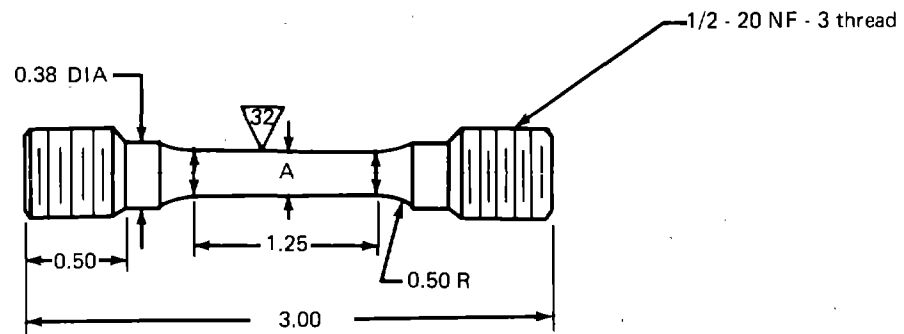
A = 0.250 max to 0.247 min

All dimensions in inches

FIGURE 24.—TENSILE SPECIMEN CONFIGURATION

86
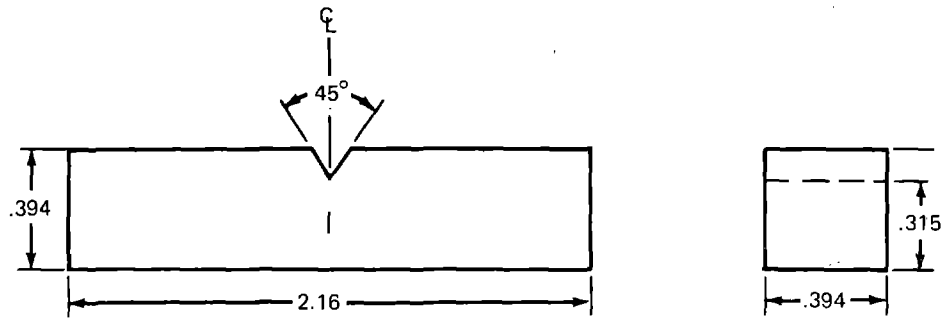
All dimensions in inches

Dynamic fracture toughness specimens
have a fatigue crack grown at the notch
root

FIGURE 25.—CHARPY AND DYNAMIC FRACTURE TOUGHNESS SPECIMEN
CONFIGURATION
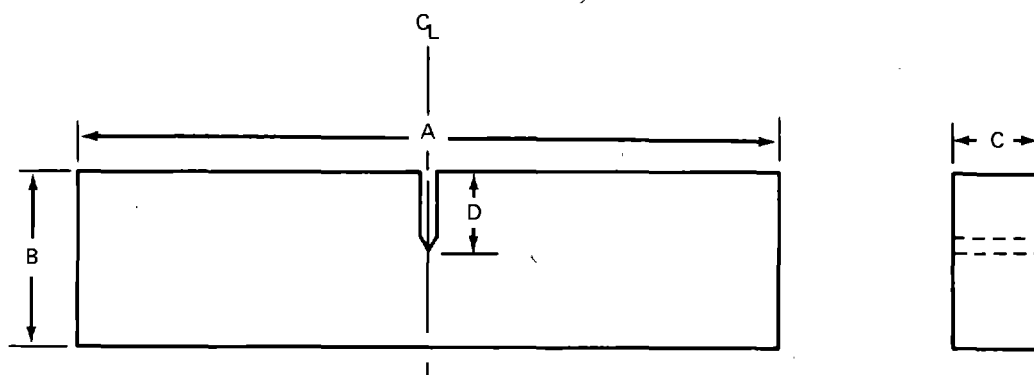
Wheel number		Dimensions			
		A	B	C	D[a]
1	Rim	8.2	2.00	1.00	0.90
	Plate	7.0	1.71	0.75	0.75
2	Rim	8.2	2.00	1.00	0.90
	Plate	7.0	1.71	0.75	0.75
3	Rim	8.2	2.00	1.00	0.90
	Plate	8.2	2.00	0.75	0.90
4	Rim	8.2	2.00	1.00	0.90
	Plate	8.2	2.00	0.75	0.90
5	Rim	8.2	2.00	1.00	0.90
	Plate	8.2	2.00	0.75	0.90
6[b]	Rim	7.0	1.70	0.70	0.75
	Plate	7.0	1.70	0.70	0.75
7	Rim	8.2	2.00	1.00	0.90
	Plate	8.2	2.00	0.75	0.90

[a]Notch dimension before fatigue precracking.

[b]One plate specimen from wheel 6 measured A = 4.2; B = 100;
C = 0.50 and D = 0.45 (tested at -40 F).

FIGURE 26.—SLOW BEND FRACTURE TOUGHNESS SPECIMEN AND SIZES TESTED
FOR EACH WHEEL

Letters A, B, C, and D indicate
hardness traverses

Letters X, Y, and Z indicate metallographic sections

Letter Q indicates area where chemical
analysis taken
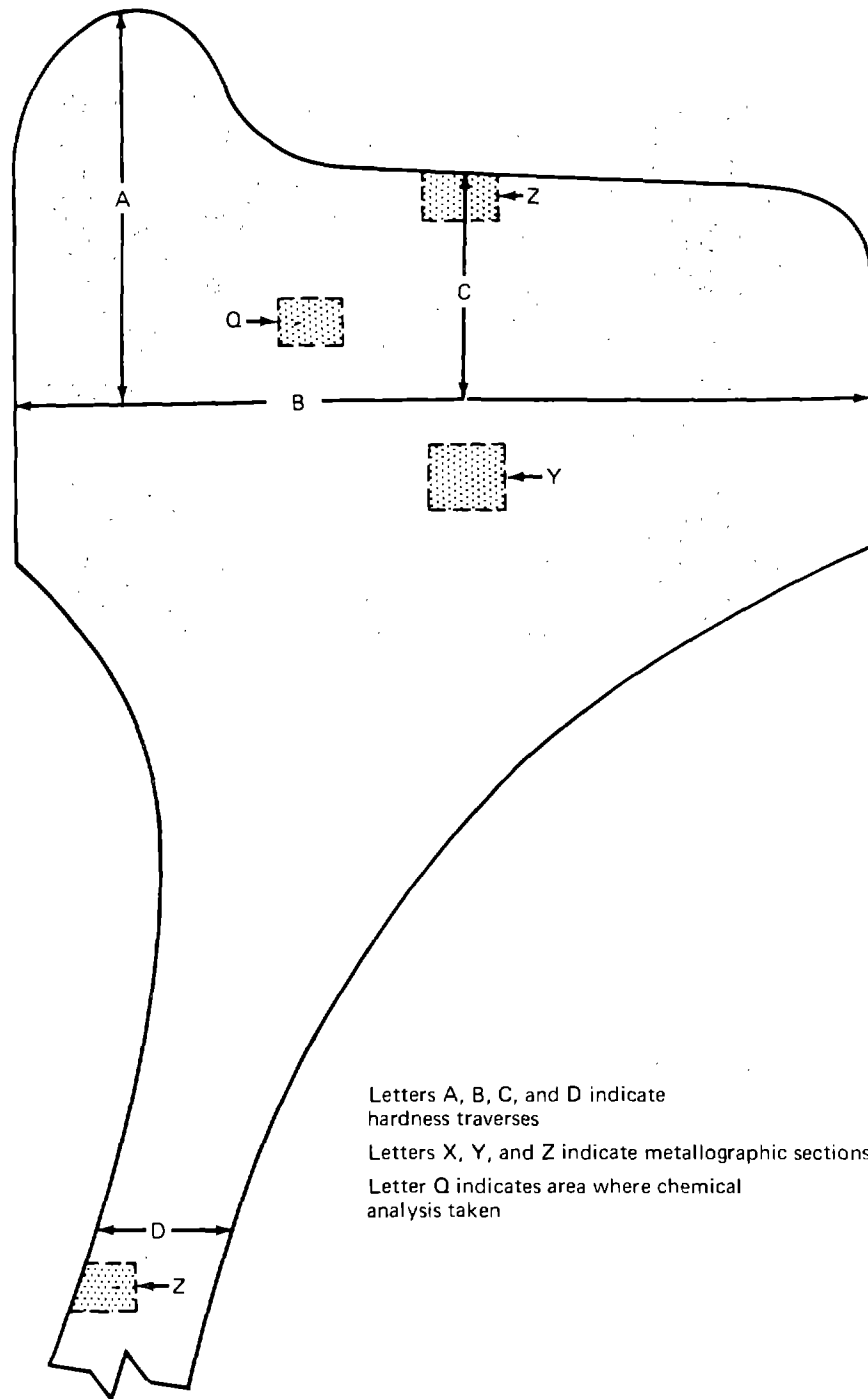
FIGURE 27.—LOCATION OF HARDNESS TRAVERSES, MICROSECTIONS, AND
CHEMICAL ANALYSES WITHIN WHEEL CROSS SECTION
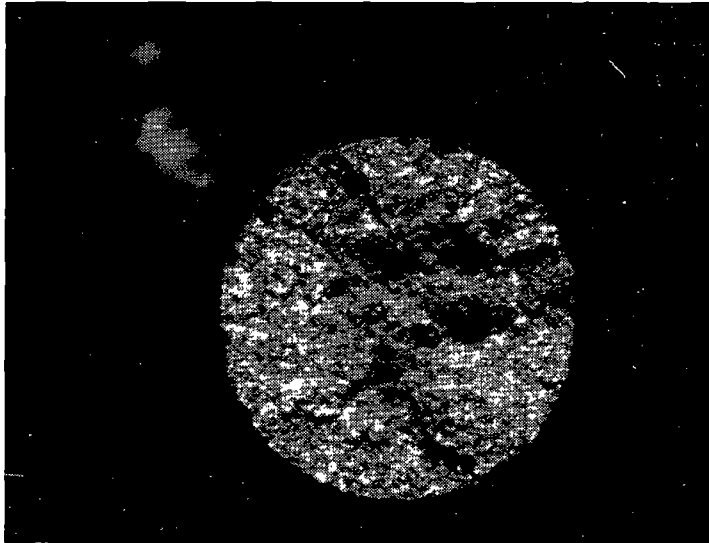
FIGURE 28.—FRACTURE FACE OF TENSILE SPECIMEN TAKEN FROM THE RIM
OF THE WROUGHT CLASS-C WHEEL (THE FIBROUS FRACTURE IS
THE DULL NONREFLECTING AREA IN THE CENTER AND OCCUPIES
ABOUT 22% OF THE FRACTURE FACE; THE OUTER BOUNDARY
OF SHINY REFLECTING FACETS IS CLEAVAGE), X9 MAGNIFICATION
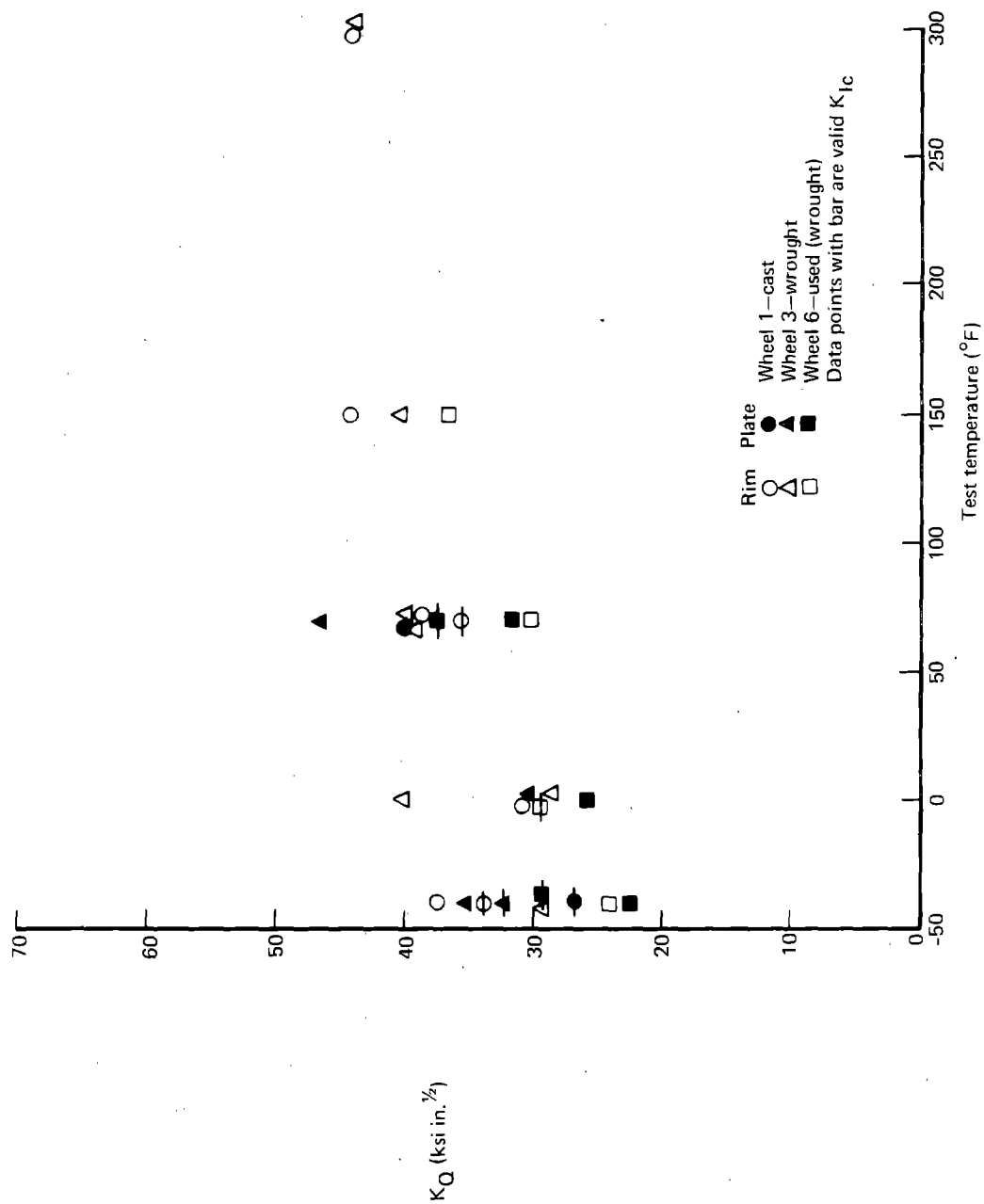
FIGURE 29.—EFFECT OF TEMPERATURE ON FRACTURE TOUGHNESS, CLASS U WHEELS
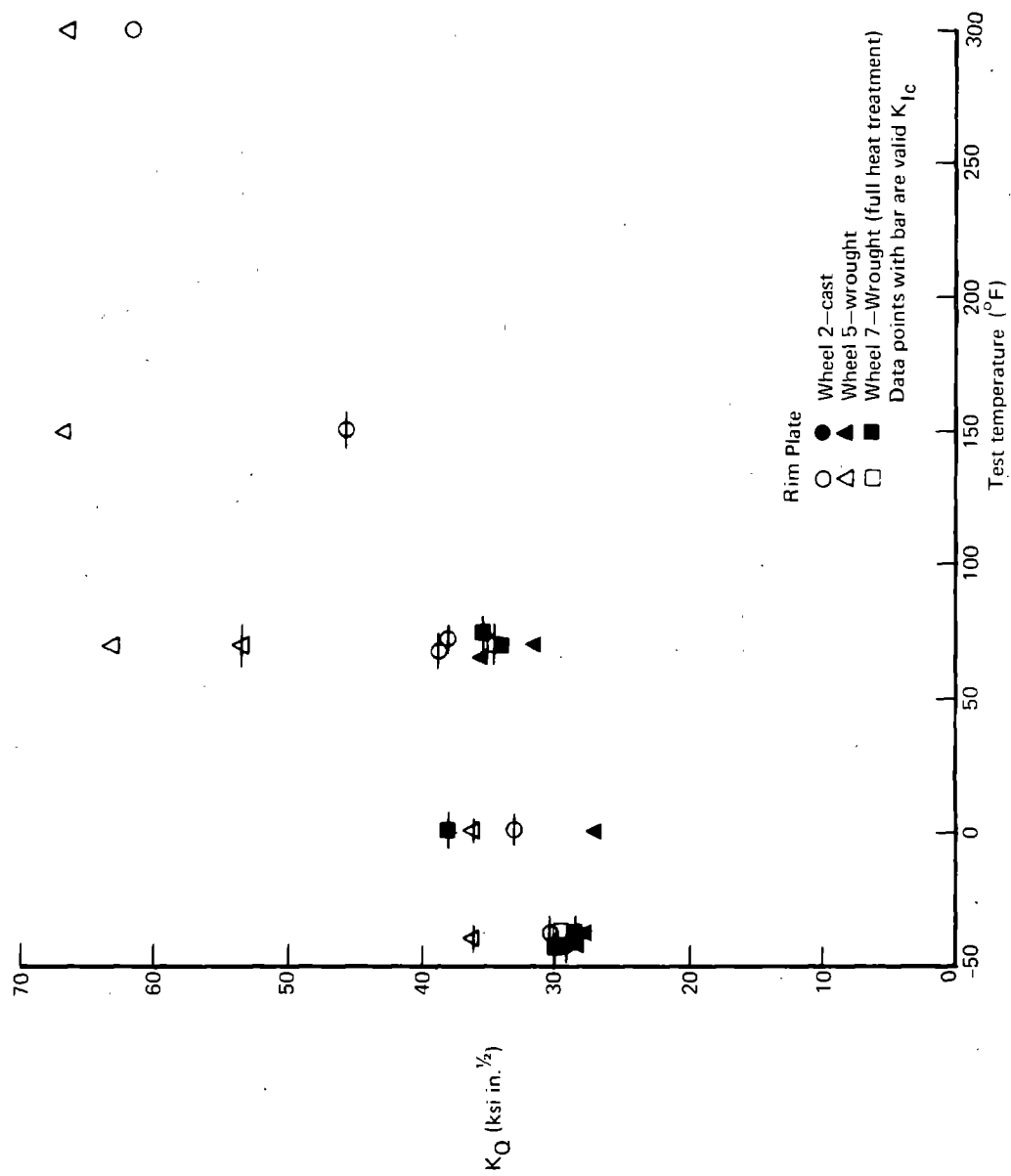
FIGURE 30.—EFFECT OF TEMPERATURE ON FRACTURE TOUGHNESS, CLASS C WHEELS

92
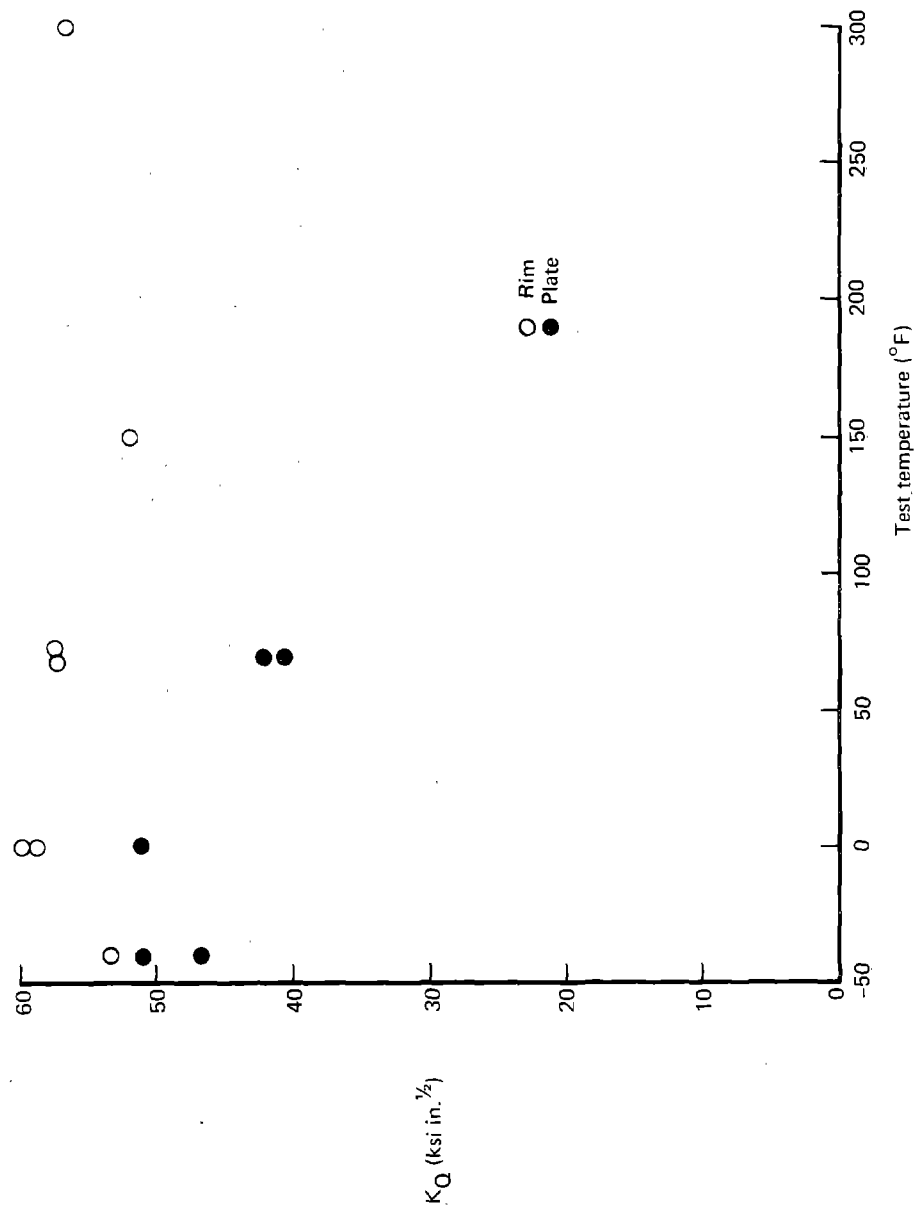
FIGURE 31.—EFFECT OF TEMPERATURE ON FRACTURE TOUGHNESS, CLASS A WHEEL

93
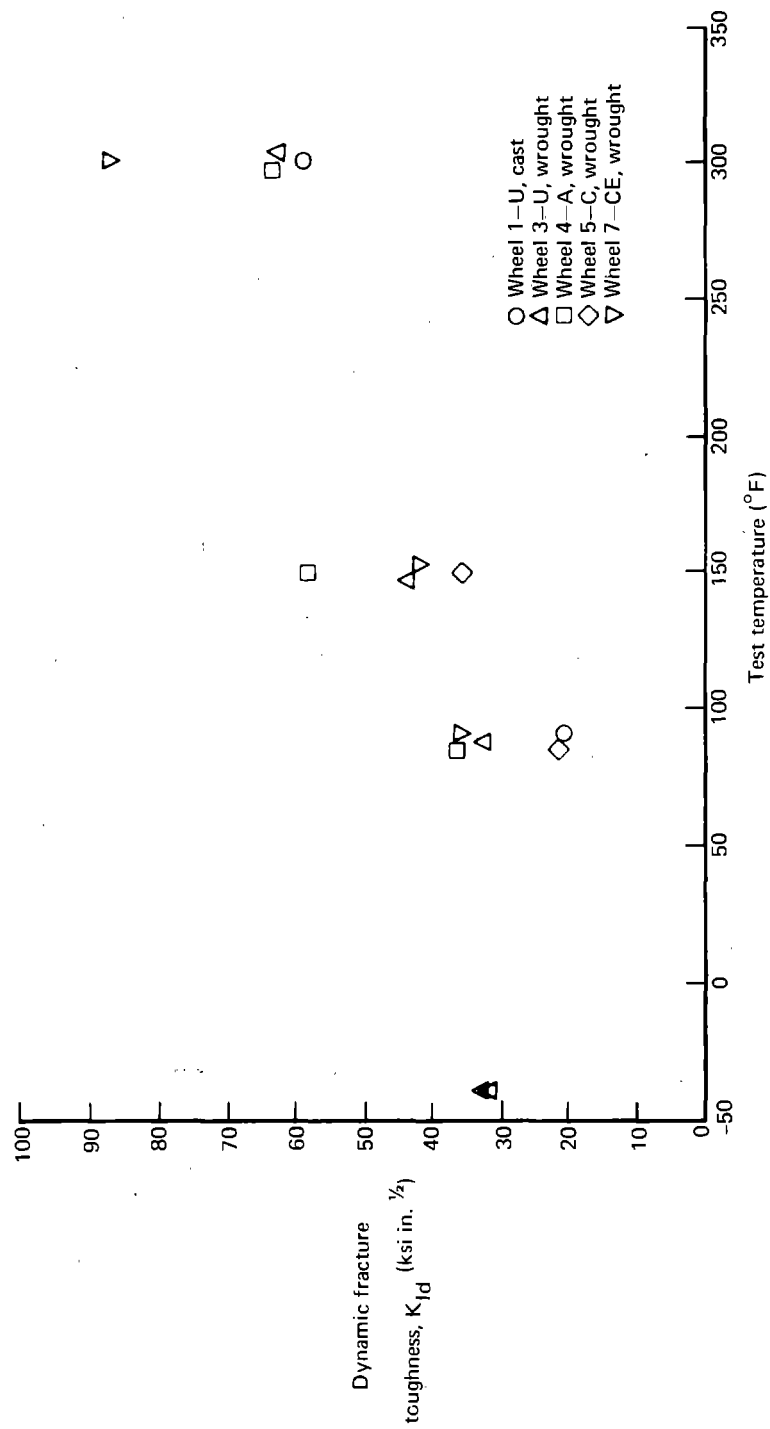
FIGURE 32.—EFFECT OF TEMPERATURE ON DYNAMIC FRACTURE TOUGHNESS (K_{Id})

+230 (241)
+225
+230 (220)
+247
+247 (220)
+253
+241 (236)
+241
+235 (235)
+225
+225 (235)
+230
+230 (241)
+241
+235 (230)
+235
+235 (235)
+235
+241 (225)
+259
+241 (225)
+230
+235 (220)

+247 (210)
+241
+241 (225)
+241
+241 (225)
+241
+241 (225)
+247
+253 (230)
+241
+241 (235)
+247

+235
+235 (230)
+241

Numbers shown are BHN values

Numbers in parenthesis are for the GF 2 location (fig. 22)
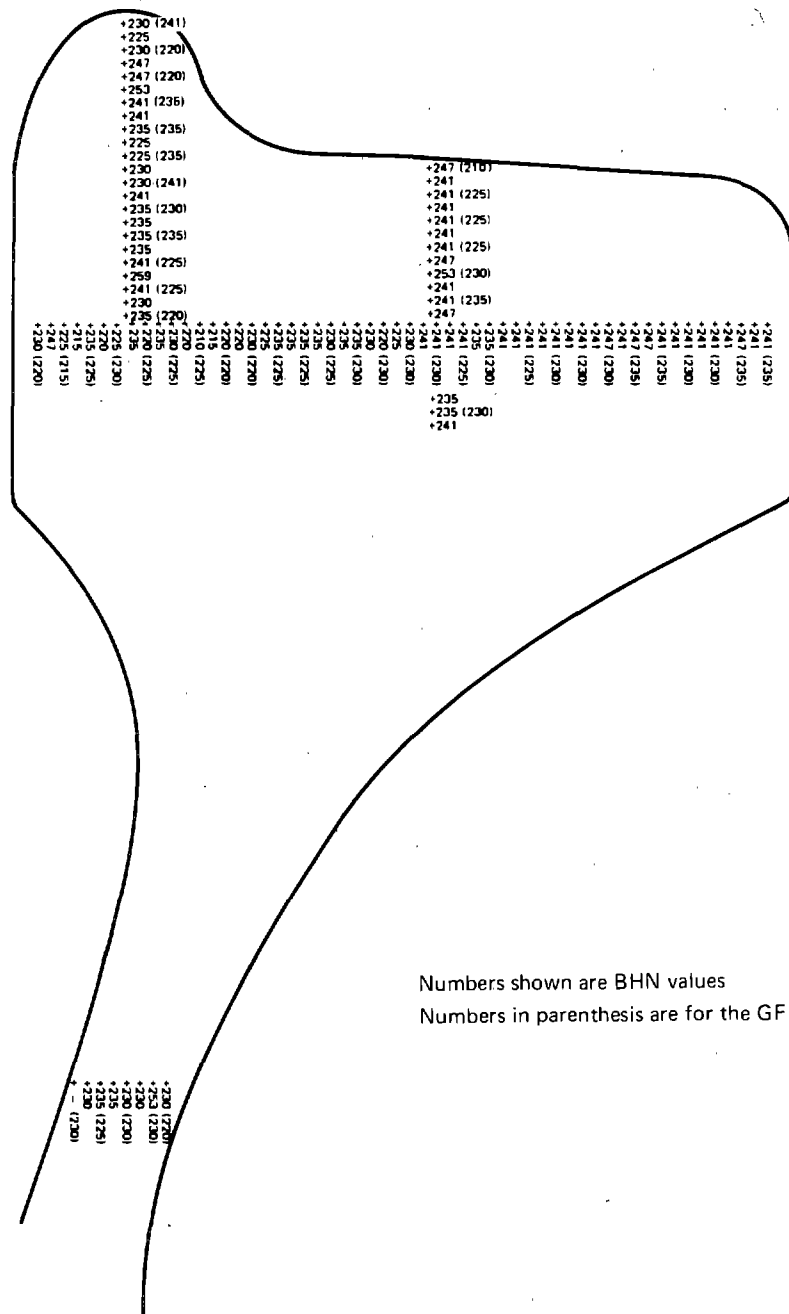
FIGURE 33.—HARDNESS TRAVERSE FOR THE CAST CLASS-U WHEEL, NO. 1

Numbers shown are BHN values
Numbers in parenthesis are for the GF 2 location (fig. 22)

FIGURE 34.—HARDNESS TRAVERSE FOR THE CAST CLASS-C WHEEL, NO. 2
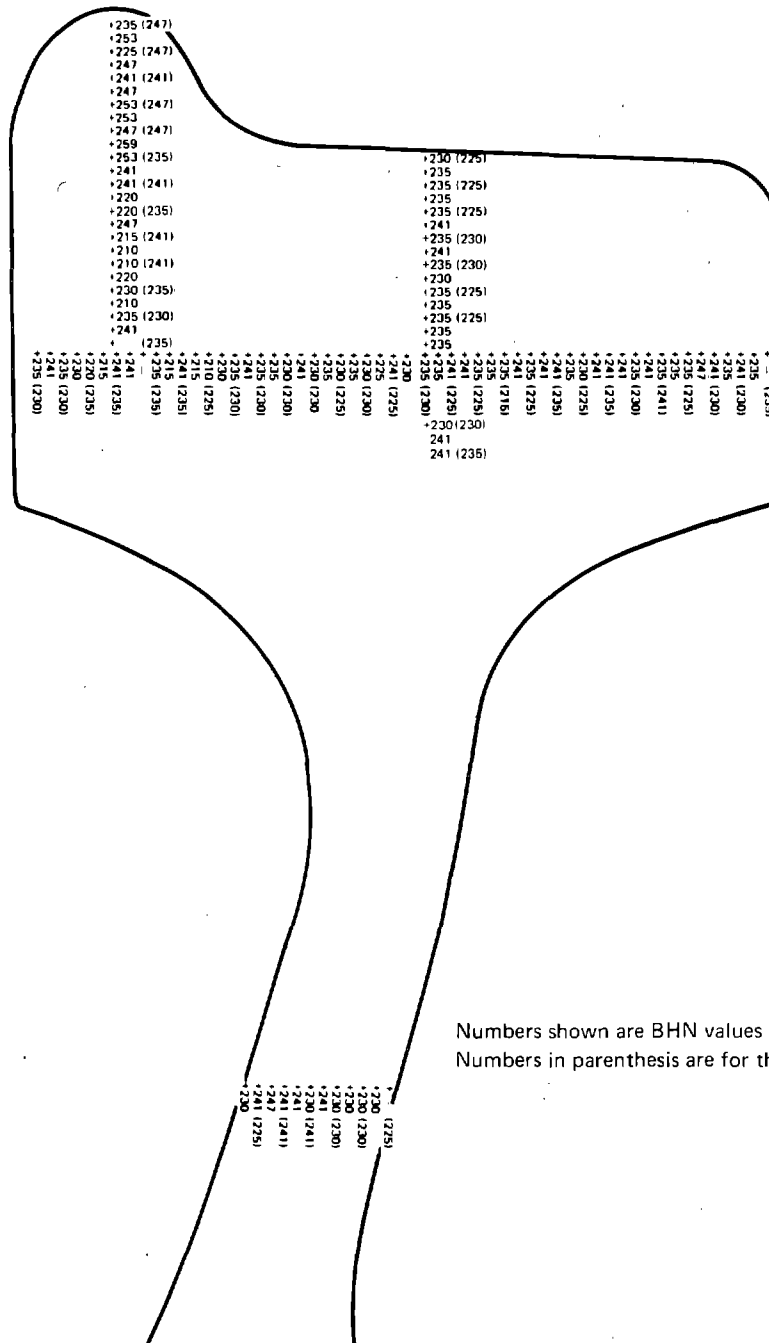
FIGURE 35.—HARDNESS TRAVERSE FOR THE CLASS-U WROUGHT WHEEL NO. 3
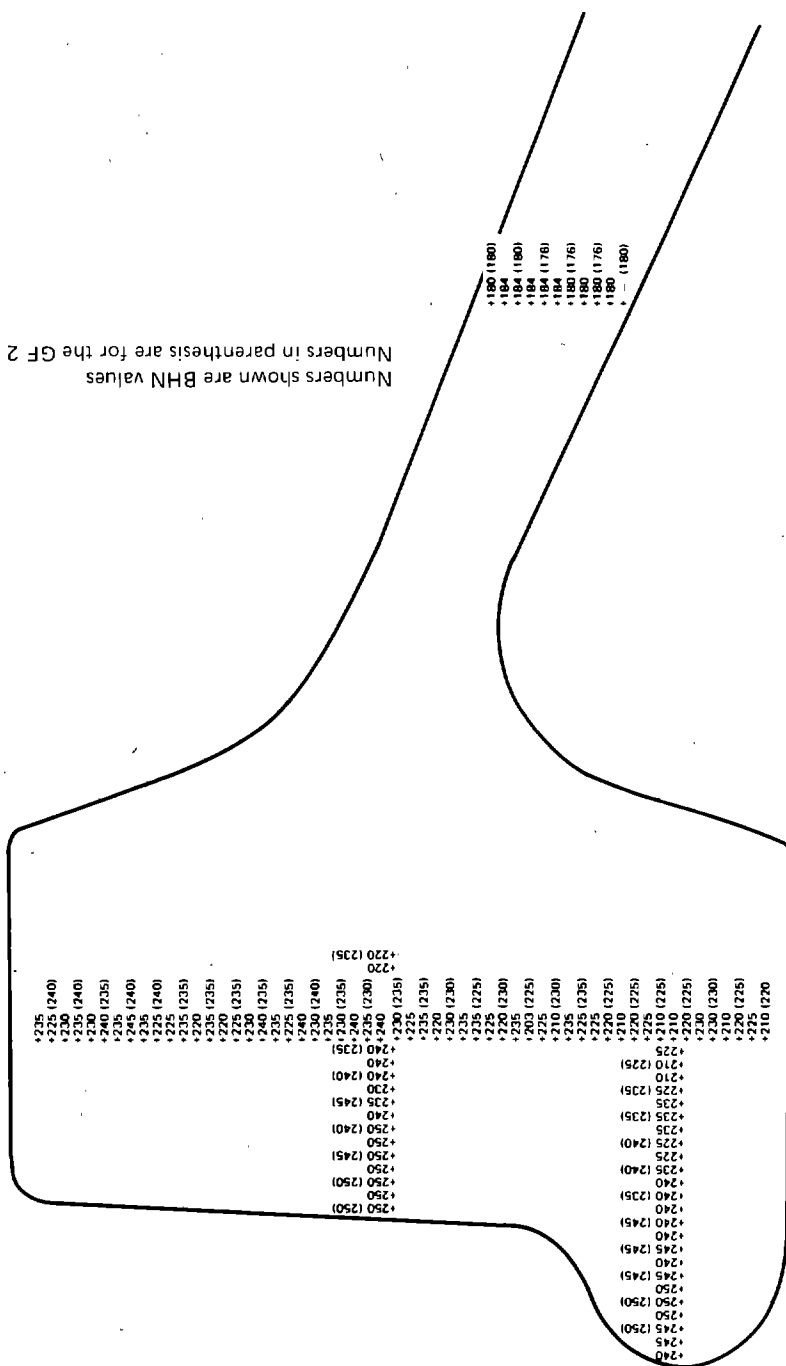
FIGURE 36.—HARDNESS TRAVERSE FOR THE CLASS-A WROUGHT WHEEL, NO. 4

Numbers shown are BHN values
Numbers in parenthesis are for the GF 2 location (fig. 22)

Numbers shown are BHN values
Numbers in parenthesis are for the GF 2 location (fig. 22)

FIGURE 37.—HARDNESS TRAVERSE FOR THE CLASS-C WROUGHT WHEEL, NO. 5

Numbers shown are BHN values
Numbers in parenthesis are for the GF 2 location (fig. 22)

FIGURE 38.—HARDNESS TRAVERSE FOR THE USED WHEEL, NO. 6

100

Numbers shown are BHN values
Numbers in parenthesis are for the GF 2 location (fig. 22)

FIGURE 39.—HARDNESS TRAVERSE FOR THE CLASS-CE WROUGHT WHEEL, NO. 7

101

FIGURE 40.—MACROSECTION OF CAST CLASS-U WHEEL (WHEEL 1),
1.1 APPROXIMATE MAGNIFICATION
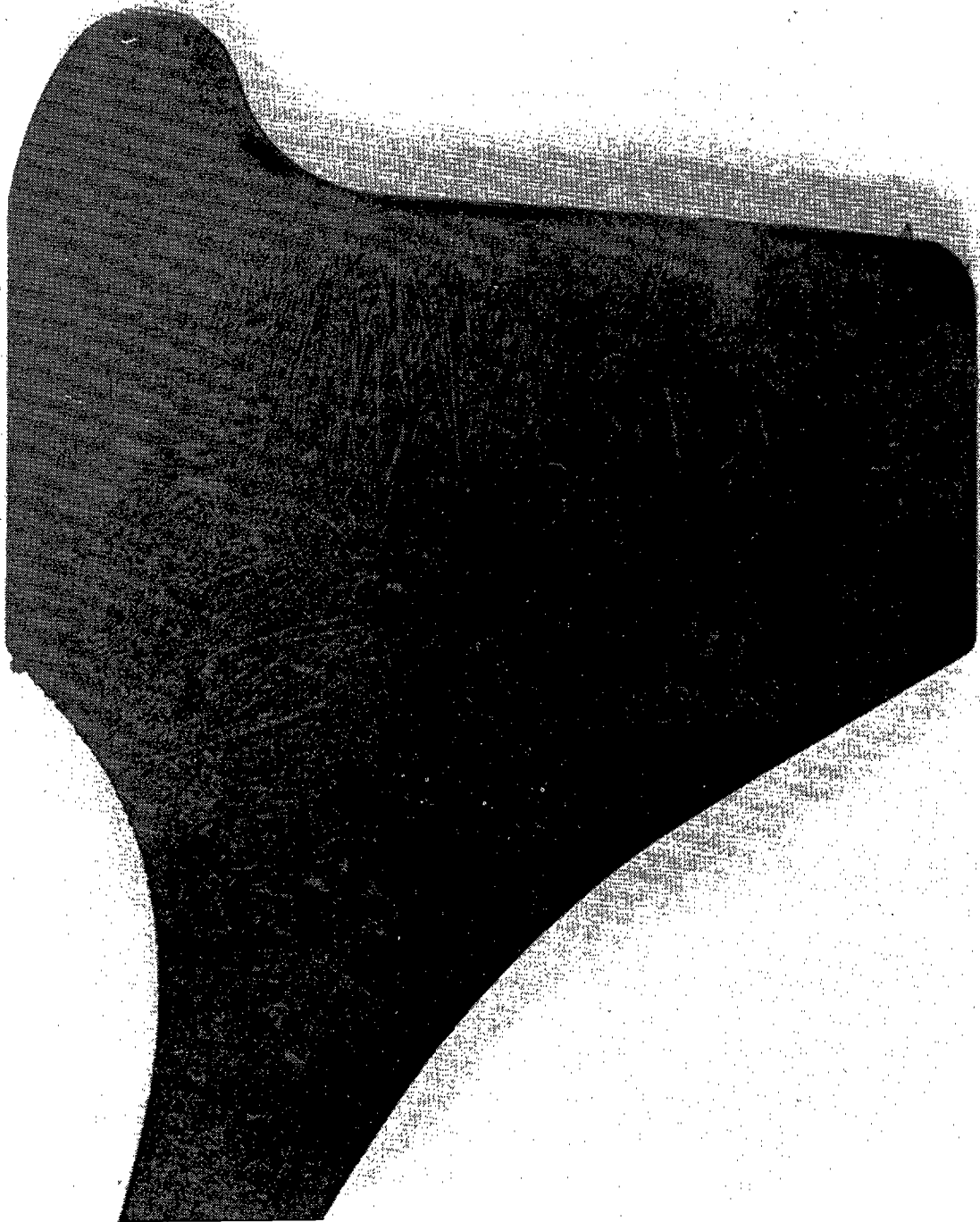
FIGURE 41.—MACROSECTION OF CAST CLASS-C WHEEL (WHEEL 2),
1.1 APPROXIMATE MAGNIFICATION
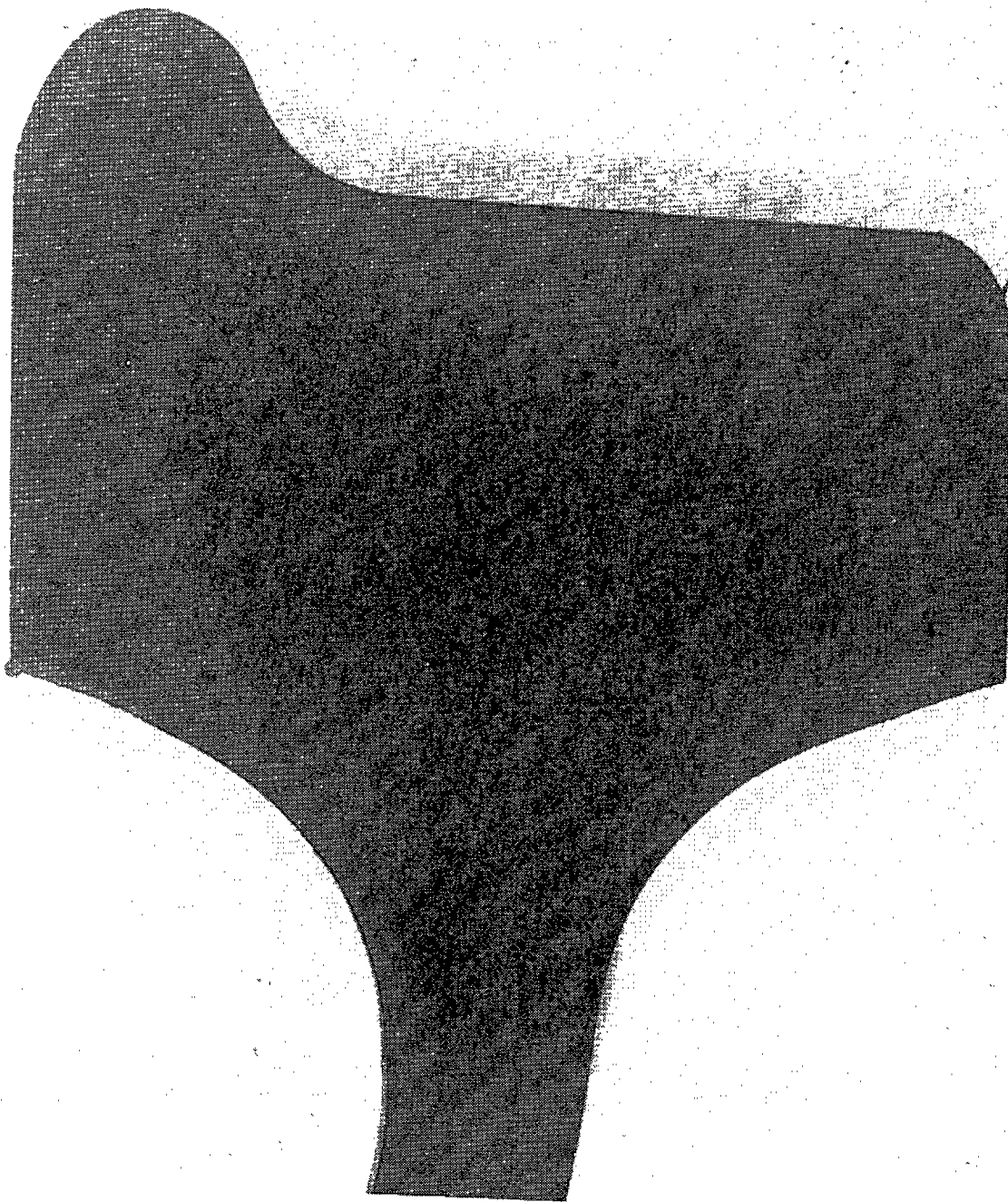
FIGURE 42.—MACROSECTION OF WROUGHT CLASS-U WHEEL (WHEEL 3),
1.1 APPROXIMATE MAGNIFICATION
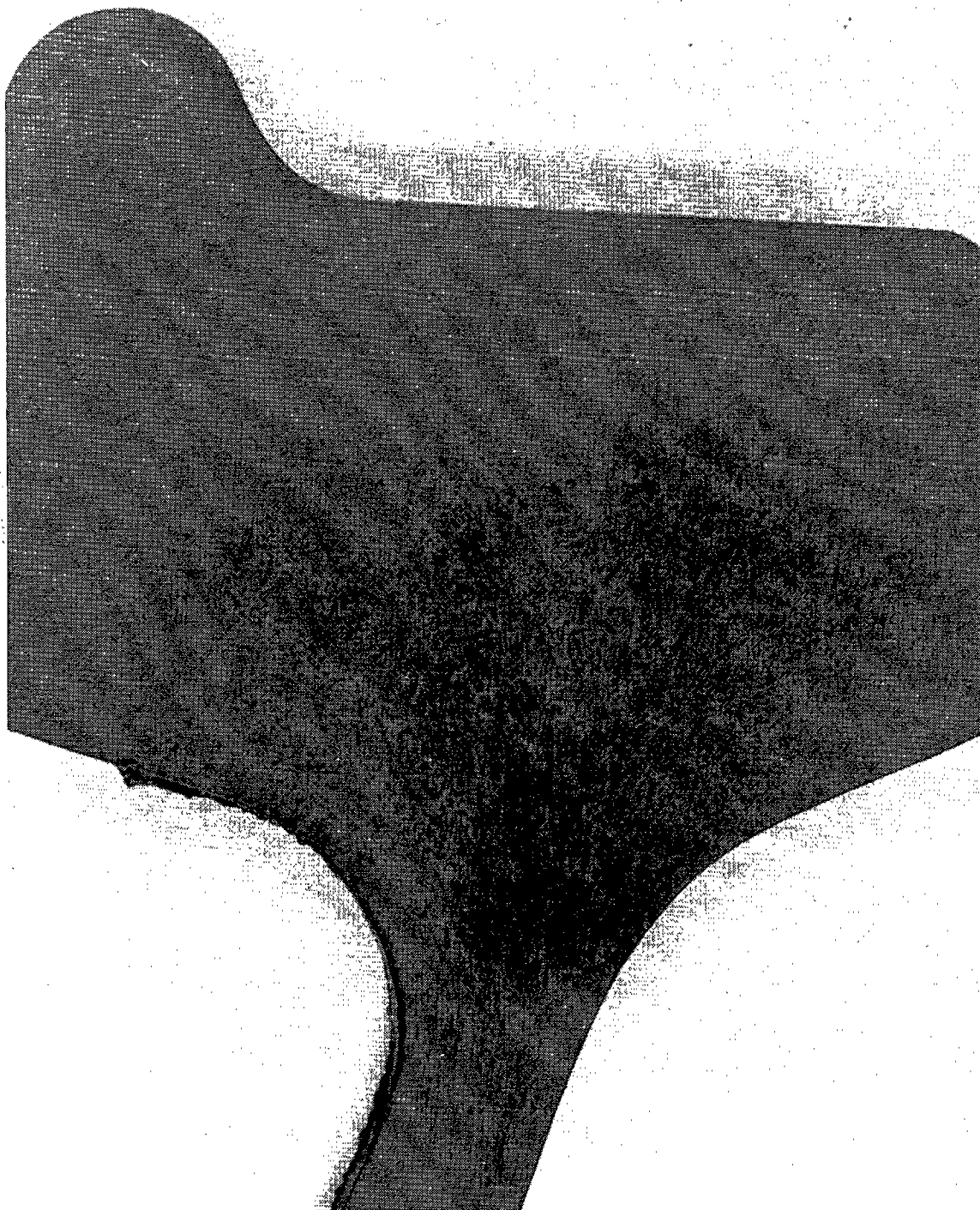
FIGURE 43.—MACROSECTION OF WROUGHT CLASS-A WHEEL (WHEEL 4),
1.1 APPROXIMATE MAGNIFICATION
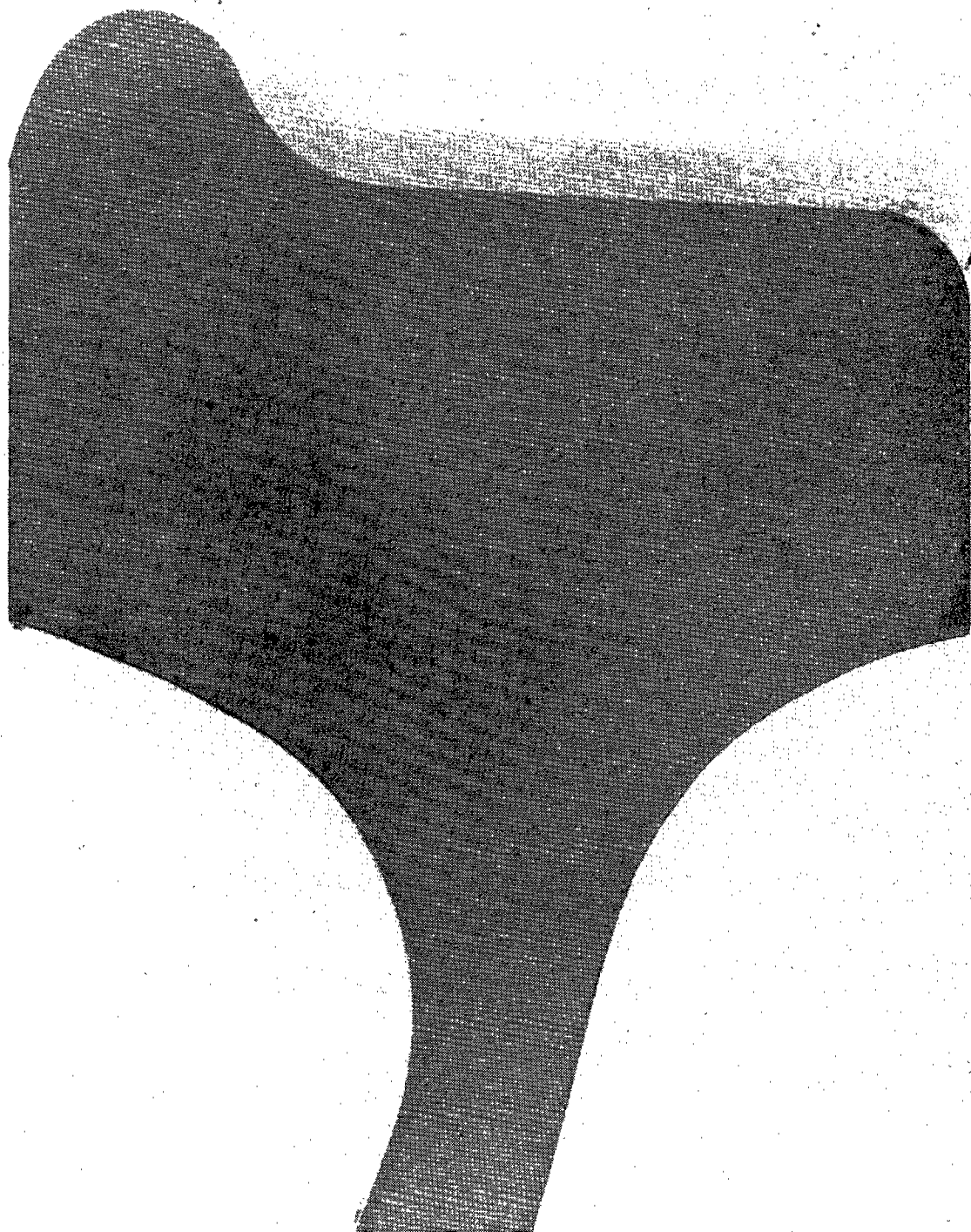
FIGURE 44.—MACROSECTION OF WROUGHT CLASS-C WHEEL (WHEEL 5),
1.1 APPROXIMATE MAGNIFICATION
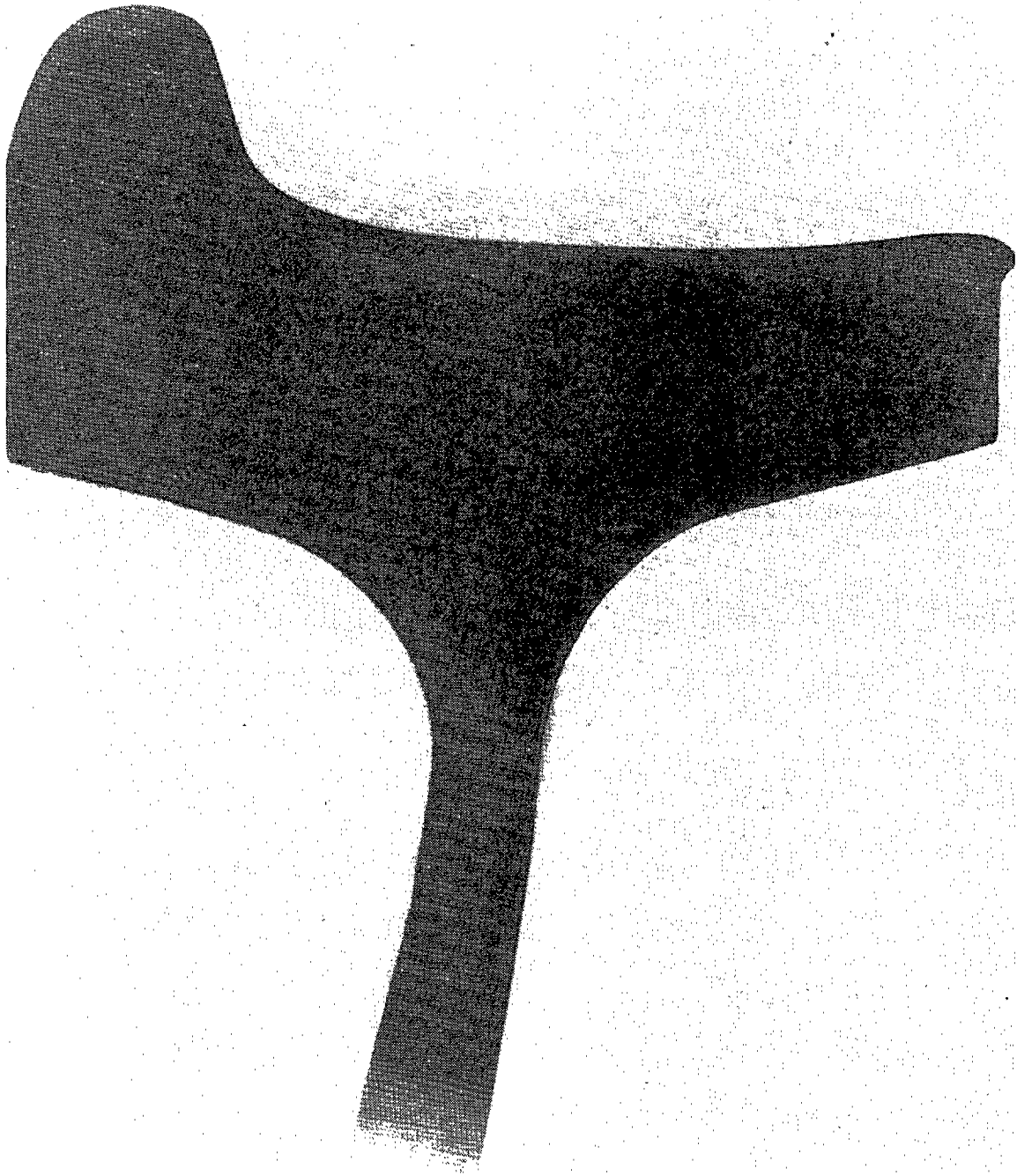
FIGURE 45.—MACROSECTION OF WORN-WROUGHT CLASS-U WHEEL (WHEEL 6),
1.1 APPROXIMATE MAGNIFICATION
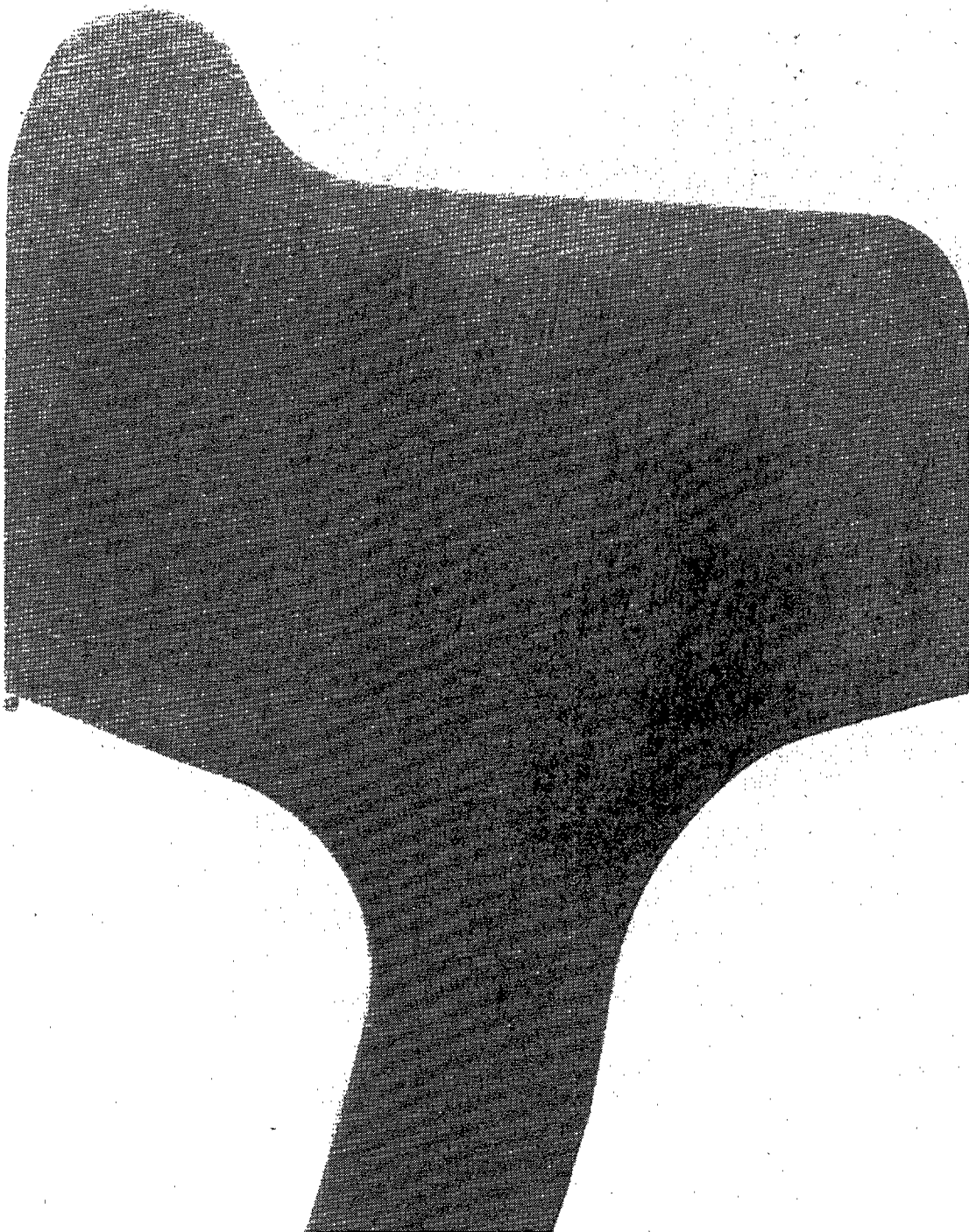
FIGURE 46.—MACROSECTION OF WROUGHT CLASS-CE WHEEL (WHEEL 7),
1.1 APPROXIMATE MAGNIFICATION
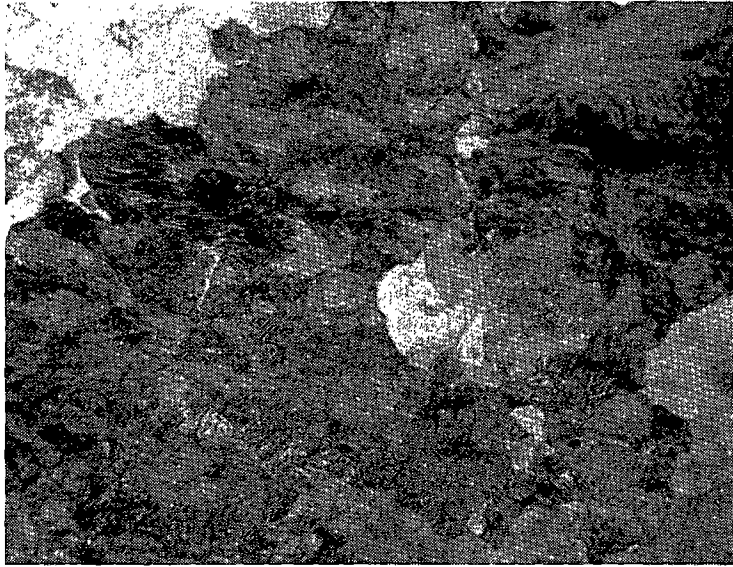
a) RIM (LOCATION Y)
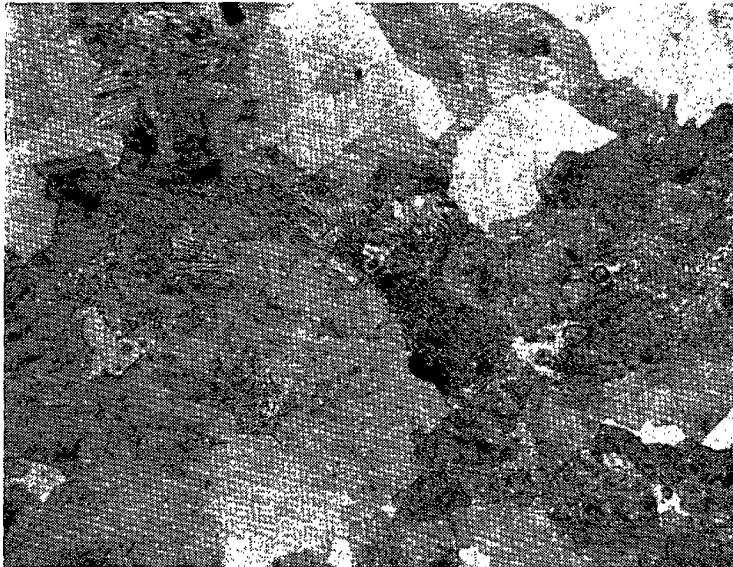
b) PLATE (LOCATION Z)

FIGURE 47.–PHOTOMICROGRAPHS OF CAST CLASS-U WHEEL (WHEEL 1), X360 MAGNIFICATION, ETCH: 2% NITAL

109
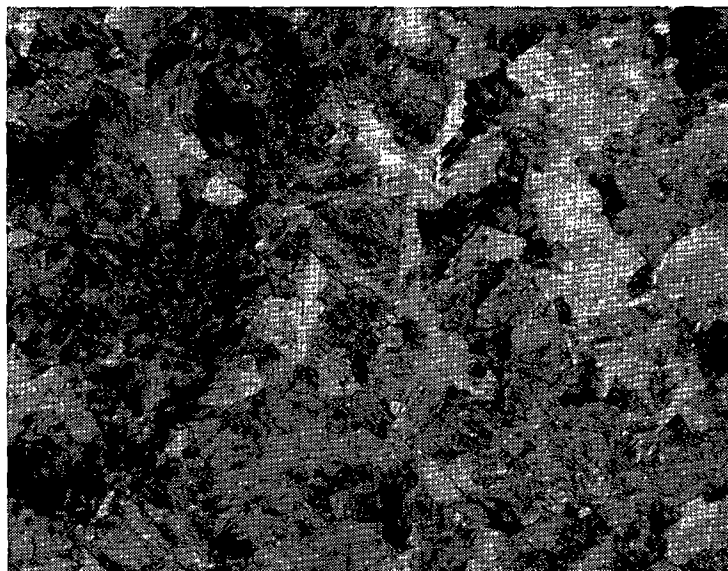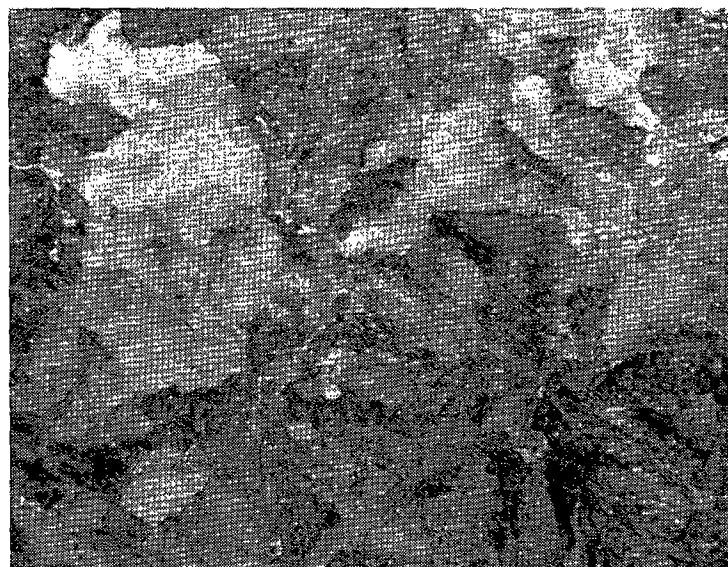
a) RIM (LOCATION Y)

b) PLATE (LOCATION Z)

FIGURE 48.—PHOTOMICROGRAPHS OF CAST CLASS-C WHEEL (WHEEL 2),
X360 MAGNIFICATION, ETCH: 2% NITAL
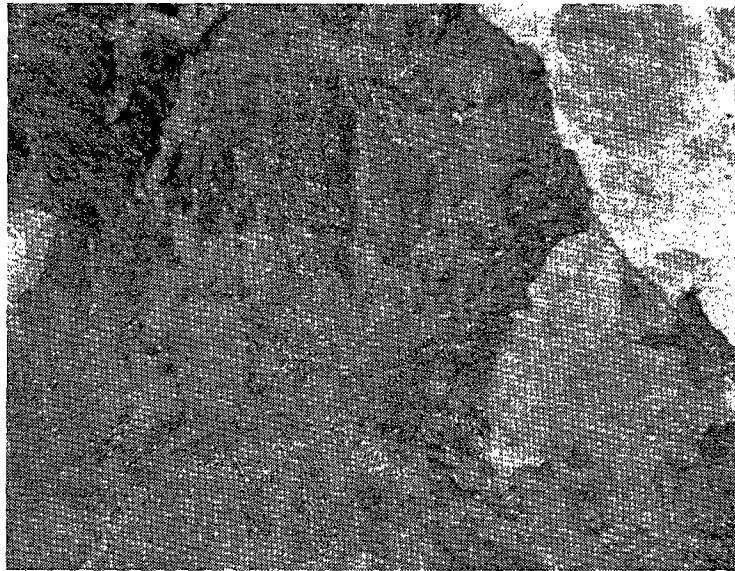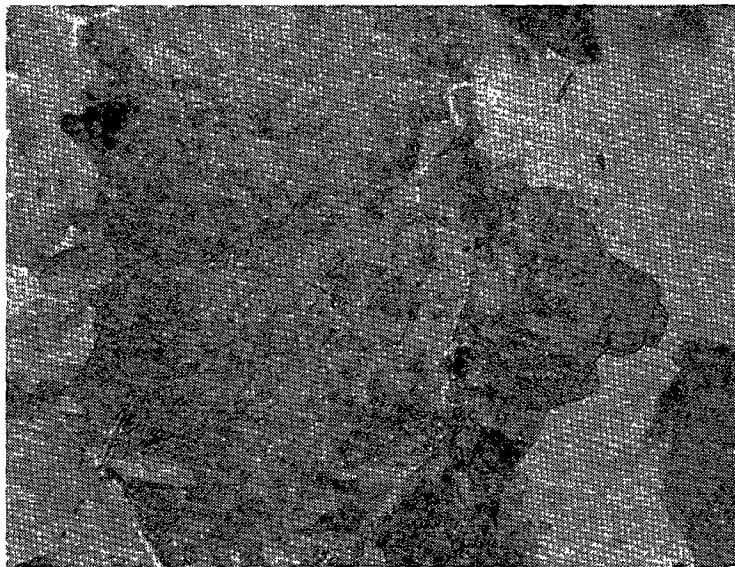
a) RIM (LOCATION Y)

b) PLATE (LOCATION Z)

FIGURE 49.—PHOTOMICROGRAPHS OF WROUGHT CLASS-U WHEEL (WHEEL 3),
X360 MAGNIFICATION, ETCH: 2% NITAL
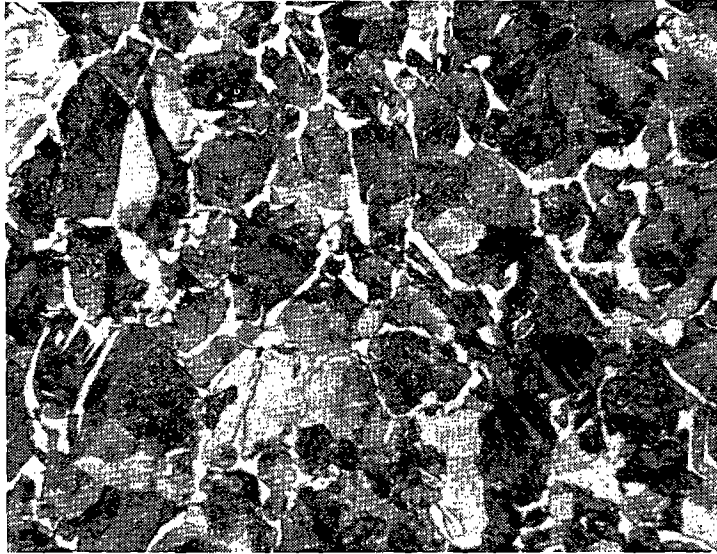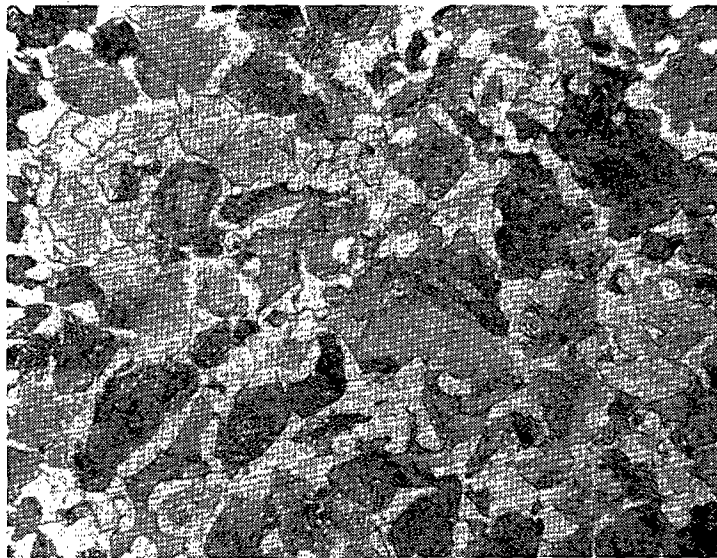
a) RIM (LOCATION Y)

b) PLATE (LOCATION Z)

FIGURE 50.—PHOTOMICROGRAPHS OF WROUGHT CLASS-A WHEEL (WHEEL 4),
X360 MAGNIFICATION, ETCH: 2% NITAL

112
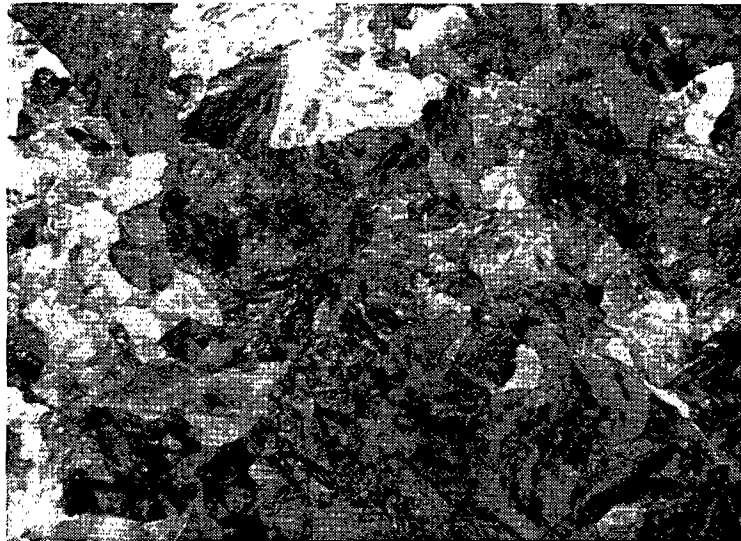
a) RIM (LOCATION (Y)

b) PLATE (LOCATION Z)

FIGURE 51.—PHOTOMICROGRAPHS OF WROUGHT CLASS-C WHEEL (WHEEL 5),
X360 MAGNIFICATION, ETCH: 2% NITAL
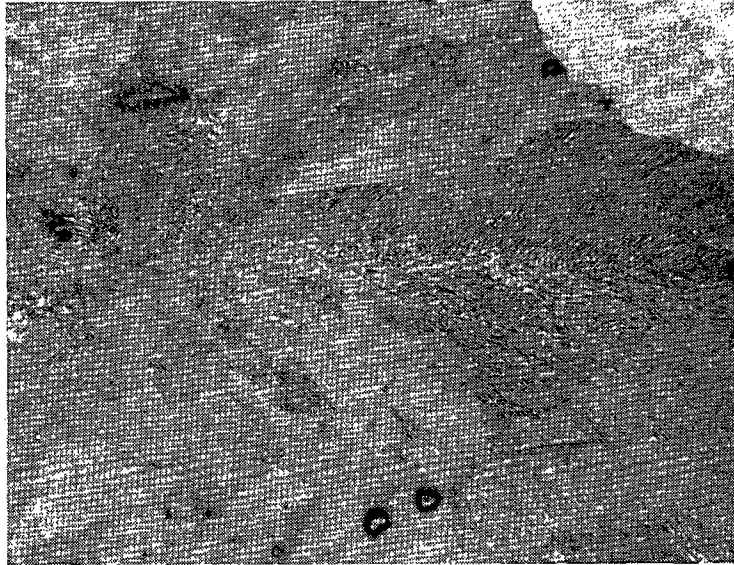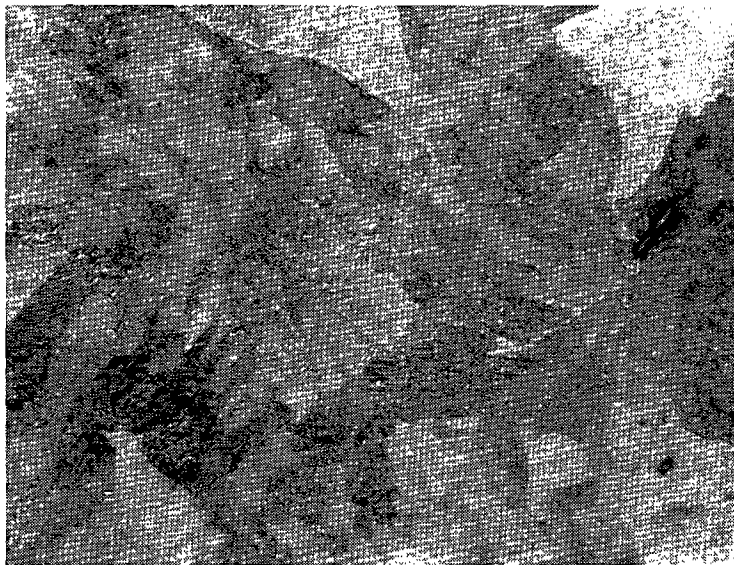
a) RIM (LOCATION Y)

b) PLATE (LOCATION Z)

FIGURE 52.—PHOTOMICROGRAPHS OF USED WROUGHT CLASS-U WHEEL (WHEEL 6),
X360 MAGNIFICATION, ETCH: 2% NITAL

a) RIM (LOCATION Y)
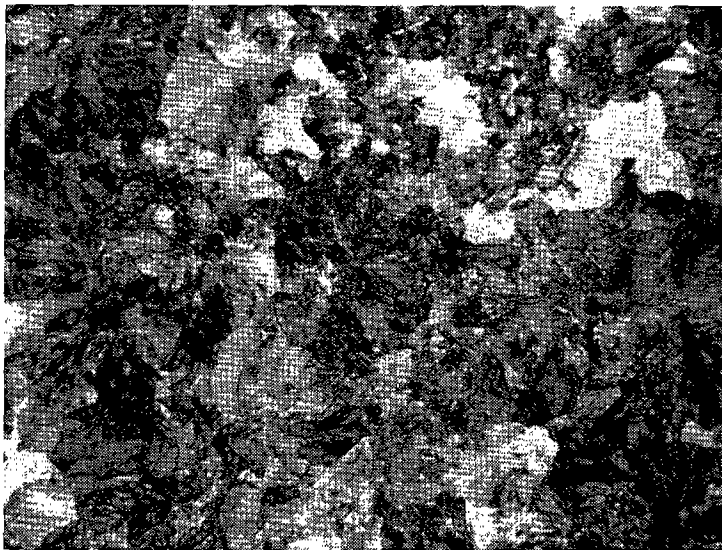
b) PLATE (LOCATION Z)

FIGURE 53.--PHOTOMICROGRAPHS OF WROUGHT CLASS-CE (WHEEL 7),
X360 MAGNIFICATION, ETCH: 2% NITAL
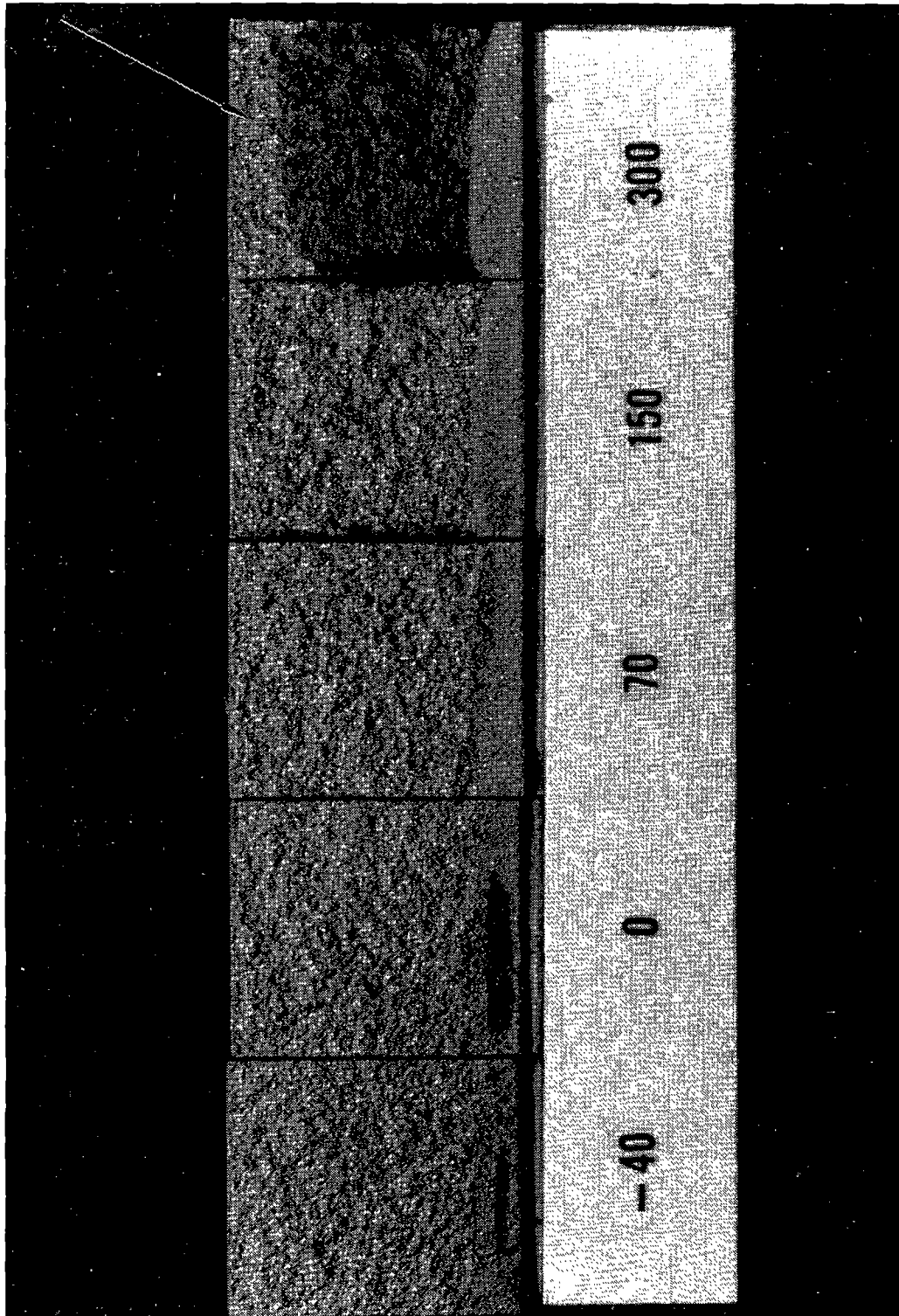
FIGURE 54.—K_{IC} FRACTURES FROM THE CAST CLASS-U WHEEL RIM—ARROW INDICATES THE CLEAVAGE CAUSED BY BREAKING OPEN THE SPECIMEN AT ROOM TEMPERATURE SINCE COMPLETE SEPARATION DID NOT OCCUR AT 300°F (NUMBERS INDICATE TEST TEMPERATURES), X1.7 MAGNIFICATION
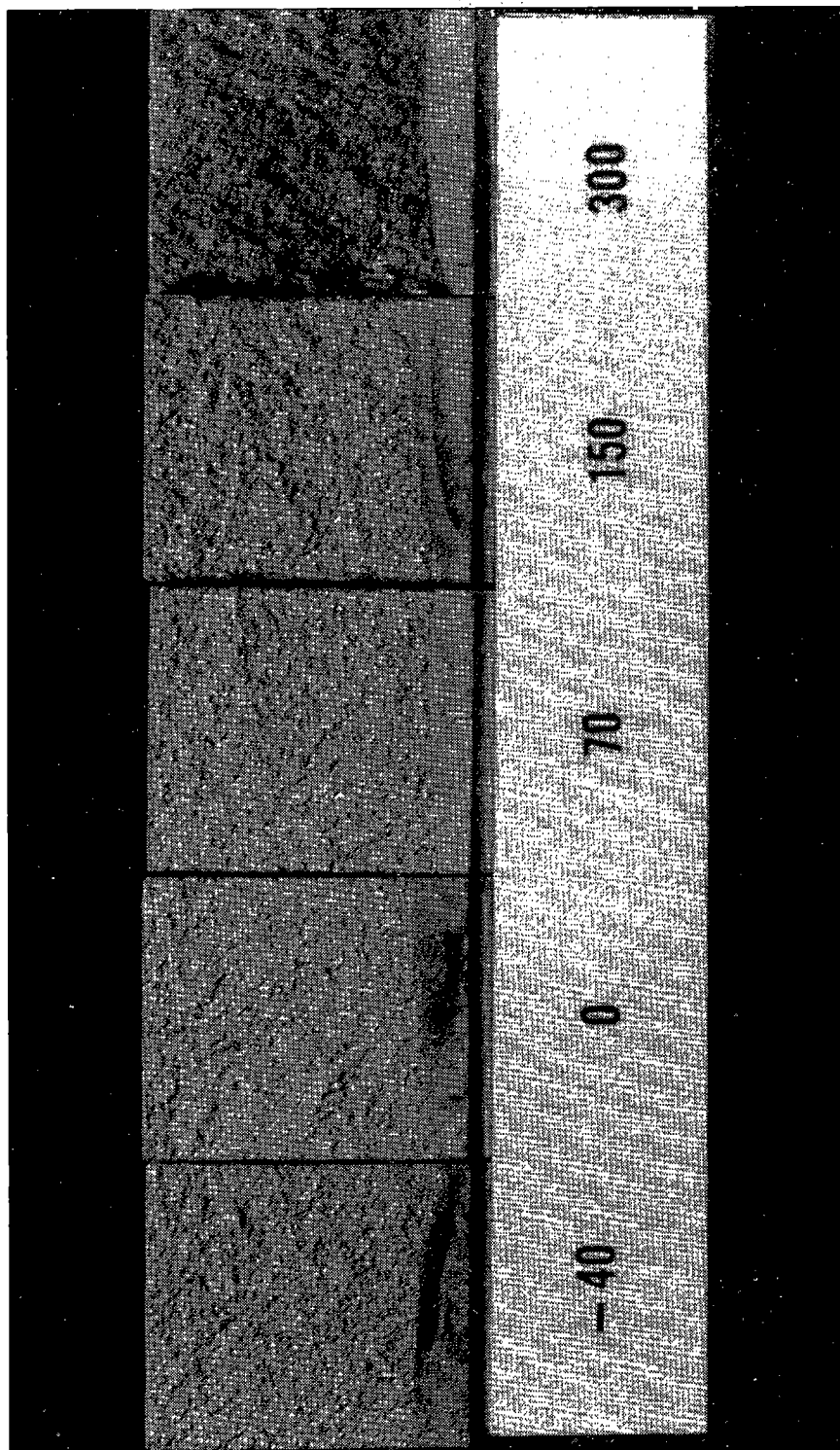
FIGURE 55.—K_{IC} FRACTURES FROM THE CAST CLASS-C WHEEL RIM (NUMBERS INDICATE TEST TEMPERATURE), X1.7 MAGNIFICATION
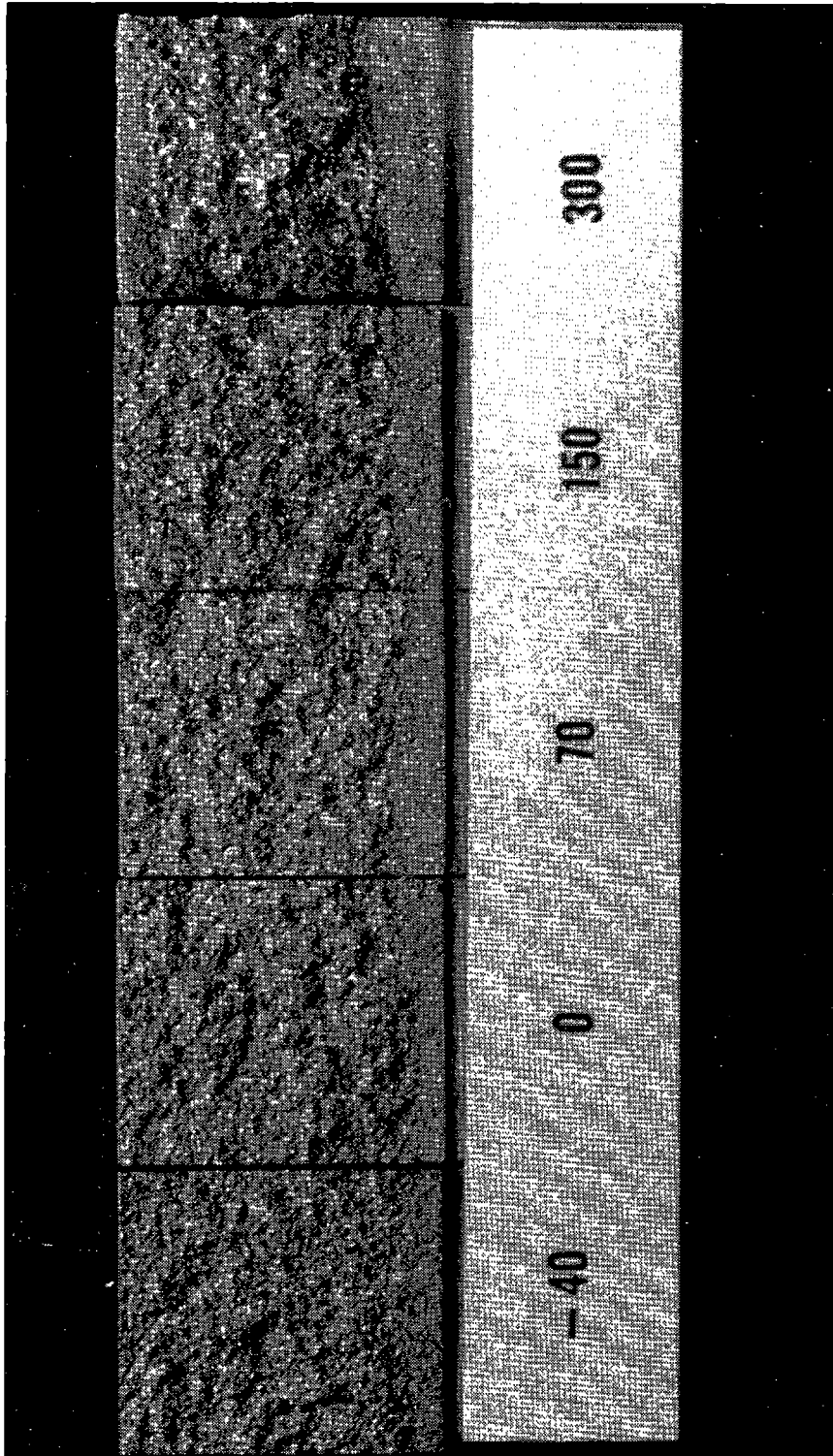
FIGURE 56.—K_{IC} FRACTURES FROM THE WROUGHT CLASS-U WHEEL RIM (NUMBERS INDICATE TEST TEMPERATURE), X1.7 MAGNIFICATION
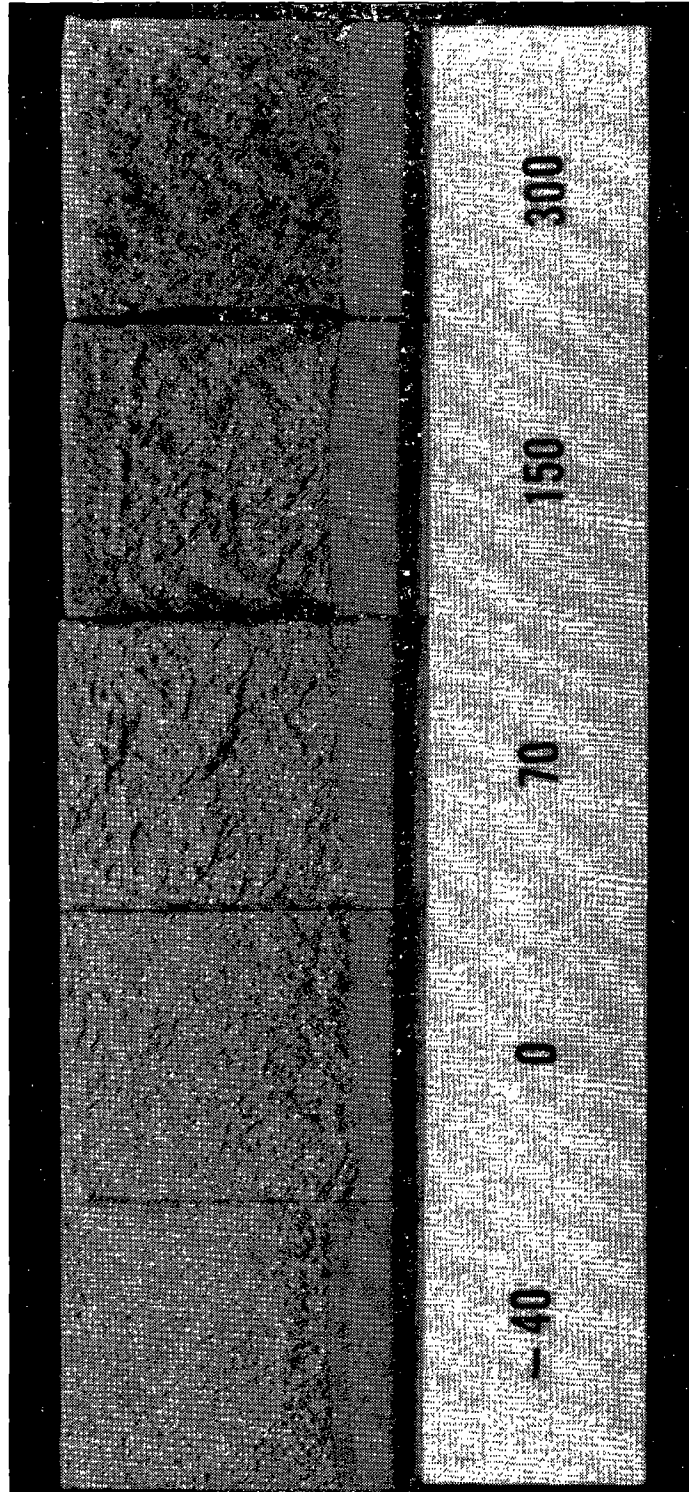
FIGURE 57.—K_{Ic} FRACTURES FROM THE WROUGHT CLASS A WHEEL RIM (NUMBERS INDICATE TEST TEMPERATURES), X1.7 MAGNIFICATION
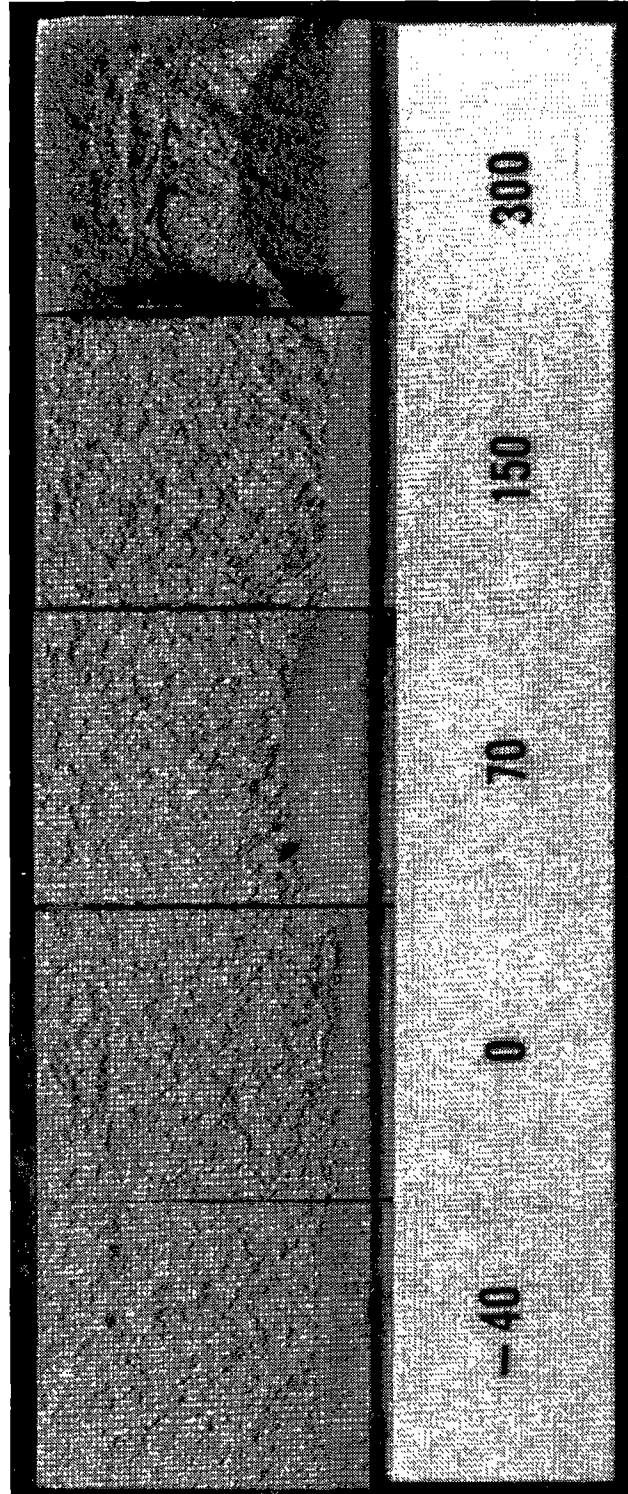
FIGURE 58.—K_{IC} FRACTURES FROM THE WROUGHT CLASS-C WHEEL RIM (NUMBERS INDICATE TEST TEMPERATURES), X1.7 MAGNIFICATION
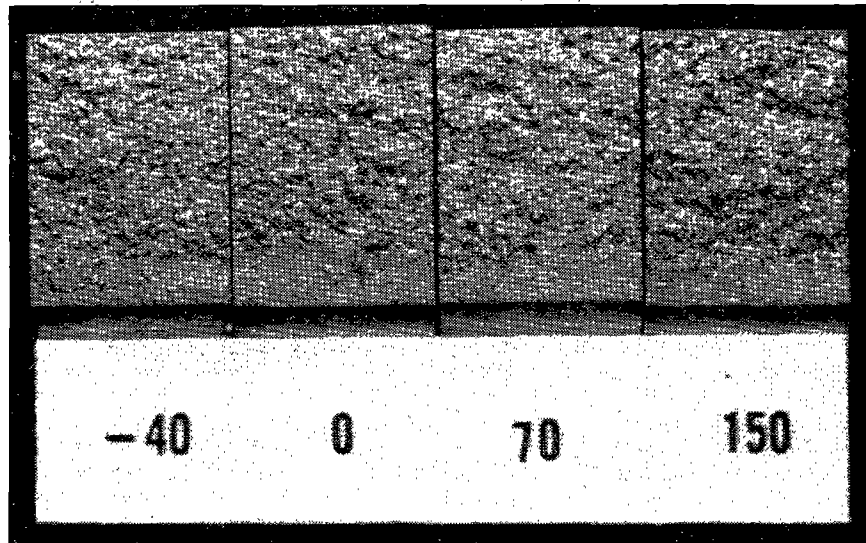
FIGURE 59.—K_{IC} FRACTURES FROM THE USED (WROUGHT CLASS-U) WHEEL
RIMS (NUMBERS INDICATE TEST TEMPERATURES), X1.7 MAGNIFICATION
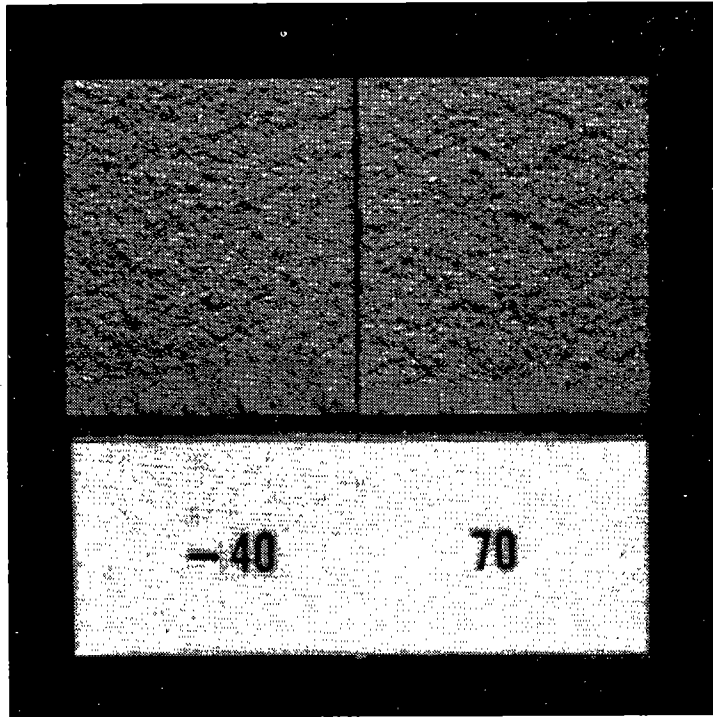
FIGURE 60.—K_{IC} FRACTURES FROM THE WROUGHT CLASS-CE WHEEL (NUMBERS INDICATE TEST TEMPERATURES), X1.7 MAGNIFICATION
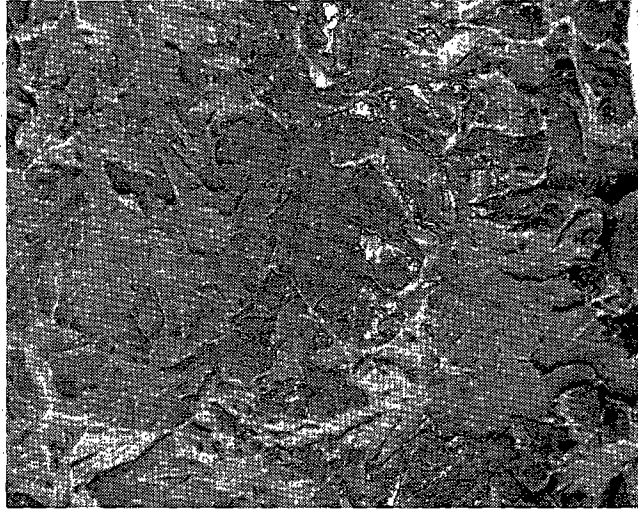
FIGURE 61.—FRACTOGRAPH (SEM) OF K_{IC} SPECIMEN FROM CAST CLASS-U WHEEL RIM (70°F), X110 MAGNIFICATION
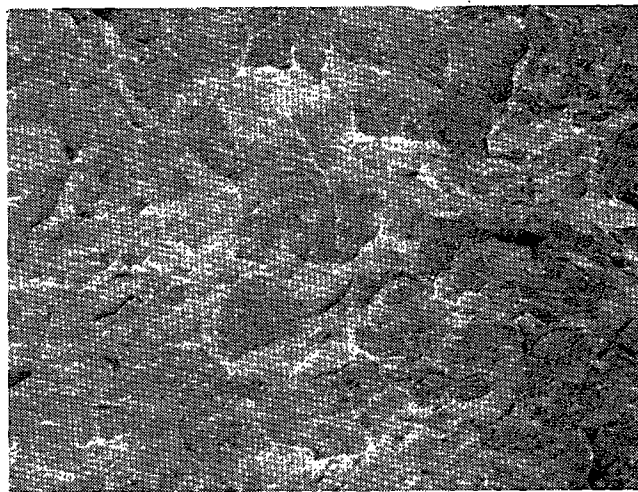
FIGURE 62.—FRACTOGRAPH (SEM) OF K_{IC} SPECIMEN FROM CAST CLASS-C WHEEL RIM (70°F), X110 MAGNIFICATION
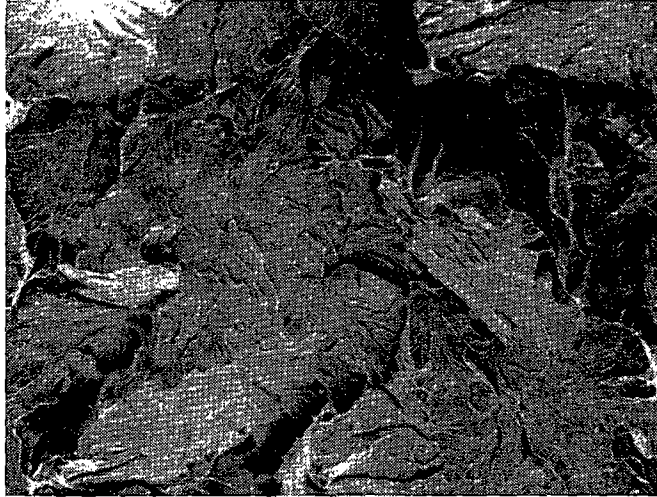
FIGURE 63.—FRACTOGRAPH (SEM) OF K_{IC} SPECIMEN FROM WROUGHT CLASS-U
WHEEL RIM (70°F), X110 MAGNIFICATION
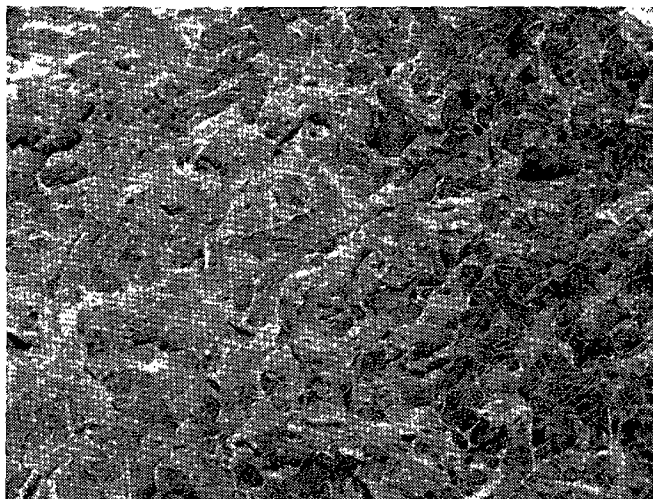
FIGURE 64.—FRACTOGRAPH (SEM) OF K_{IC} SPECIMEN FROM WROUGHT CLASS-A
WHEEL RIM (70°F), X110 MAGNIFICATION
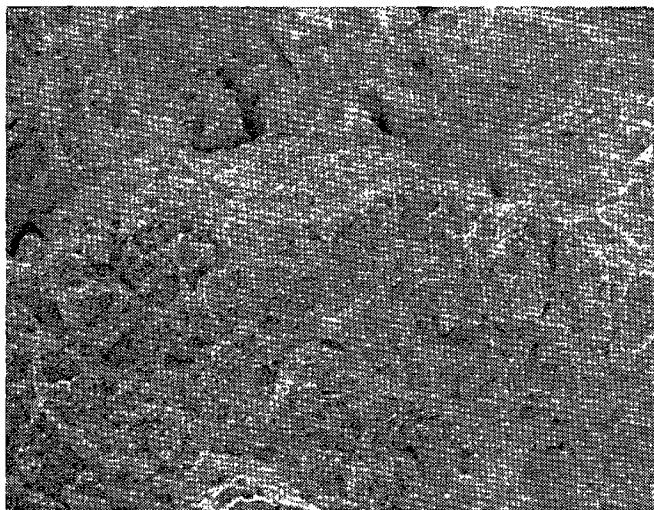
FIGURE 65.—FRACTOGRAPH (SEM) OF K_{IC} SPECIMEN FROM WROUGHT CLASS-A
WHEEL RIM (300°F), X110 MAGNIFICATION
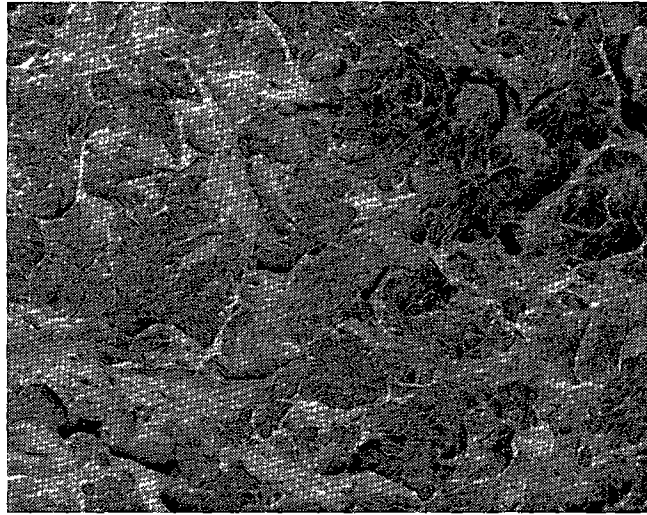
FIGURE 66.—FRACTOGRAPH (SEM) K_{IC} SPECIMEN FROM WROUGHT CLASS-C WHEEL RIM (70°F), X110 MAGNIFICATION

FIGURE 67.—FRACTOGRAPH (SEM) OF K_{IC} SPECIMEN FROM USED WROUGHT CLASS-U WHEEL RIM (70°F), X110 MAGNIFICATION
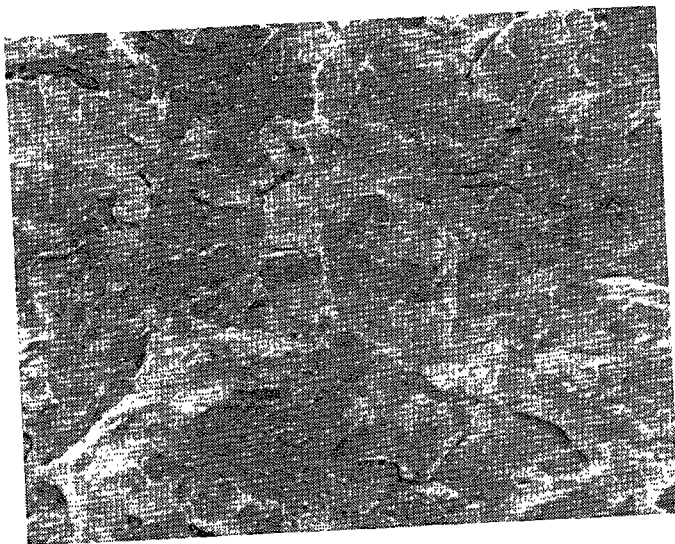
FIGURE 68.—FRACTOGRAPH (SEM) OF K_{IC} SPECIMEN FROM WROUGHT CLASS-CE
WHEEL RIM (70°F), X110 MAGNIFICATION
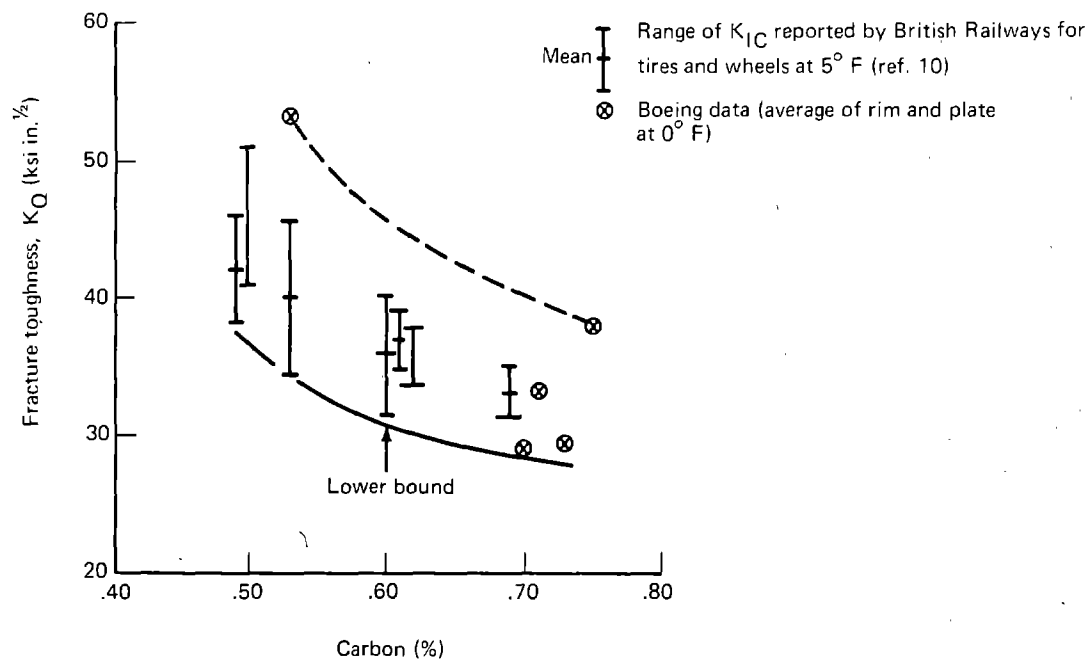
FIGURE 69.—EFFECT OF CARBON CONTENT ON FRACTURE TOUGHNESS (0°-5°F)
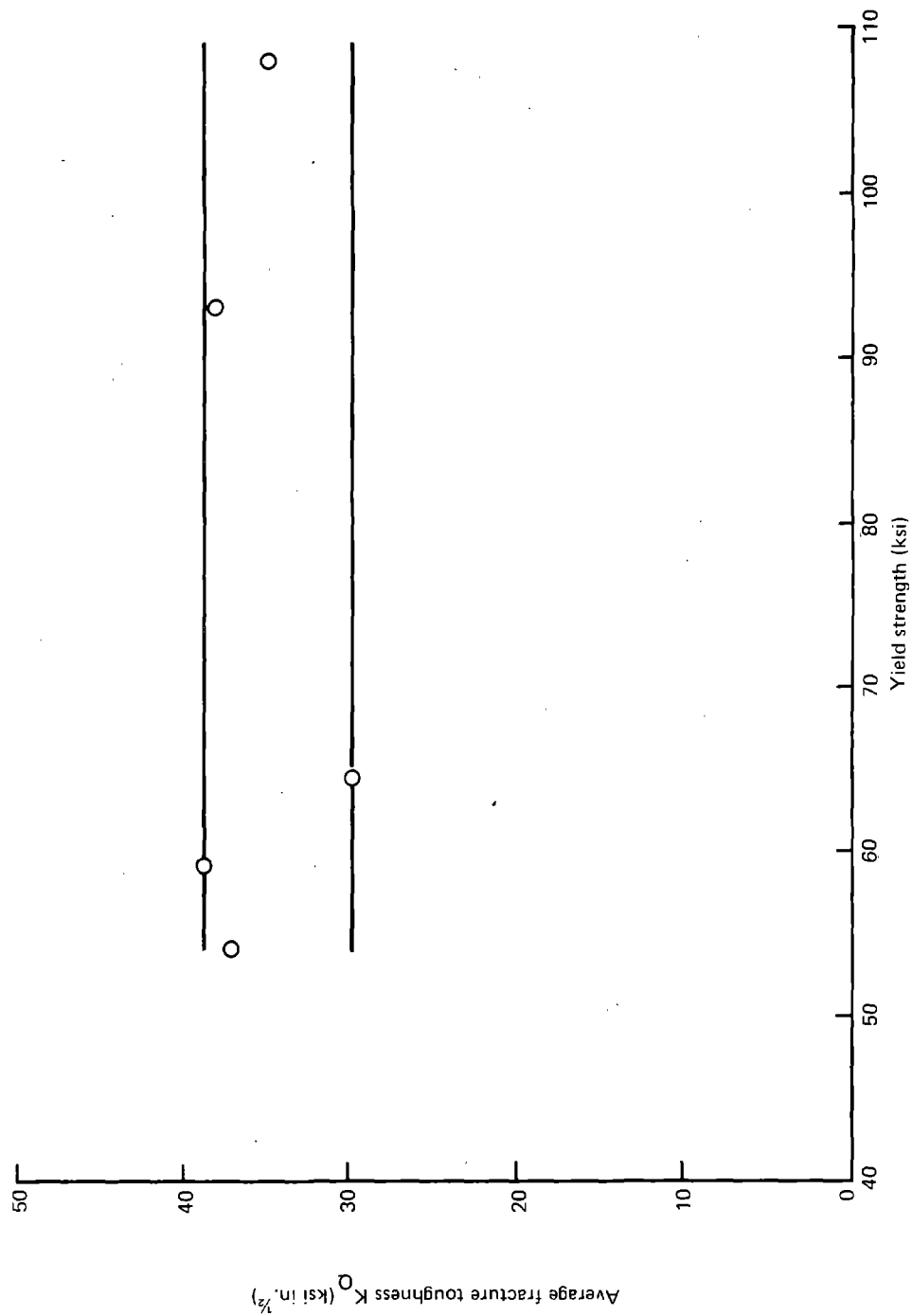
FIGURE 70.—RELATIONSHIP BETWEEN FRACTURE TOUGHNESS (AT 70°F) AND
YIELD STRENGTH FOR WHEEL RIMS CONTAINING 0.70-0.75% CARBON

129

O U, wrought
× U1, cast
△ A, wrought
□ B, wrought
◊ C, wrought
M = diesel locomotive wheel

Note: One crack in a U1 wheel that
extended completely through the
rim and into the plate to depth of
2 1/8 in. below the tread is not shown

Corner cracks identified as E

E ← through rim thickness
X
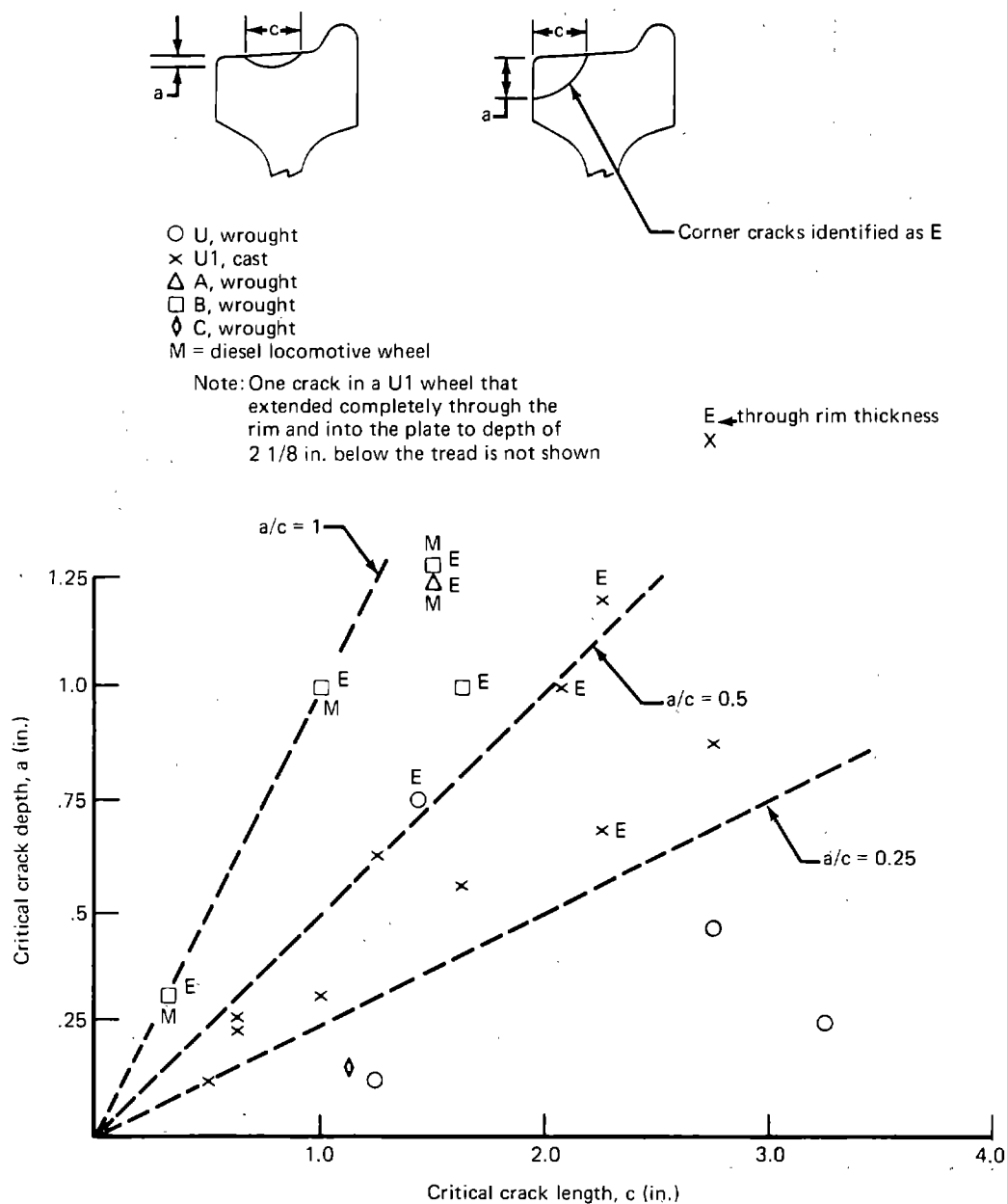
FIGURE 71.—CRITICAL SIZE OF TREAD THERMAL CRACKS FOR WHEEL FRACTURE

130
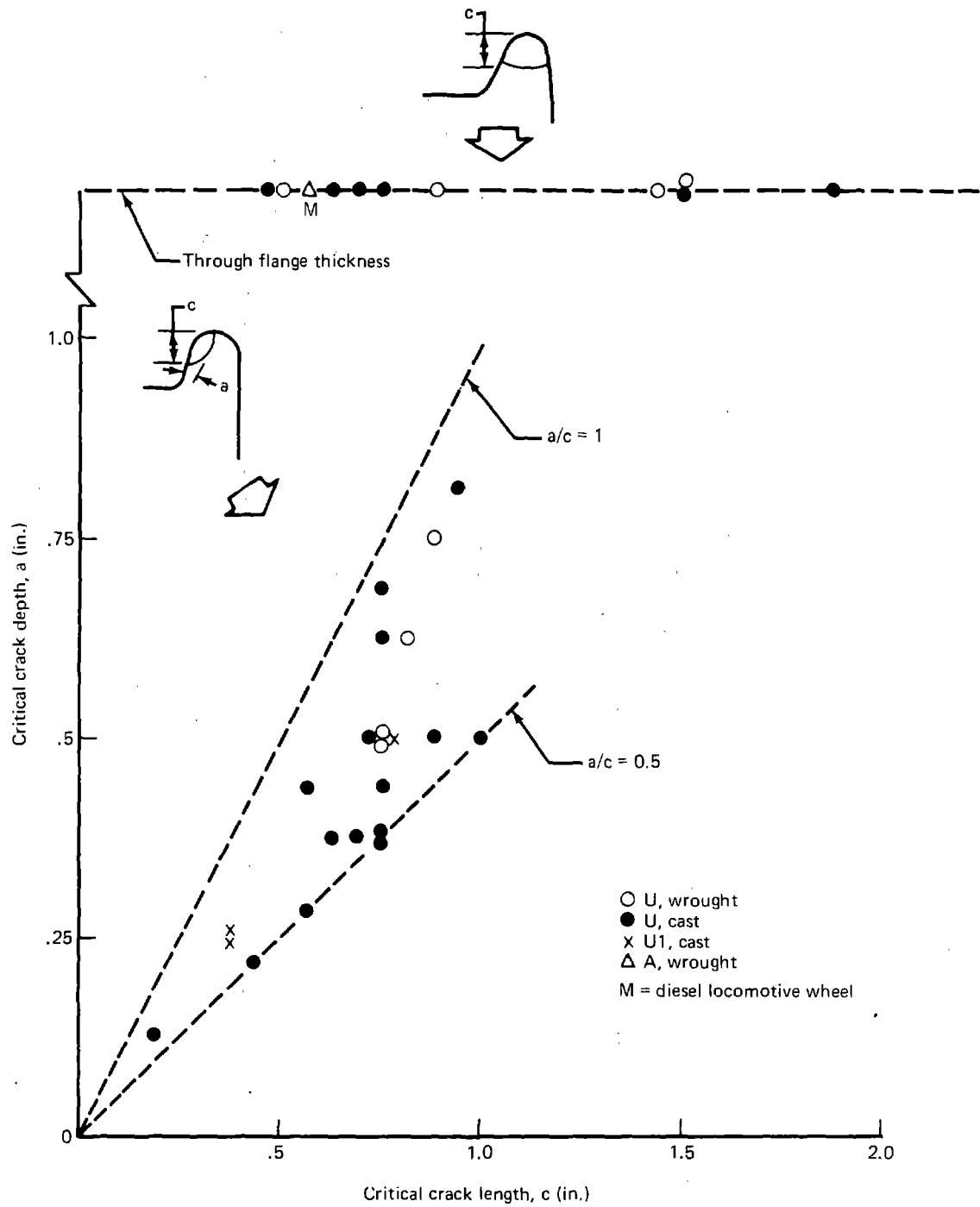
FIGURE 72.—CRITICAL CRACK SIZE AT FLANGE FOR WHEEL FRACTURE

131
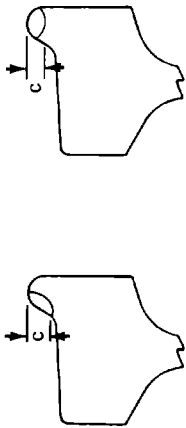
FIGURE 73.—HISTOGRAM OF CRITICAL CRACK LENGTH OF FLANGE THERMAL CRACKS FOR
WHEEL FRACTURE
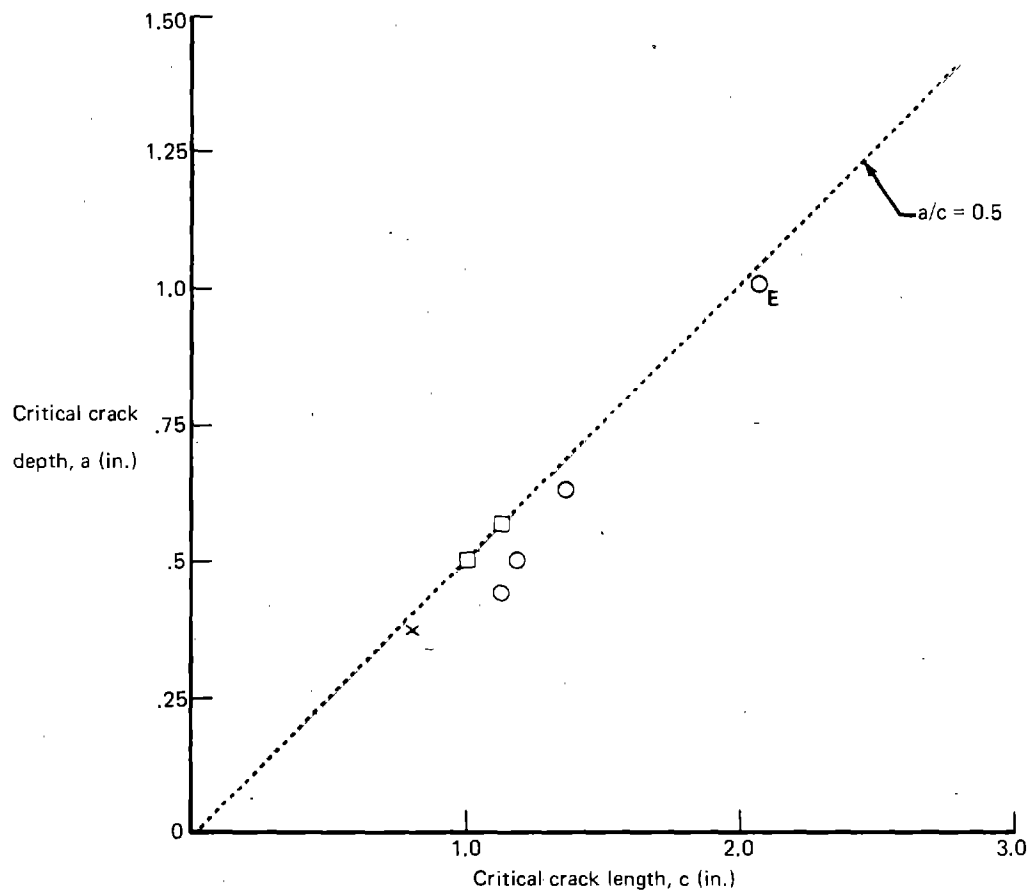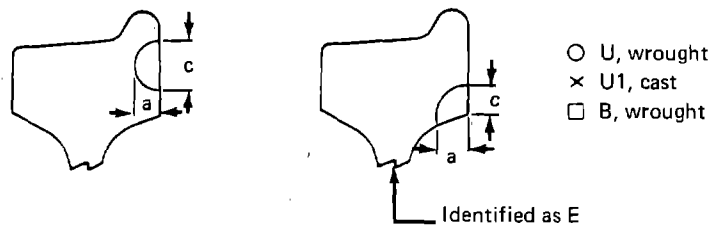
FIGURE 74.—CRITICAL SIZE OF THERMAL CRACKS AT REAR-RIM FACE FOR
WHEEL FRACTURE
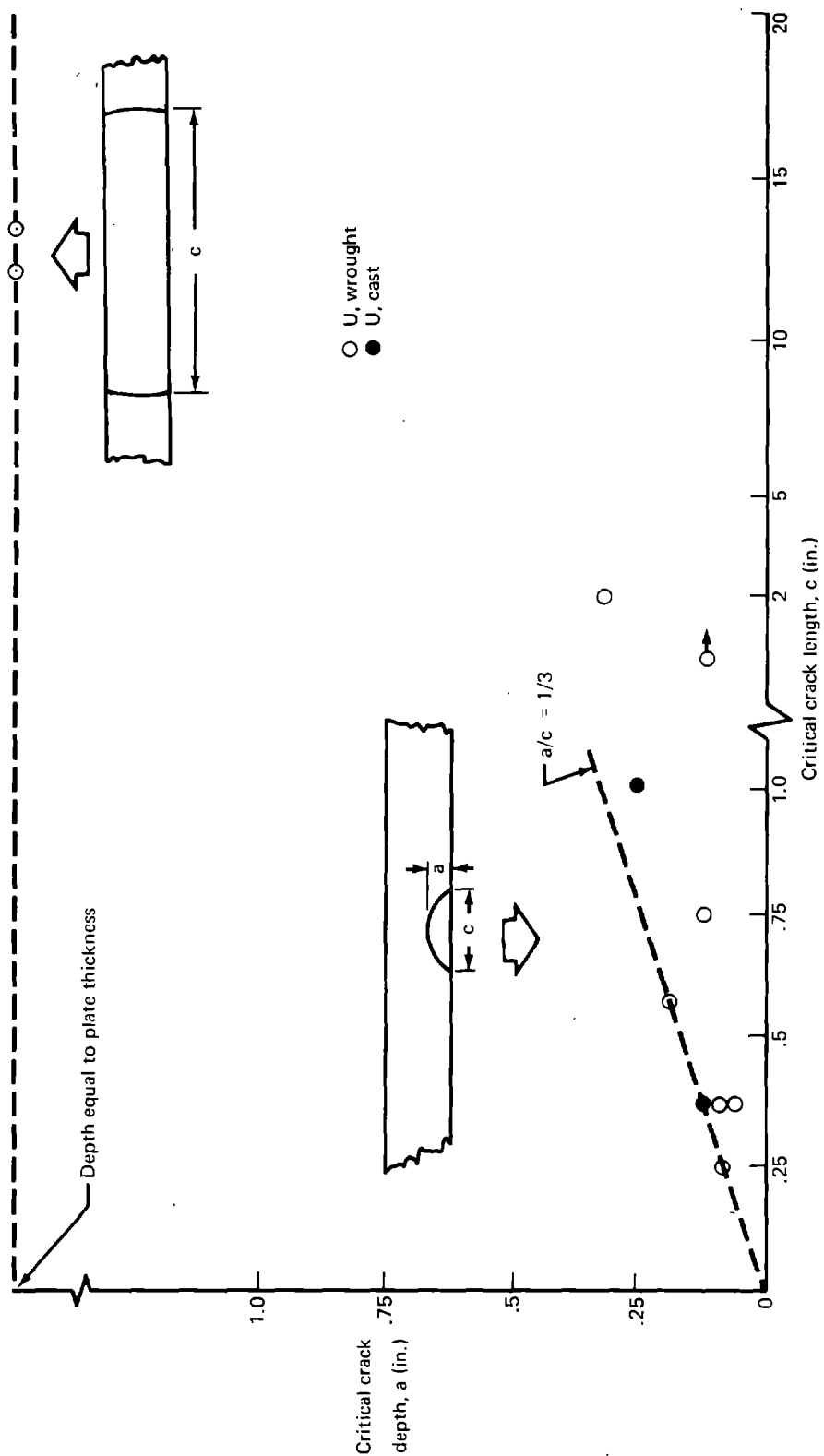
FIGURE 75.—CRITICAL CRACK SIZE AT FRONT HUB FILLET FOR PLATE FRACTURE
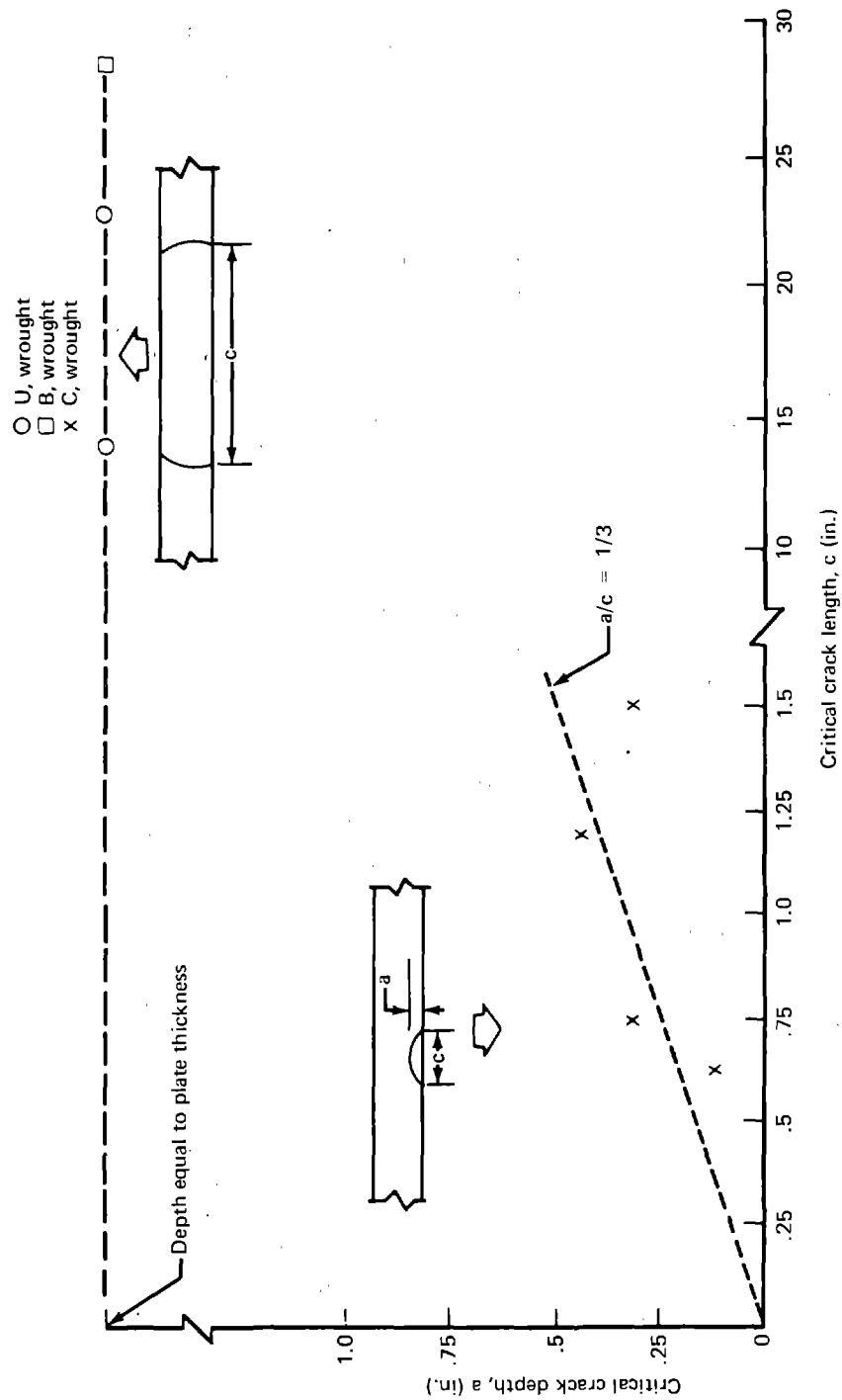
FIGURE 76.—CRITICAL CRACK SIZE AT REAR RIM FILLET FOR PLATE FRACTURE
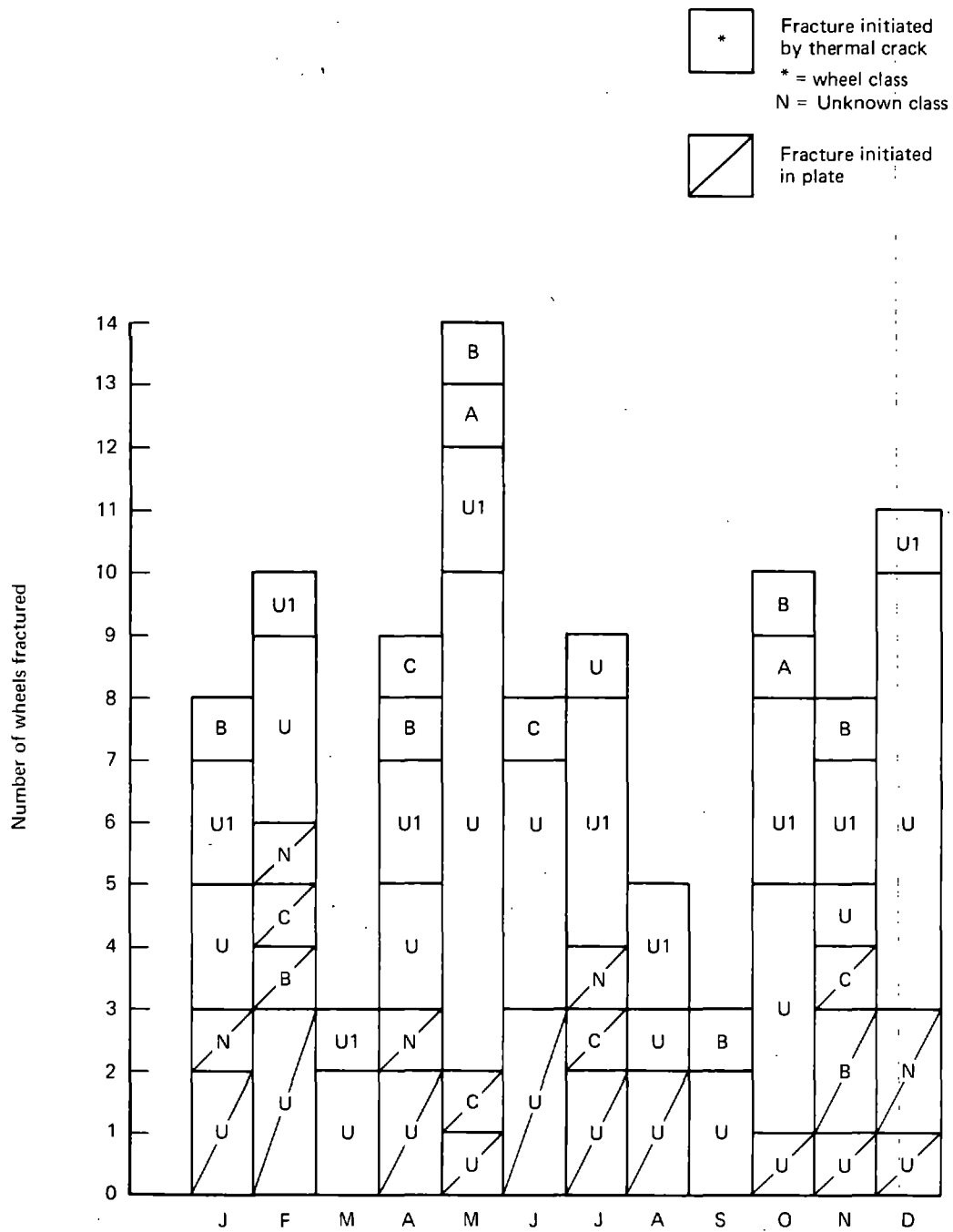
FIGURE 77.—INCIDENCE OF WHEEL FRACTURE WITH RESPECT TO TIME OF YEAR
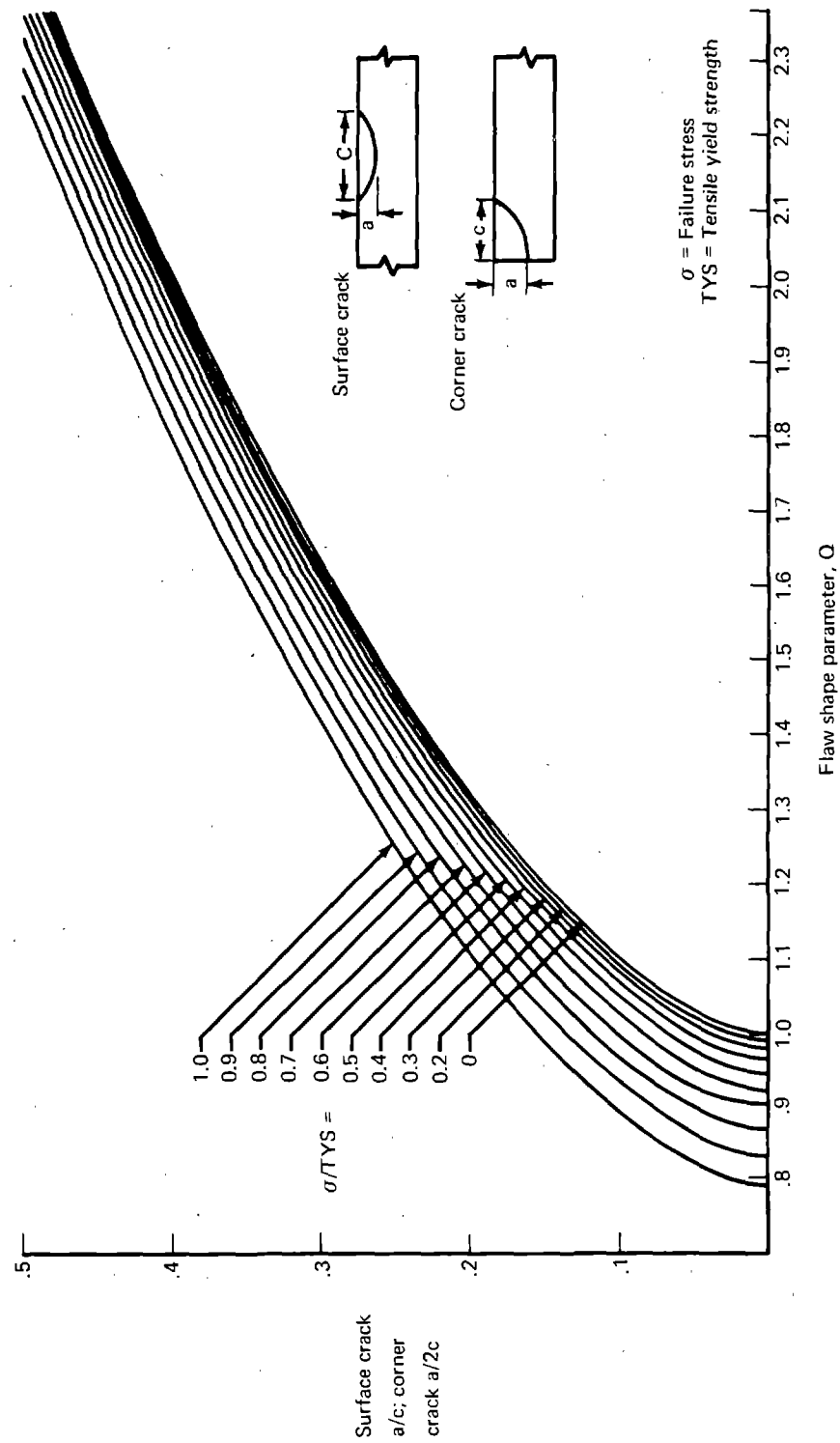
FIGURE 78.—SHAPE PARAMETER CURVES FOR SURFACE AND CORNER CRACKS

137
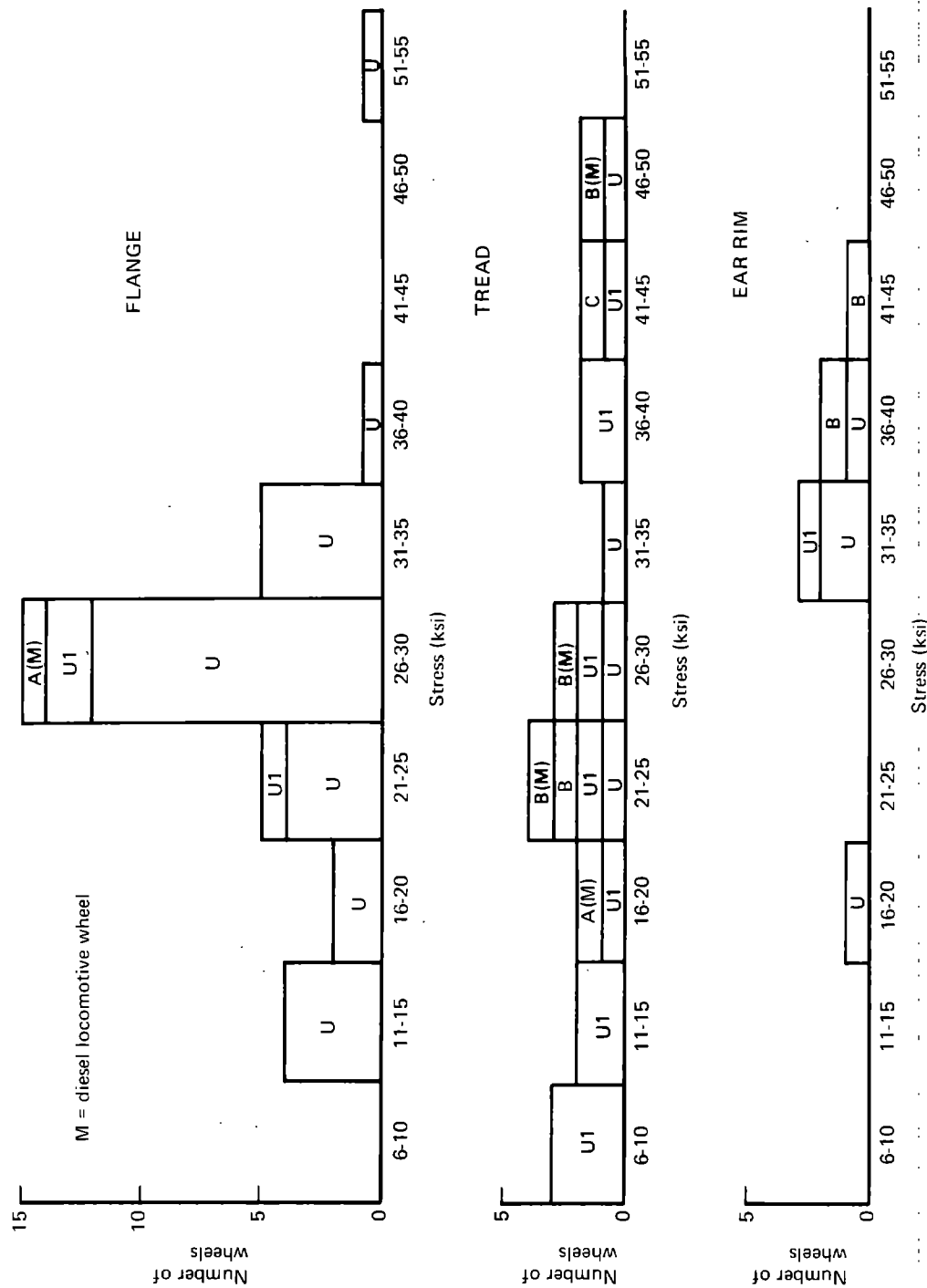
FIGURE 79.–SUMMARY OF ESTIMATED FAILURE STRESS FOR WHEELS THAT FRACTURED FROM THERMAL CRACKS

138

a) FRONT HUB FILLET,
   CLASS-U WHEELS
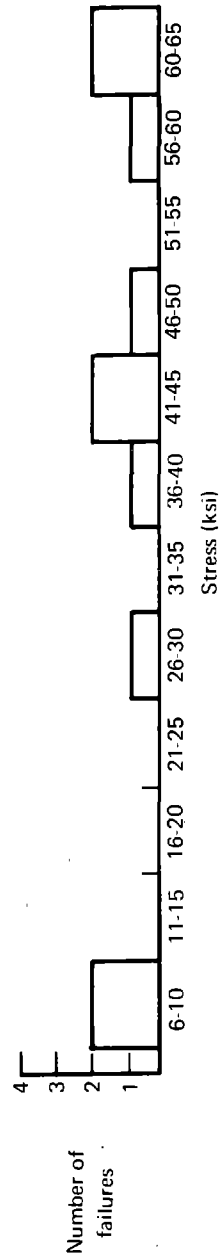
b) REAR RIM FILLET,
   CLASS-C WHEELS EXCEPT WHERE INDICATED
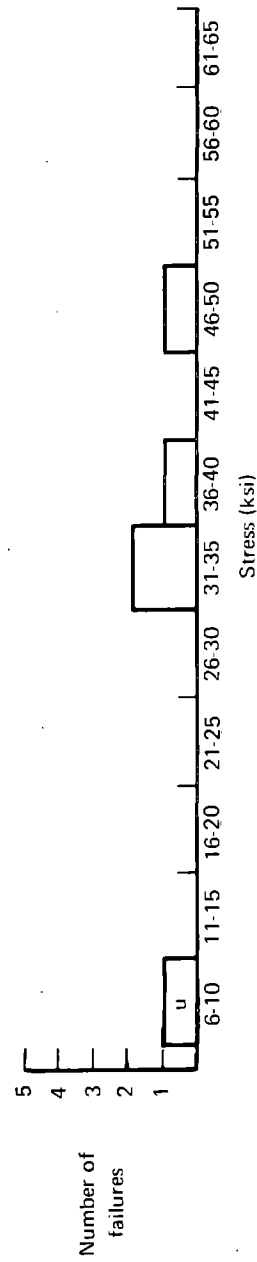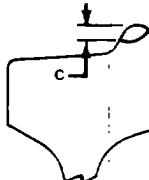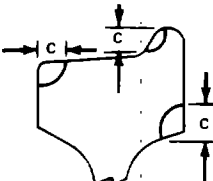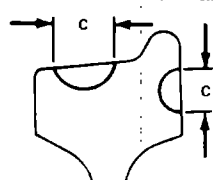
*FIGURE 80.—SUMMARY OF ESTIMATED FAILURE STRESSES THAT FRACTURED
FROM PLATE CRACKS*

Curve	Type of crack	Typical location
1	Through-thickness edge crack	
2	Corner crack	
3	Surface crack	
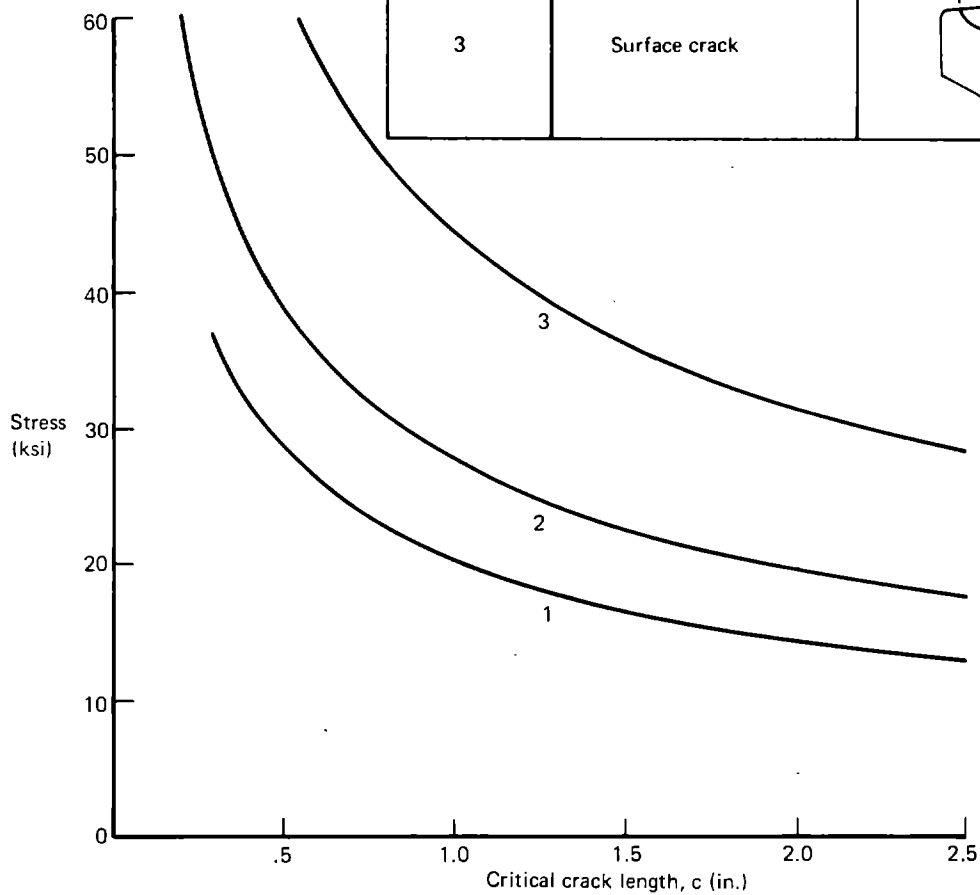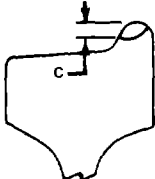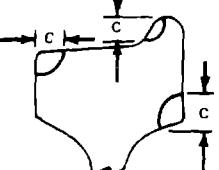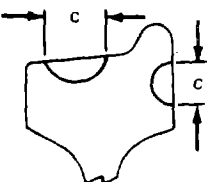
FIGURE 81.—APPLIED STRESS/CRITICAL CRACK LENGTH RELATIONSHIPS FOR THERMAL CRACKS IN CLASS-A WHEELS ($K_{IC} = 40$ KSI IN.$^{1/2}$)

Curve	Type of crack	Typical location
1	Through-thickness edge crack	
2	Corner crack	
3	Surface crack	
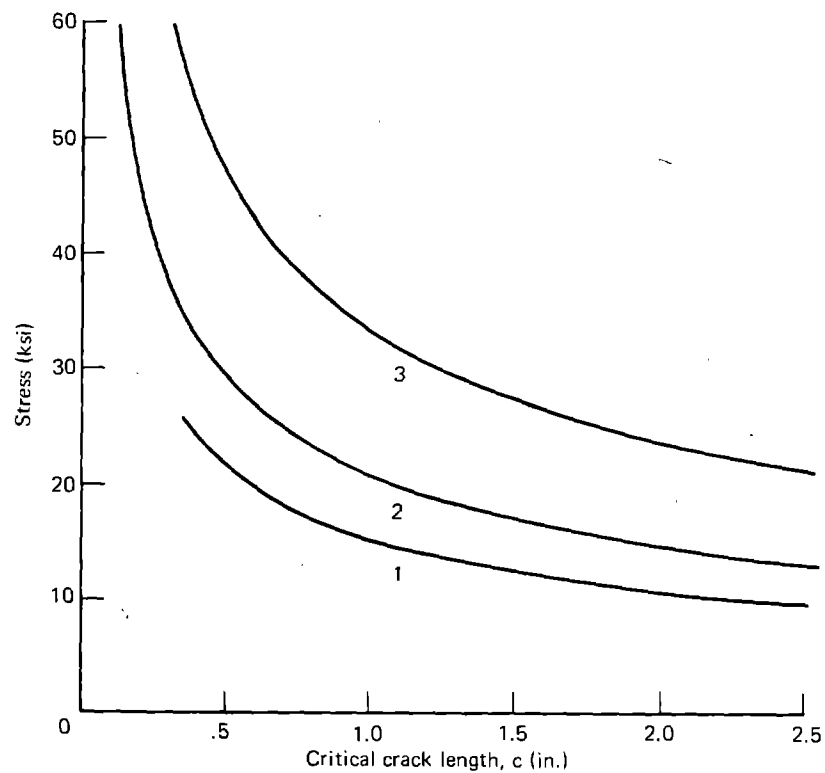
FIGURE 82.—APPLIED STRESS/CRITICAL CRACK LENGTH RELATIONSHIPS FOR THERMAL CRACKS IN CLASS-B WHEELS $(K_{IC} = 30\ KSI\ IN.\ ^{1/2})$

Curve	Type of crack	Typical location
1	Through-thickness edge crack	
2	Corner crack	
3	Surface crack	
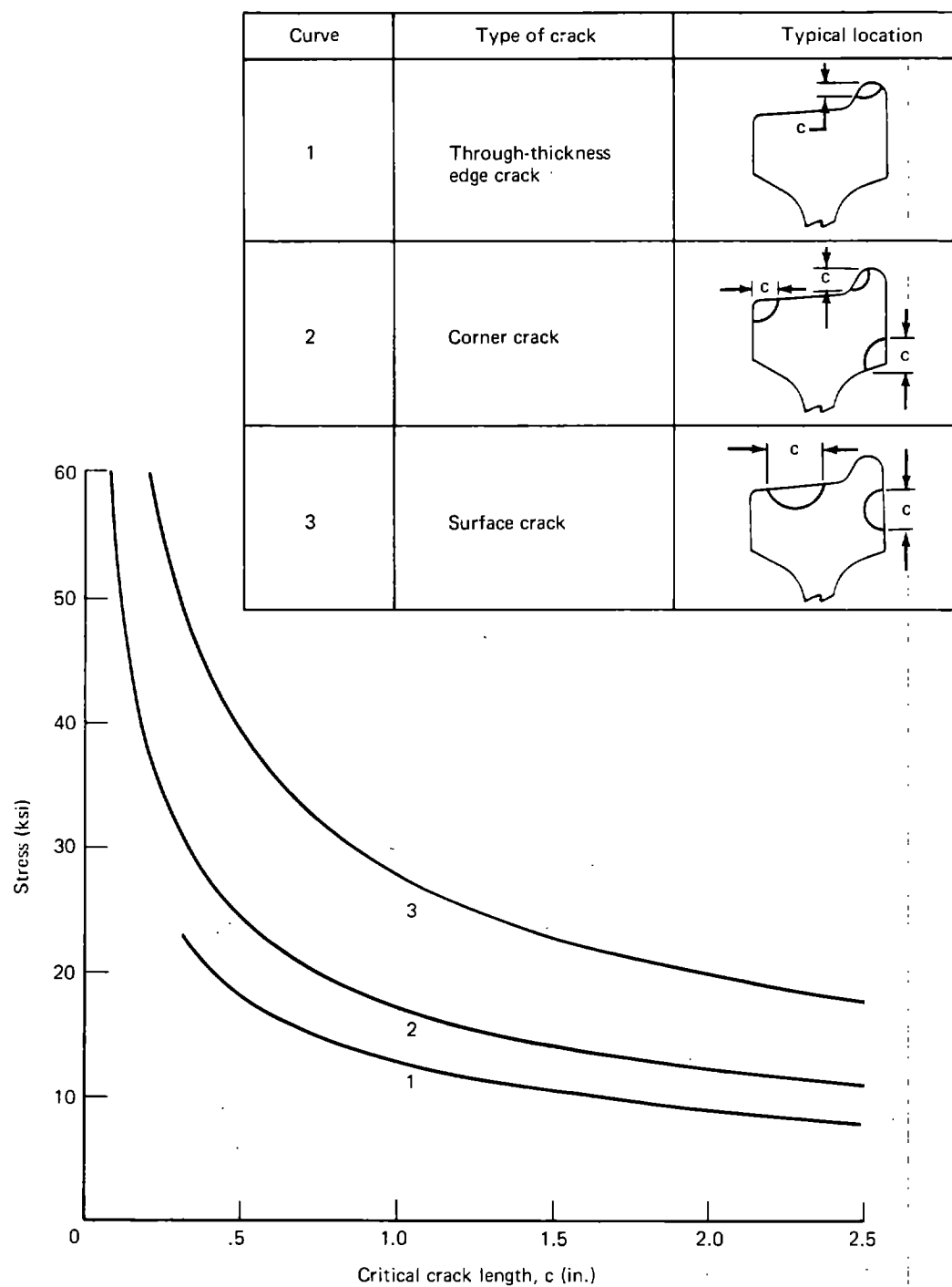
FIGURE 83.—APPLIED STRESS/CRITICAL CRACK LENGTH RELATIONSHIPS FOR
THERMAL CRACKS IN CLASS-C AND CLASS-U WHEELS (K_{IC} = 25 KSI IN.$^{1/2}$)

142
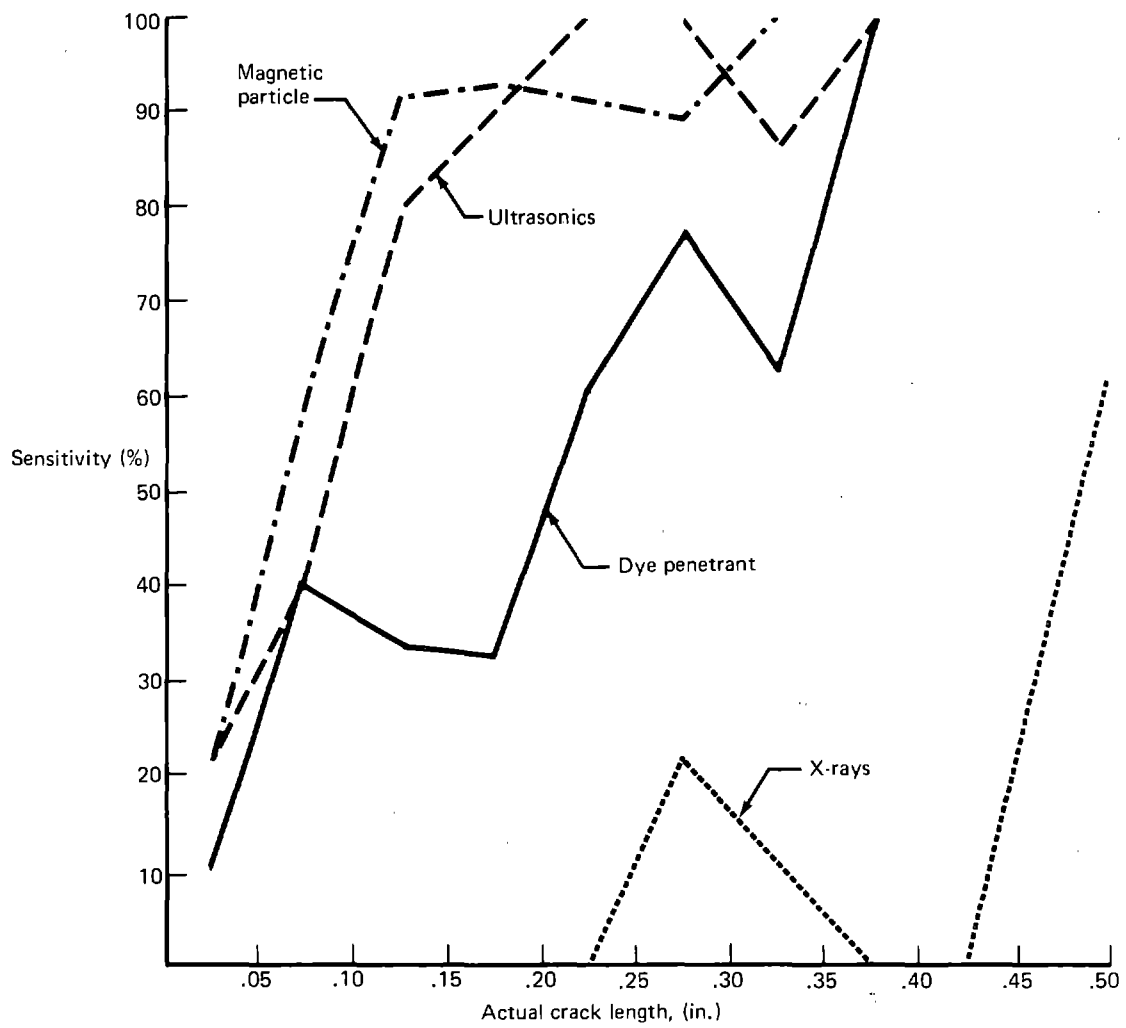
FIGURE 84.—SENSITIVITY OF NDT INDICATIONS IN DETECTING SURFACE FATIGUE
CRACKS IN 4330V MODIFIED STEEL SPECIMENS (AFTER PACKMAN ET
AL., REF. 41)

143
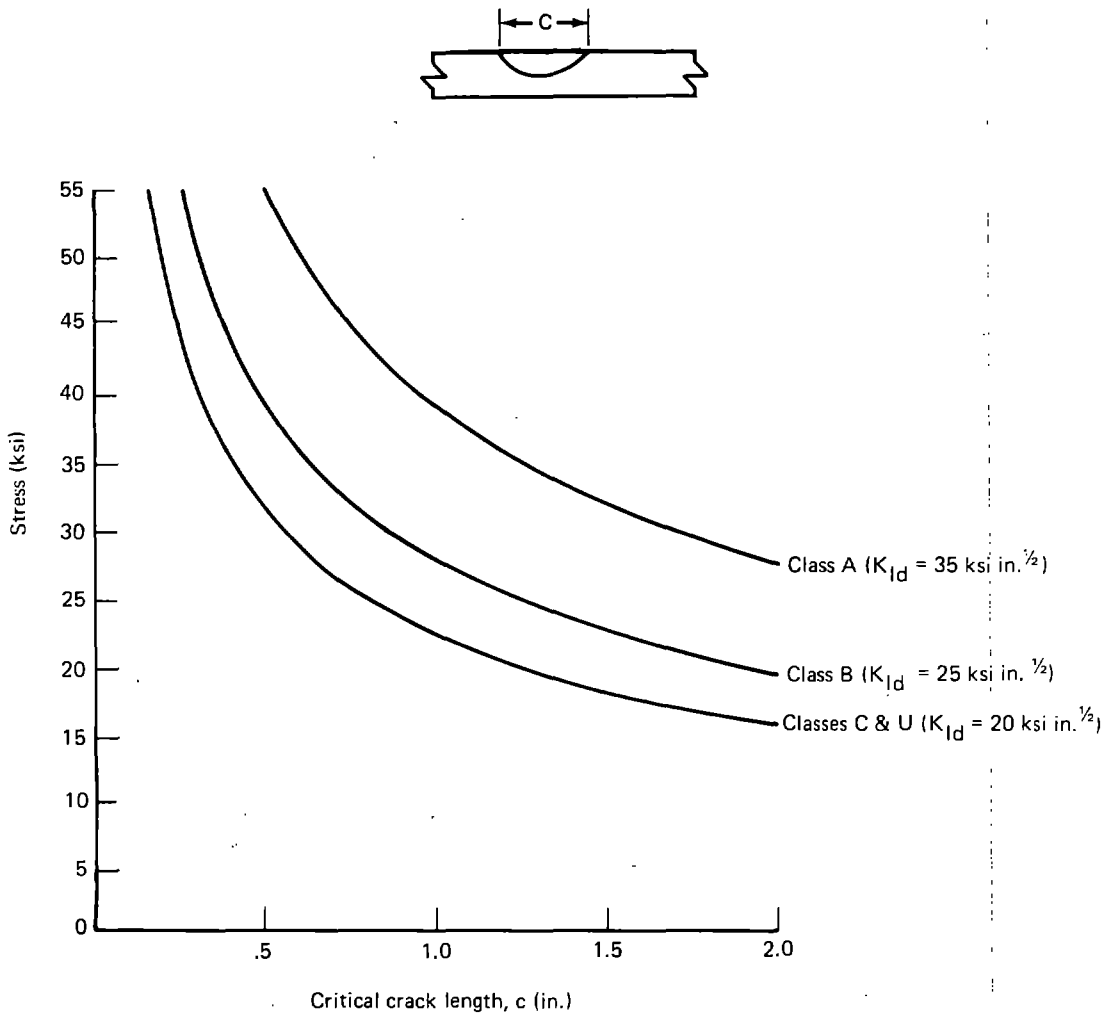
FIGURE 85.—APPLIED STRESS/CRITICAL CRACK LENGTH RELATIONSHIPS FOR
SURFACE CRACKS IN WHEEL PLATES

144
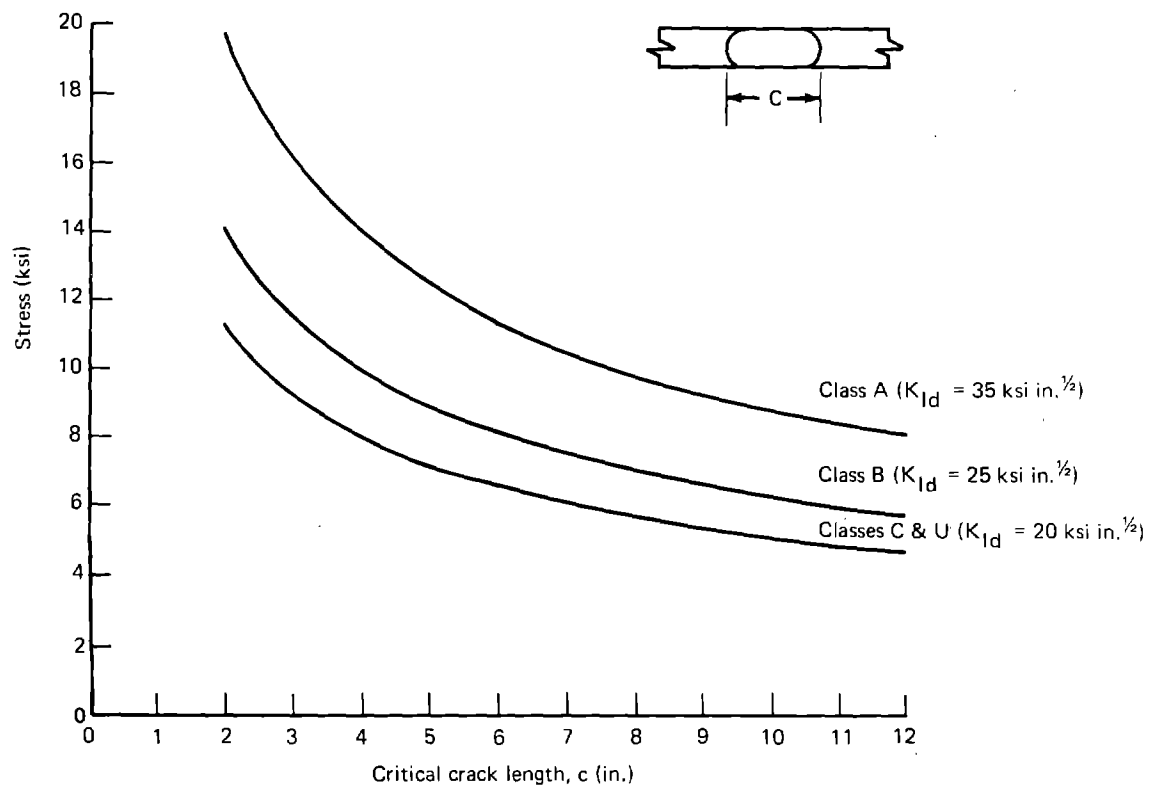
FIGURE 86.—APPLIED STRESS/CRITICAL CRACK LENGTH RELATIONSHIPS FOR
THROUGH-THICKNESS CRACKS IN WHEEL PLATES

APPENDIX A

TABLE A1.—MINIMUM JANUARY TEMPERATURES ENCOUNTERED BY U.S. RAILROADS FOR THE PERIOD 1931-1960

State	Location	Major railroads	Mean minimum (° F)	Lowest recorded (° F)
Alabama	Birmingham	L&N, IC, SCL, SLSF, SOU	36.3	- 4
	Mobile	L&N, SOU, GM&O	43.7	8
Alaska	Anchorage	Alaska	4.3	-38
	Fairbanks	Alaska	-21.4	-61
Arizona	Flagstaff	AT&SF	14.1	-20
	Phoenix	AT&SF, SP	35.3	20
Arkansas	Fort Smith	MP, SLSF	29.4	0
	Little Rock	MP, CRI&P	30.5	- 4
California	Bakersfield	AT&SF, SP	37.4	25
	Sacramento	SP, WP	37.2	23
Colorado	Alamosa	D&RGW	- 0.8	-50
	Denver	D&RGW, UP, BN	14.8	-25
Connecticut	Hartford	NYNH&H	17.3	-26
Delaware	Wilmington	B&O, PC	25.5	- 4
D.C.	Washington	B&O, PC	29.5	3
Florida	Jacksonville	SOU, SCL	45.0	12
	Tallahassee	SCL	42.7	10
Georgia	Atlanta	SCL, SOU, L&N	37.3	- 3
	Savannah	SCL	40.9	9
Idaho	Lewiston	UP, BN	23.7	-22
	Pocatello	UP	13.0	-19
Illinois	Chicago	BN, AT&SF, B&O, CRI&P, N&W, C&NW	19	-16
	Springfield	N&W, GM&O, IC, B&O	20.5	-22
Indiana	Fort Wayne	N&W, PC	19.6	-18
	Indianapolis	N&W, B&O, PC, IC	21.0	-18
Iowa	Des Moines	C&NW, CRI&P, BN, N&W, CGW	11.3	-24
	Waterloo	CGW, CRI&P, IC	8.9	-34
Kansas	Topeka	AT&SF, UP, CRI&P, MP	19.0	- 9
	Wichita	AT&SF, CRI&P, MP, SLSF	22.3	-12
Kentucky	Louisville	L&N, SOU, PC, IC	26.5	-20
Louisiana	Baton Rouge	IC	42.3	10
	Shreveport	IC, SLSW	38.3	3
Maine	Caribou	CP	1.1	-41
	Portland	MC, B&M	11.7	-39
Maryland	Baltimore	B&O, PC	44.1	- 7
Massachusetts	Boston	B&M, PC, NYNH&H	23.0	- 4
	Pittsfield	PC, NYNH&H	13.1	-25
Michigan	Escanaba	C&NW, SL	10	-31
	Detroit	PC, C&O	20.7	-16
Minnesota	International Falls	BN	- 8.1	-46
	Minneapolis	C&NN, BN, SL	2.3	-34
Mississippi	Meridian	GM&O, SOU, IC	36.8	6

State	Location	Major railroads	Mean minimum (°F)	Lowest recorded (°F)
Missouri	St. Joseph	CRI&P, MP, AT&SF, UP, BN	17.1	-14
	St. Louis	GM&O, CRI&P, SLSF, MP, N&W	23.5	-11
Montana	Butte	BN, CMSP&P, UP	0.4	-52
	Great Falls	BN, CMSP&P	12.5	-43
Nebraska	Lincoln	BN, UP, C&NW	16.2	-18
	Omaha	C&NW, UP, BN, CRI&P	12.9	-17
Nevada	Winnemuca	SP, WP	14.7	-24
New Hampshire	Concord	B&M	10.6	-23
New Jersey	Trenton	PC, READ	26.2	-14
New Mexico	Alburquerque	AT&SF	23.5	- 7
	Clayton	BN	20.2	-21
New York	New York	PC, EL, NYNH&H	26.9	-15
	Syracuse	PC, EL	16.5	-26
N. Carolina	Asheville	SOU	30.4	- 7
	Raleigh	SCL, SOU	31.3	0
N. Dakota	Bismarck	SL, BN	0.1	-43
	Devils Lake	SL, BN	-4.7	-46
Ohio	Cleveland	N&W, PC, EL, B&O	21.3	-19
	Columbus	B&O, PC, C&O	22.0	-19
Oklahoma	Oklahoma City	MKT, SLSF, CRI&P, AT&SF	28.1	1
	Tulsa	MKT, SLSF, AT&SF	26.5	- 3
Oregon	Pendleton	UP, BN	25.1	-22
	Portland	UP, BN, SP	35.5	3
Pennsylvania	Philadelphia	PC, READ	24.3	- 5
	Pittsburg	B&O, PC	24.7	-13
Rhode Island	Providence	N/NH&H	21.0	- 5
S. Carolina	Greenville	SOU, G&N, SCL	35.0	8
	Charleston	SCL	38.3	8
S. Dakota	Aberdeen	CMSP&P, C&NW, BN	0	-39
	Sioux Falls	C&NW, BN, CMSP&P	5.2	-36
Tenessee	Memphis	IC, L&N, SOU, SLSF, MP	32.4	-13
Texas	Houston	MKT, SP, MP, AT&SF	46.6	10
	Lubbock	AT&SF, BN	25.4	-16
Utah	Milford	UP	12.1	-28
	Salt Lake City	D&RGW	17.5	-18
Vermont	Burlington	VT	6.9	-27
Virginia	Lynchburg	C&O, N&W, SOU	29	- 4
	Richmond	SCL, SOU, C&O	29	-12
Washington	Spokane	BN, UP	19.2	-25
	Walla Walla	BN, UP	27.4	-16
West Virginia	Charleston	C&O, PC	27.9	-12
	Parkersburg	B&O	26.3	-27
Wisconsin	Green Bay	CMSP&P, C&NW	8.5	-29
	Madison	CMSP&P, C&NW	9.1	-30
Wyoming	Casper	C&NW, BN	13.9	-31
	Cheyenne	UP, BN	13.6	-27

APPENDIX B

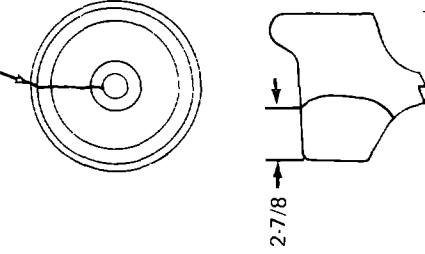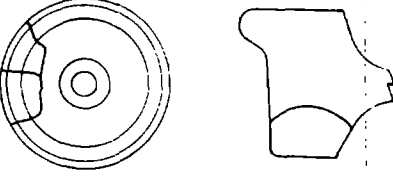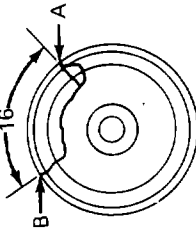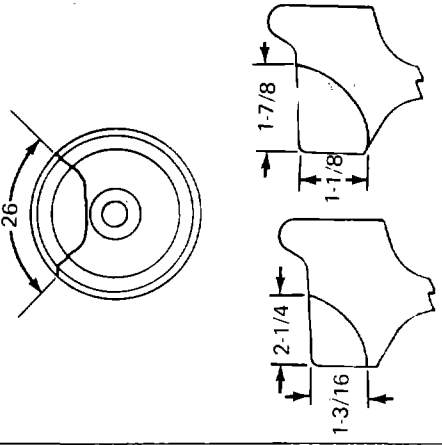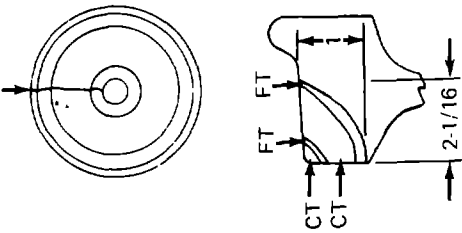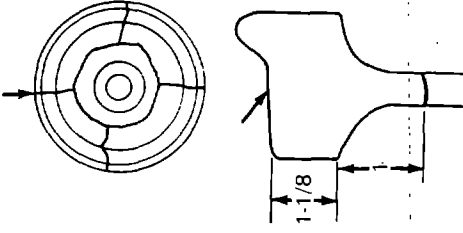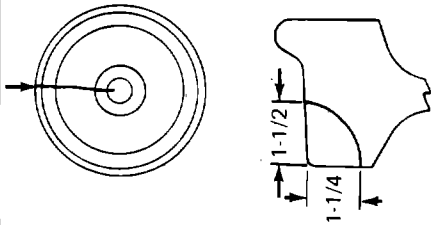*TABLE B1.—FRACTURES INITIATED AT THE TREAD SURFACE*
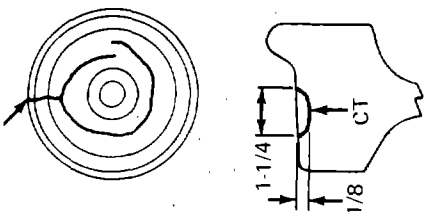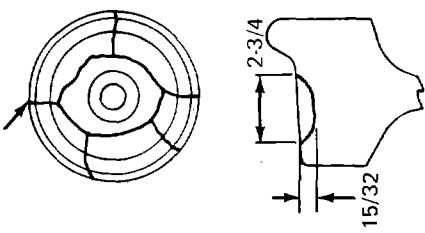
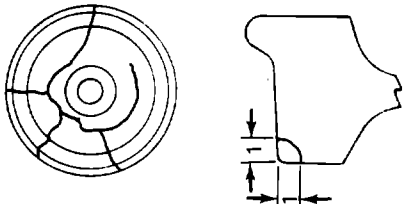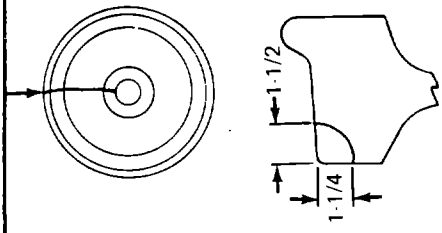| Wheel design	Class	Age (yr)	Rim thickness (in.)	Month failed	Sketch of cracked wheel and initial crack	Calculated failure stress (ksi)	Remarks
36 in (Wr) 1W	U (0.72C, 0.72 Mn)	5	1-5/16	April		47	1) Tread microstructure altered by heat to depth of 1/8 in. over 1-1/2 in. in initiation area.
36 in (Wr) 1W	U	3	1-7/16	December		29	Tread microstructure altered by heat in initiation area.
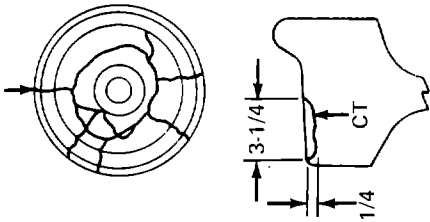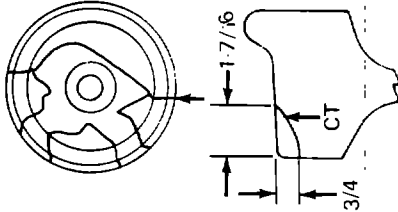
149

TABLE B1.—CONTINUED

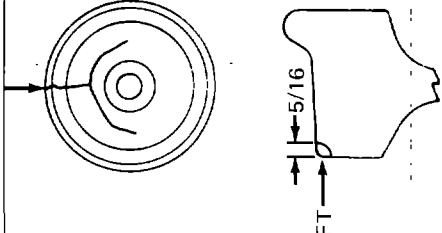| Wheel design	Class	Age (yr)	Rim thickness (in.)	Month failed	Sketch of cracked wheel and initial crack	Calculated failure stress (ksi)	Remarks
36 in (Wr) 1W	U (0.75C, 0.77 Mn)	3	1-7/16	March		35	Tread microstructure altered by heat to a max. depth of 5/16 over outer 3 in. of tread.
H36 (Wr) 1W	U (0.82C, 1.58 Mn)	5	—	December		22	1) Tread microstructure altered by heat to a depth of 1/16 in. in initiation area. 2) Mn content exceeds spec M107 maximum.
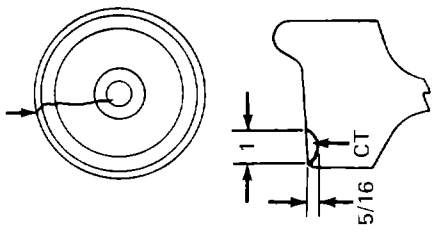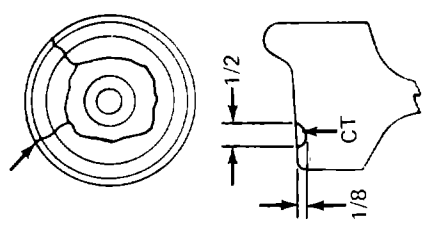
150

TABLE B1.—CONTINUED

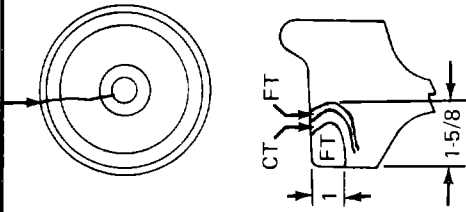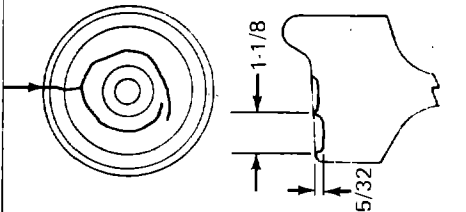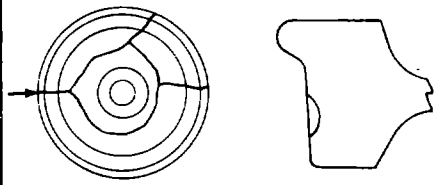| Wheel design	Class	Age (yr)	Rim thickness (in.)	Month failed	Sketch of cracked wheel and initial crack	Calculated failure stress (ksi)	Remarks
33 in (cast)	U1 (1.10C, 0.61 Mn)	8	1-9/32	April		29	
33 in (cast)	U1 (1.14C, 0.78 Mn)	8	1-3/8	November		43	
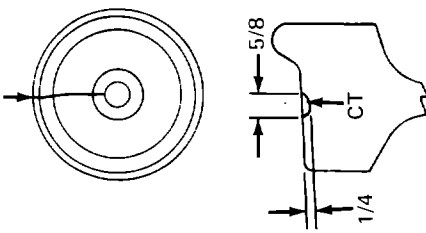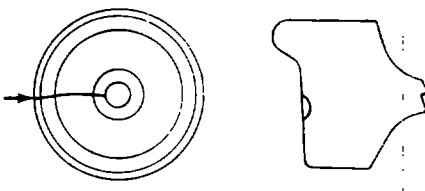
151

TABLE B1.—CONTINUED

Wheel design	Class	Age (yr)	Rim thickness (in.)	Month failed	Sketch of cracked wheel and initial crack	Calculated failure stress (ksi)	Remarks
33 in. (cast) 1W	U1 (1.19C 0.61 Mn)	13	1-1/4	January		36	Tread area showed evidence of metallurgical change due to heat in initiation area.
33 in (cast)	U1 (1.22C 0.72 Mn)	5	1-1/4	October		—	1) Tread microstructure altered by heat to 3/16 depth in initiation area. 2) Crack size not established due to damage.
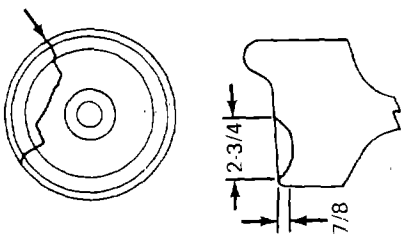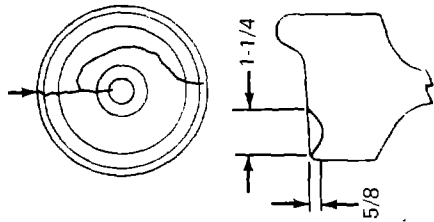
152

Wheel design	Class	Age (yr)	Rim thickness (in.)	Month failed	Sketch of cracked wheel and initial crack	Calculated failure stress (ksi)	Remarks
33 in (cast) 1W	U1	13	—	July	(2-3/4, 7/8)	18	
33 in (cast) 1W	U1	14	—	March	(1-1/4, 5/8)	25	

TABLE B1. -CONTINUED
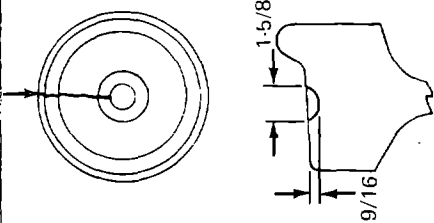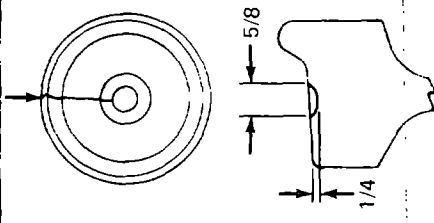
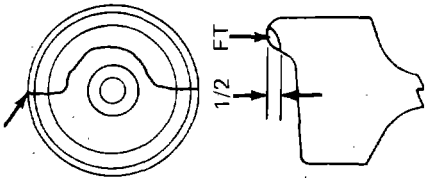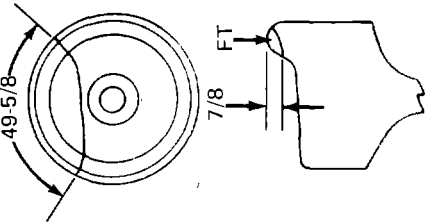| Wheel design	Class	Age (yr)	Rim thickness (in)	Month failed	Sketch of cracked wheel and initial crack	Calculated failure stress (ksi)	Remarks
33 in (cast)	U1 (1.18C, 0.63 Mn)	5	1	November	1-5/8, 9/16	23	1) Tread microstructure altered by heat to a depth of 1/8 in. in initiation area.
33 in (cast) 1W	U1 (1.19C, 0.61 Mn)	13	1-1/4	January	5/8, 1/4	36	1) Tread microstructure altered by heat to a depth exceeding 1/16 in. in initiation area.
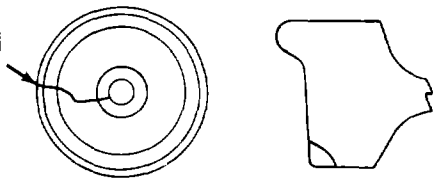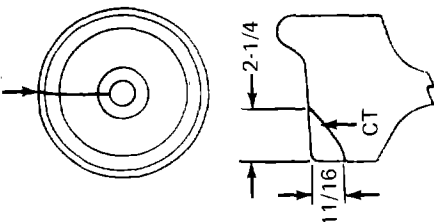
154

TABLE B1.—CONTINUED

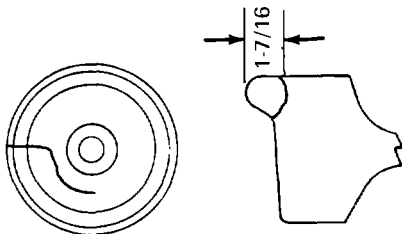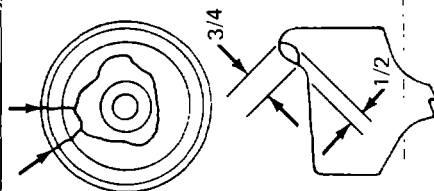| Wheel design	Class	Age (yr)	Rim thickness (in.)	Month failed	Sketch of cracked wheel and initial crack	Calculated failure stress (ksi)	Remarks
33 in (cast) 1W	U1	9	1	August		—	Crack size not recorded
33 in (cast)	U1	14	1-1/16	May		15	

TABLE B1.—CONTINUED

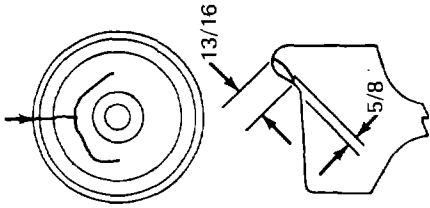| Wheel design	Class	Age (yr)	Rim thickness (in.)	Month failed	Sketch of cracked wheel and initial crack	Calculated failure stress (ksi)	Remarks
33 in (cast)	U1 (1.27C, 0.80 Mn)	4	—	July	2-7/8	7	Tread microstructure altered by heat to a depth of 3/32 in. along outer 1 in. of thread.
33 in (cast)	U1 (1.20C, 0.83 Mn)	8	1-3/8	December		—	Crack dimensions not established due to fracture face damage but a secondary fracture contained a thermal crack which extended thru the rim thickness for 1-1/2 in. from outer edge of rim.

156

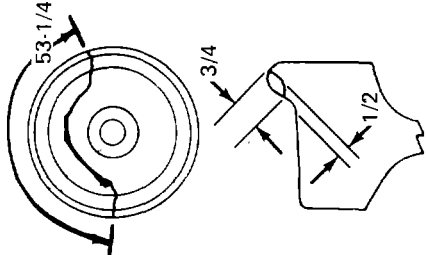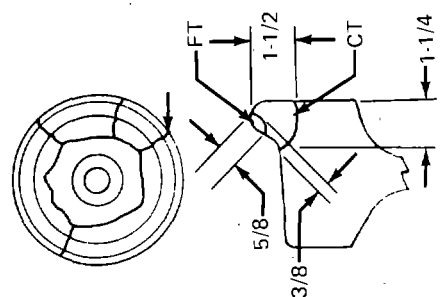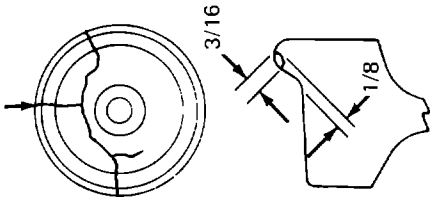| Wheel design	Class	Age (yr)	Rim thickness (in.)	Month failed	Sketch of cracked wheel and initial crack	Calculated failure stress (ksi)	Remarks
33 in (cast)	U1	9	1-1/8	May		—	Large thermal crack at A initiated rapid brittle crack which extended radially into plate to a depth of 2-1/2 in. below tread. A thru thickness plate fatigue crack developed from the arrested crack and extended for 10 in., eventually connecting with a second thermal crack (B) which had extended into plate.
33 in (cast) 1W	U1	8	1-3/16	October		9	Failure initiated from two thermal cracks which were 26 in. apart.

TABLE B1.—CONTINUED

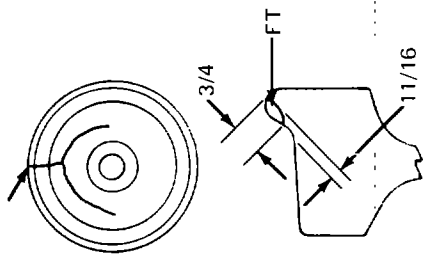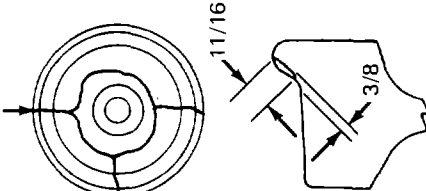| Wheel design	Class	Age (yr)	Rim thickness (in.)	Month failed	Sketch of cracked wheel and initial crack	Calculated failure stress (ksi)	Remarks
33 in (cast) 1W	U1	8	1-3/16	August		9	Note alternate mode of thermal crack propogation.
33 in (cast) 1W	U1	8	1-1/8	July		12	1) Crack initiated in a heat checked band which extended full circumference of wheel. 2) Thermal crack extended through rim; possibly arrested cleavage.

158

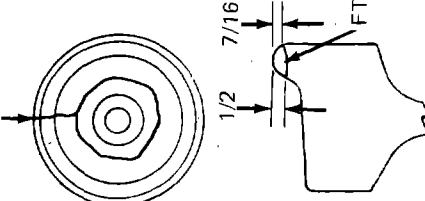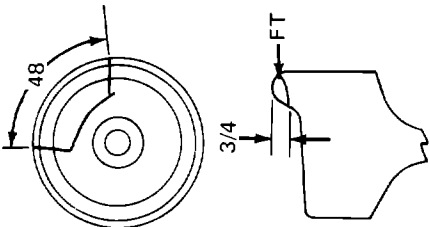| Wheel design	Class	Age (yr)	Rim thickness (in.)	Month failed	Sketch of cracked wheel and initial crack	Calculated failure stress (ksi)	Remarks
40 in (Wr) MW Diesel Loco	A	2	1-5/16	October		18	
40 in (Wr) MW Diesel Loco	B (0.63c, 0.72 Mn)	1	2-11/16	April		27	Tread microstructure altered by heat over outer 2-3/4 in. of tread to a depth of 7/8 in.

TABLE B1. CONTINUED

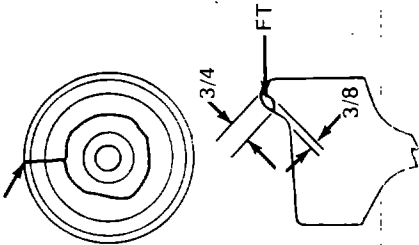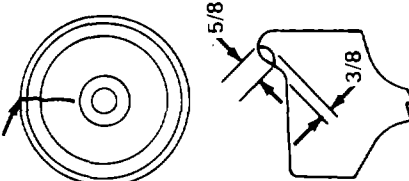| Wheel design	Class	Age (yr)	Rim thickness (in.)	Month failed	Sketch of cracked wheel and initial crack	Calculated failure stress (ksi)	Remarks
40 in. (Wr) MW Diesel Loco	B	1	2-13/16	—	(1-1/2, 1-1/4)	22	
40 in. (Wr) — Diesel Loco	B (0.67C, 0.74 Mn)	3	1-7/16	September	(5/16, FT)	48	Crack iniated at flowed area at outer edge of tread. Slight microstructural change in this area due to heat.

TABLE B1.—CONTINUED

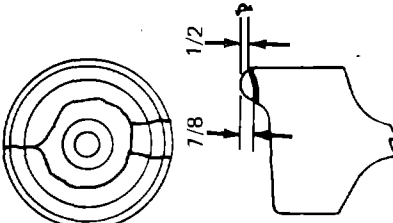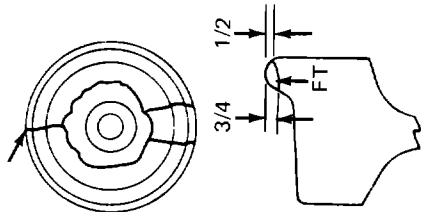| Wheel design	Class	Age (yr)	Rim thickness (in.)	Month failed	Sketch of cracked wheel and initial crack	Calculated failure stress (ksi)	Remarks
33 in (Wr) MW	BR	8	1-15/16	January		22	
36 in (Wr) 1W	CR (0.79C, 0.72Mn)	2	1-7/16	April		42	Tread microstructure altered by heat to a depth of 1/4 over 1-3/4 in. of tread width.

TABLE B1.—CONCLUDED

Wheel design	Class	Age (yr)	Rim thickness (in.)	Month failed	Sketch of cracked wheel and initial crack	Calculated failure stress (ksi)	Remarks
33 in (Wr) 1W	C (0.75C, 0.72 Mn)	8	1-7/16	June			1) Microstructure at tread surface altered by heat. 2) Dimensions of thermal crack not established due to damaged fracture face.

NOTE: 1) Crack initiation was generally associated with heat checked areas, the tread being frequently discolored due to excessive heating.

2) F.T.-- Thermal fatigue thermal cr: C.T.—Cleavage type thermal crack
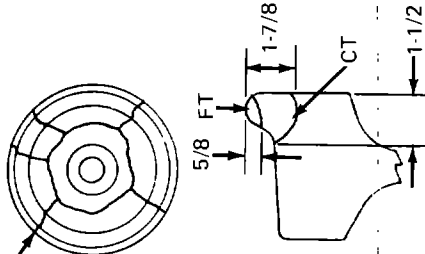
162

TABLE B2.—FRACTURES INITIATED AT THE FLANGE

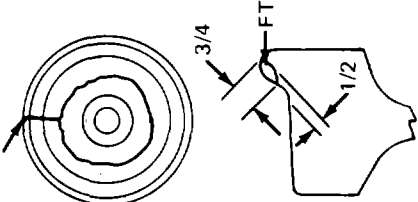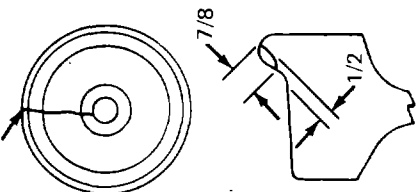| Wheel design	Class	Age (yr)	Rim thickness (in)	Month failed	Sketch of cracked wheel and initial crack	Calculated failure stress (ksi)	Remarks
J33 (Wr)	U	2	1-3/8	May	1/2 FT	25	
J33 (Wr) 1W	U	4	1-3/8	September	49-5/8 7/8 FT	19	

163

TABLE B2.—CONTINUED

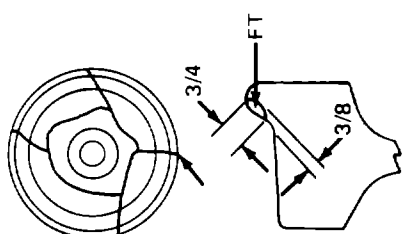| Wheel design	Class	Age (yr)	Rim thickness (in.)	Month failed	Sketch of cracked wheel and initial crack	Calculated failure stress (ksi)	Remarks
33 in (Wr) 1W	U	5	1-1/4	October	1-7/16	15	
J33 (Wr)	U	4	1-5/16	October	3/4 1/2	29	Another thermal crack (1/2 x 3/4 in.) caused a second radial fracture.

164

TABLE B2.—CONTINUED

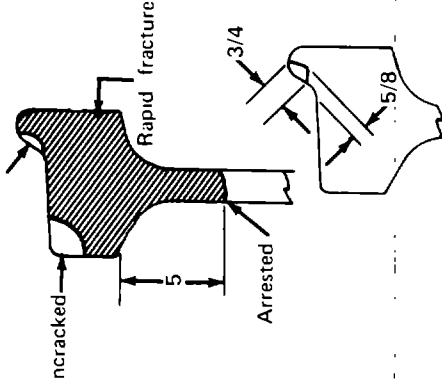| Wheel design	Class	Age (yr)	Rim thickness (in.)	Month failed	Sketch of cracked wheel and initial crack	Calculated failure stress (ksi)	Remarks
J33 (Wr) 1W	U	5	1-1/4	October		27	

165

TABLE B2.—CONTINUED

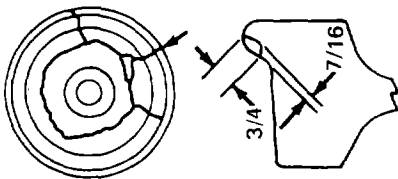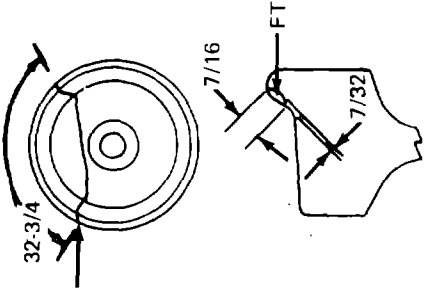| Wheel design	Class	Age (yr)	Rim thickness (in.)	Month failed	Sketch of cracked wheel and initial crack	Calculated failure stress (ksi)	Remarks
J33 (Wr) 1W	U	5	1-5/16	December		14	Dual mode of thermal crack growth.
J33 (Wr)	U	1	1-5/16	July		26	

166

TABLE B2.—CONTINUED

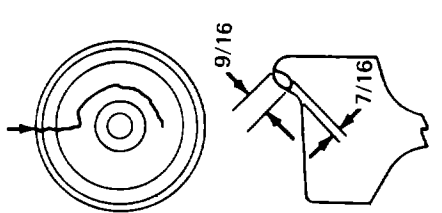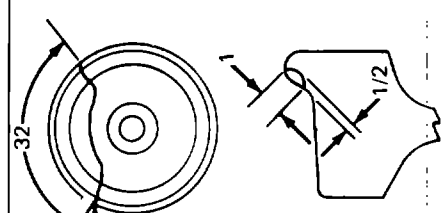| Wheel design	Class	Age (yr)	Rim thickness (in.)	Month failed	Sketch of cracked wheel and initial crack	Calculated failure stress (ksi)	Remarks
33 in (Wr) 1W	U (0.79C, 0.74 Mn)	7	1-1/16	April		29	
33 in (cast) 1W	U (0.82C, 0.61 Mn)	6	1-3/16	December		14	Dual mode of thermal crack growth

167

TABLE B2.—CONTINUED

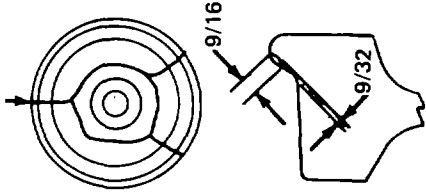| Wheel design	Class	Age (yr)	Rim thickness (in.)	Month failed	Sketch of cracked wheel and initial crack	Calculated failure stress (ksi)	Remarks
33 in (cast)	U	10	—	June		54	
33 in (cast)	U	3	1-1/4	December		28	

TABLE B2.—CONTINUED

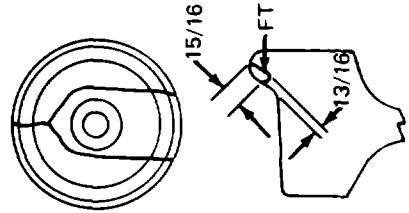| Wheel design	Class	Age (yr)	Rim thickness (in.)	Month failed	Sketch of cracked wheel and initial crack	Calculated failure stress (ksi)	Remarks
33 in (cast)	U	5	1-1/4	January		31	
33 in (cast)	U	9	1-3/16	September		26	

169

TABLE B2.—CONTINUED

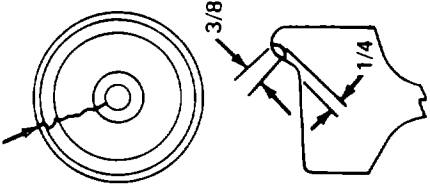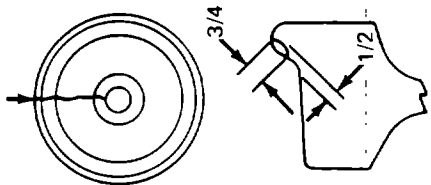| Wheel design	Class	Age (yr)	Rim thickness (in)	Month failed	Sketch of cracked wheel and initial crack	Calculated failure stress (ksi)	Remarks
33 in (cast)	U	5	1-3/16	July		20	
33 in (cast)	U	4	1-1/16	October		30	

TABLE B2.—CONTINUED

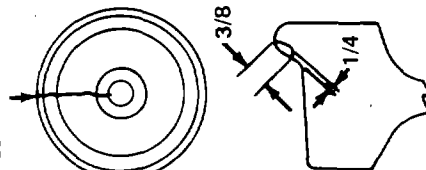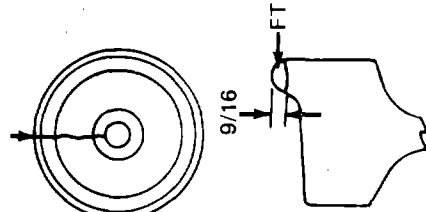| Wheel design	Class	Age (yr)	Rim thickness (in.)	Month failed	Sketch of cracked wheel and initial crack	Calculated failure stress (ksi)	Remarks
33 in (cast)	U	5	1-1/8	May		32	
CJ33 (cast)	U	<1	1-1/2	August		21	

171

TABLE B2.–CONTINUED

Wheel design	Class	Age (yr)	Rim thickness (in.)	Month failed	Sketch of cracked wheel and initial crack	Calculated failure stress (ksi)	Remarks
33 in (cast) 1W	U	6	1-3/32	May		22	Other radial cracks due to thermal cracks.
33 in (cast) 1W	U	6	1-5/16	May		13	1) Dual mode of thermal crack growth. 2) Thermal crack in other locations were responsible for 3 out of the 5 radial breaks.

TABLE B2.—CONTINUED

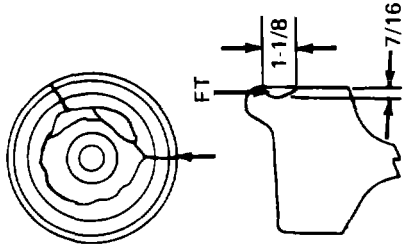| Wheel design	Class	Age (yr)	Rim thickness (in.)	Month failed	Sketch of cracked wheel and initial crack	Calculated failure stress (ksi)	Remarks
33 in (cast) 2W	U (0.88C, 0.75 Mn)	12	1-1/32	November		27	
CM33 (cast) 2W	U	4	2	December		28	

TABLE B2.—CONTINUED

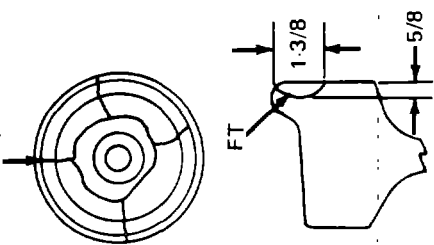| Wheel design	Class	Age (yr)	Rim thickness (in.)	Month failed	Sketch of cracked wheel and initial crack	Calculated failure stress (ksi)	Remarks
33 in (cast) 1W	U	7	1-1/8	December		31	
33 in (cast) 1W	U	7	1	February		28	

174

TABLE B2.—CONTINUED

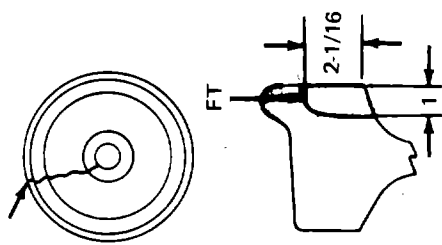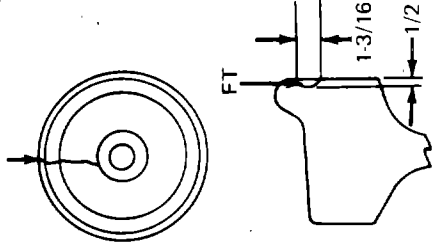| Wheel design	Class	Age (yr)	Rim thickness (in.)	Month failed	Sketch of cracked wheel and initial crack	Calculated failure stress (ksi)	Remarks
33 in (cast) 1W	U	6	1	March		29	
CJ33 (cast)	U	2	1-1/2	May		39	

TABLE B2.—CONTINUED

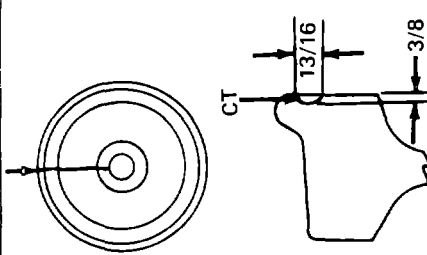| Wheel design	Class	Age (yr)	Rim thickness (in.)	Month failed	Sketch of cracked wheel and initial crack	Calculated failure stress (ksi)	Remarks
CJ33 (cast) 1W	U	<1	1-3/8	June		33	
CA33 (cast) 1W	U	2	—	February		26	

176

TABLE B2.—CONTINUED

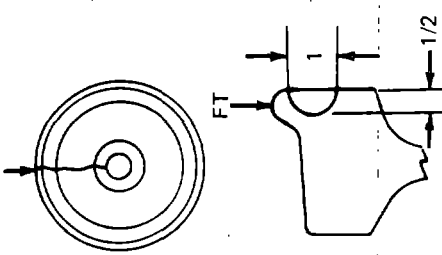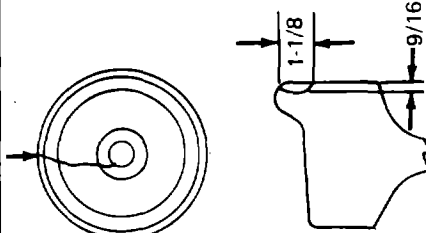| Wheel design	Class	Age (yr)	Rim thickness (in.)	Month failed	Sketch of cracked wheel and initial crack	Calculated failure stress (ksi)	Remarks
33 in (cast) 1W	U	7	1-1/4	May		35	
CJ33 (cast) 1W	U	3	1-1/4	May		25	

177

Wheel design	Class	Age (yr)	Rim thickness (in)	Month failed	Sketch of cracked wheel and initial crack	Calculated failure stress (ksi)	Remarks
33 in (cast)	U1	7	1	July		29	
CJ33 (cast)	U1 (1.19C, 0.74 Mn)	1	1-1/2	October		21	Microstructure altered by heat to 5/32 in depth in area of thermal crack.

TABLE B2.—CONCLUDED

Wheel design	Class	Age (yr)	Rim thickness (in.)	Month failed	Sketch of cracked wheel and initial crack	Calculated failure stress (ksi)	Remarks
33 in (cast)	U1	9	1-3/8	April		29	
40 in (Wr) — Diesel Switcher	A	4	1	May		30	

NOTE: 1) All above thermal cracks were reported to have initiated in heat checked areas which were frequently grooved.
2) F.T.—Thermal fatigue type thermal crack. CT—Cleavage type thermal crack.

TABEL B3.—FRACTURES INITIATED AT REAR RIM FACE

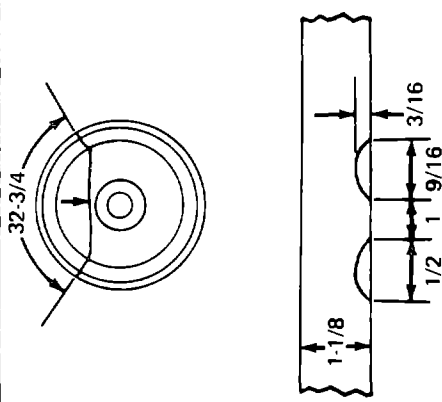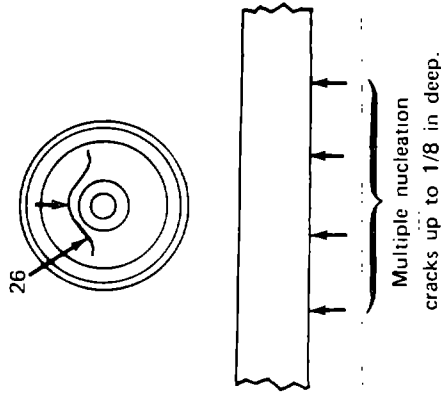| Wheel design	Class	Age (yr)	Rim thickness (in.)	Month failed	Sketch of cracked wheel and initial crack	Calculated failure stress (ksi)	Remarks
36 in (Wr) 1W	U	4	1-1/8	January		37	
J33 (Wr) 1W	U	6	1-7/16	February		34	

TABLE B3.—CONTINUED

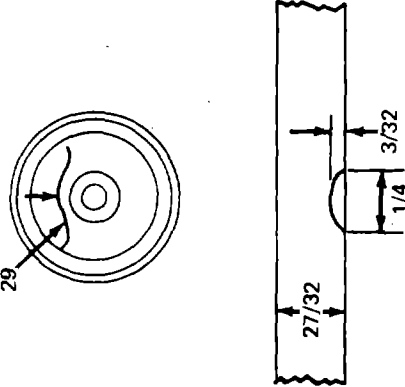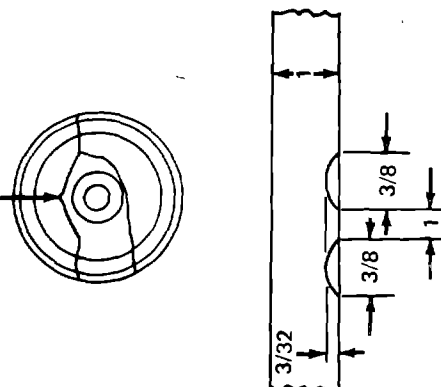| Wheel design	Class	Age (yr)	Rim thickness (in.)	Month failed	Sketch of cracked wheel and initial crack	Calculated failure stress (ksi)	Remarks
30 in (Wr)	U (0.78C 0.70 Mn)	11	1-15/16	May		19	Cracks initiated at base of a hot stamped identity numeral.
CJ36 (cast) 2W	U	5	1-3/4	June			

TABLE B3.--CONTINUED

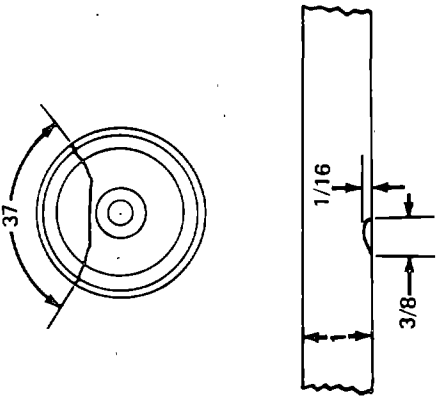| Wheel design	Class	Age (yr)	Rim thickness (in.)	Month failed	Sketch of cracked wheel and initial crack	Calculated failure stress (ksi)	Remarks
33 in (cast)	U1 (1.04C, 0.75 Mn)	3	2-3/16	February	CT — 13/16, 3/8	31	Tread showed evidence of thermal damage to 5/16 in. depth.
33 in (Wr) MW	BR	7	1-7/16	December	FT — 1, 1/2	43	Microstructure of rear rim face altered to a depth of 1/8 in. with 0.002 in. layer of untempered martensite at surface.

TABLE B3.—CONCLUDED

Wheel design	Class	Age (yr)	Rim thickness (in.)	Month failed	Sketch of cracked wheel and initial crack	Calculated failure stress (ksi)	Remarks
J36 (Wr) 2W	B (0.66C, 0.63 Mn)	4	—	May		40	

NOTE: 1) All cracks were reported to be associated with retarde, shoe action on rear rim face.

2) F.T.—Thermal fatigue type thermal crack. C.T.—Cleavage type thermal crack.

183

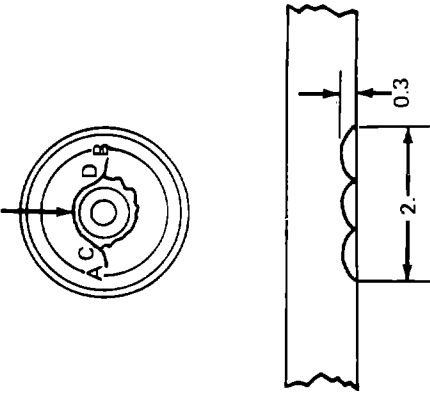*TABLE B4.—FRACTURES INITIATED AT FRONT HUB FILLET*

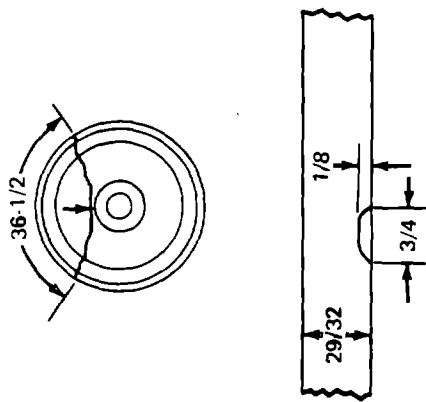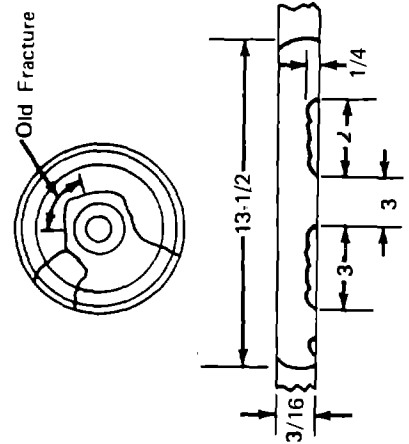| Wheel design	Class	Age (yr)	Rim thickness (in.)	Month failed	Sketch of cracked wheel and initial crack	Calculated failure stress (ksi)	Remarks
36 in (Wr)	U	—	1-13/16	June		45	1) Crack initiation associated with mill scale. 2) One stage brittle fracture.
33 in (Wr) 1W	U	—	1-1/16	April		41	1) Multiple cracks initiated in area which contained mill scale embedded to a depth of 1/32 in. 2) Brittle fracture arrested, 4-6 in. below tread.

184

TABLE B4.—CONTINUED

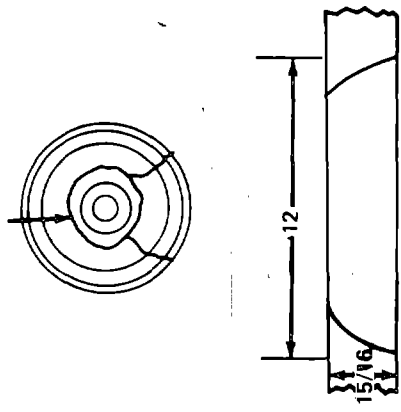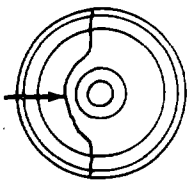| Wheel design	Class	Age (yr)	Rim thickness (in.)	Month failed	Sketch of cracked wheel and initial crack	Calculated failure stress (ksi)	Remarks
33 in (Wr) 2W	U	7	1-5/16	May		65	1) Crack initiation associated with pitting due to embedded mill scale. 2) Crack arrested 3-4 in. below tread.
33 in (Wr) 1W	U	12	1	July		56	Fatigue cracks nucleated at rough and pitted area and initiated brittle crack which arrested at rim. Final fracture through rim developed later.

185

TABLE B4.–CONTINUED

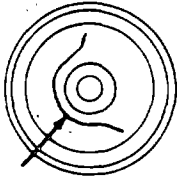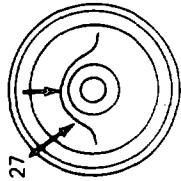| Wheel design	Class	Age (yr)	Rim thickness (in.)	Month failed	Sketch of cracked wheel and initial crack	Calculated failure stress (ksi)	Remarks
33 in (Wr) 1W	U (0.73C, 0.66 Mn)	18	1-1/16	February		62	1) Crack initiated in area of pitting (0.027 in. deep) due to entrapped mill scale. Microstructure also altered in this area by processing. 2) One stage brittle fracture.
33 in (Wr) 1W	U	7	3/4	February		30	1) Crack initiated in rough area. 2) "Cupids Bow" fracture (A-B) formed first, fracture C-D developed later. 3) Rim worn below condemnable limits.

TABLE B4.—CONTINUED

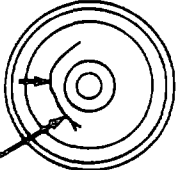| Wheel design	Class	Age (yr)	Rim thickness (in.)	Month failed	Sketch of cracked wheel and initial crack	Calculated failure stress (ksi)	Remarks
33 in (Wr) 1W	U (0.82C, 0.68 Mn)	5	1-5/16	January		46	1) Crack initiated in area of embedded scale. 2) One stage brittle fracture.
33 in (Wr) 1W	U	14	1-15/16	February		6	1) Multiple fatigue cracks initiated in rough area, and developed into 13-1/2 long crack, probably by fatigue. Final rapid fracture of wheel initiated from 13-1/2 in crack. 2) One stage brittle fracture.

187

TABLE B4.—CONTINUED

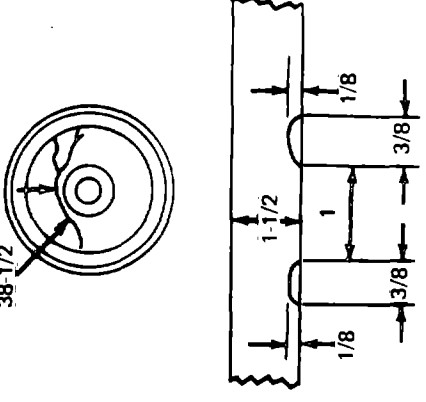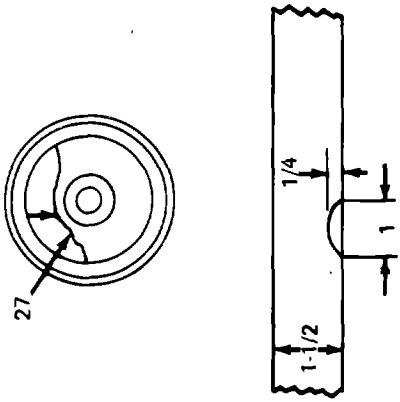| Wheel design	Class	Age (yr)	Rim thickness (in.)	Month failed	Sketch of cracked wheel and initial crack	Calculated failure stress (ksi)	Remarks
33 in (Wr) 1W	U	22	1-1/16	November		7	Cracks initiated in area of entrapped mill scale.
33 in (Wr) 1W	U	—	1-5/16	October		—	1) "Small" cracks initiated in roughly machined area, and nucleated a brittle crack which arrested close to rim. Final failure occurred later. 2) Crack dimensions not reported.

TABLE B4.—CONTINUED

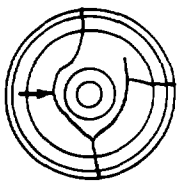| Wheel design	Class	Age (yr)	Rim thickness (in.)	Month failed	Sketch, of cracked wheel and initial crack	Calculated failure stress (ksi)	Remarks
33 in (Wr) 1W	U	20	1-1/8	April		—	1) Multiple cracks initiated in pitted area containing embedded mill scale. 2) Crack arrested 2-3 in. below tread. 3) Fracture faces not exposed.
33 in (Wr) 1W	U	7	1-5/16	August	27	—	1) Crack initiated in an area which was pitted due to embedded mill scale. 2) Crack extended to within 3 in. of tread surface. 3) Fracture faces not exposed.

189

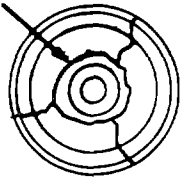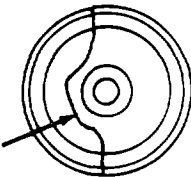| Wheel design	Class	Age (yr)	Rim thickness (in.)	Month failed	Sketch of cracked wheel and initial crack	Calculated failure stress (ksi)	Remarks
J33 (Wr) 1W	U	4	1-7/16	August		—	1) Crack initiated in rough area. 2) Fracture faces not exposed.
CH36 (cast) 1W	U	2	1-7/16	July		54	1) Crack initiated in pitted area which also contained porosity. 2) Crack arrested 4-3/4 in. below tread.

Wheel design	Class	Age (yr)	Rim thickness (in.)	Month failed	Sketch of cracked wheel and initial crack	Calculated failure stress (ksi)	Remarks
CJ33 (cast) 1W	U	3	1-1/4	June		36	1) Crack initiation associated with rough plate surface. 2) Crack arrested 3 in. below tread.
33 in (Wr)	—	7	1-1/8	December		—	1) Fatigue crack initiated in area of rolled in mill scale. 2) Crack dimension not determined. 3) One stage brittle fracture.

191

TABLE B4.—CONTINUED

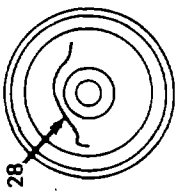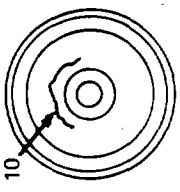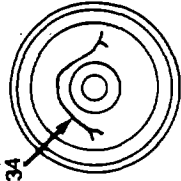| Wheel design	Class	Age (yr)	Rim thickness (in.)	Month failed	Sketch of cracked wheel and initial crack	Calculated failure stress (ksi)	Remarks
33 in (Wr) 1W	—	—	1-1/4	January		—	1) Multiple cracks initiated at rough area. 2) Crack dimensions not determined. 3) Two stage fracture, crack originally extended around circumference.
33 in (Wr) —	—	—	7/8	February		—	1) Crack initiated in a rough surface and extended to 3-1/2 in. below tread. Final failure thru rim occurred later. 2) Fracture faces not exposed.

TABLE B4.—CONTINUED

Wheel design	Class	Age (yr)	Rim thickness (in.)	Month failed	Sketch of cracked wheel and initial crack	Calculated failure stress (ksi)	Remarks
33 in (Wr) 1W	—	—	1-3/16	December	28	—	1) Crack initiated in a pitted area due to embedded mill scale. 2) Fracture faces not exposed. 3) Crack extended to 3-1/2 in. below tread.
33 in (—) 1W	—	—	1-1/4	April	10	—	1) Multiple nucleation of cracks due to rough area. 2) Fracture faces not exposed.

TABLE B4.—CONCLUDED

Wheel design	Class	Age (yr)	Rim thickness (in.)	Month failed	Sketch of cracked wheel and initial crack	Calculated failure stress (ksi)	Remarks
33 in (Wr) 1W	—	—	1-5/16	July		—	1) Crack initiation associated with rough surface. 2) Brittle crack propogation arrested approx. 4-5 in. below tread. 3) Fracture faces not exposed.

194

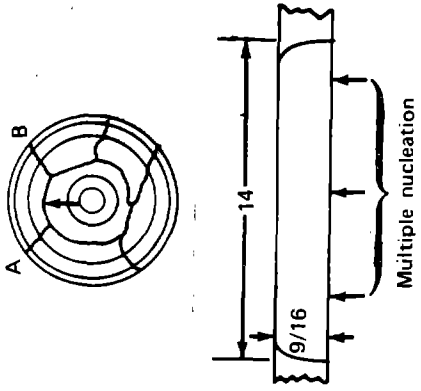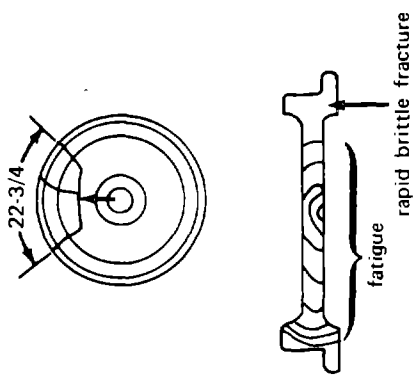TABEL B5.—FRACTURES WHICH INITIATED AT REAR RIM FILLET

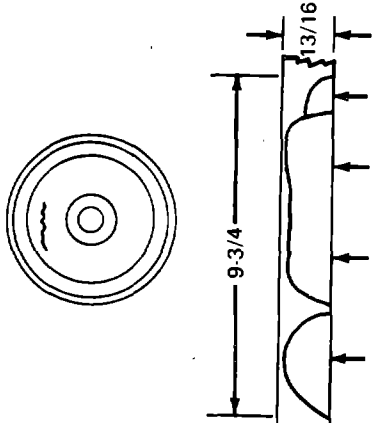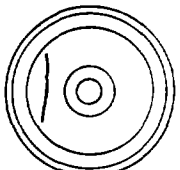| Wheel design	Class	Age (yr)	Rim thickness (in.)	Month failed	Sketch of cracked wheel and initial crack	Calculated failure stress (ksi)	Remarks
33 in (Wr) 1W	U (0.74C, 0.79 Mn)	19	1-1/8	December		6	1) Multiple fatigue cracks initiated in roughly machined area. 2) Rapid brittle fractures to A & B developed thru rim from 14 in. long fatigue crack. 3) One stage brittle fracture.
33 in (Wr) 1W	U	3	1-1/4	January		—	Crack initiated in slightly rough mill scaled area.

195

TABLE B5.—CONTINUED

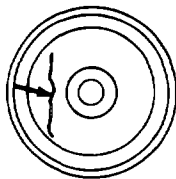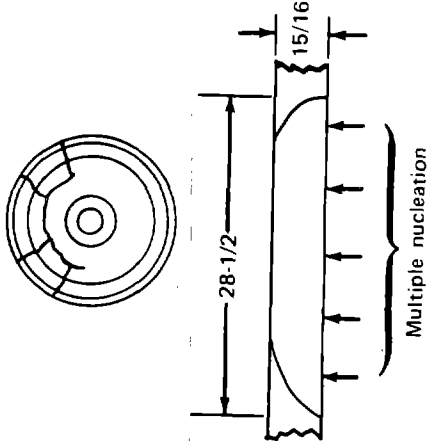| Wheel design	Class	Age (yr)	Rim thickness (in.)	Month failed	Sketch of cracked wheel and initial crack	Calculated failure stress (ksi)	Remarks
36 in (Wr) 1W	U	6	1-3/8	June		—	Multiple crack initiated in rough machined area.
28 in (Wr)	U (0.74C, 0.74 Mn)	—	—	—		—	1) No defects associated with fatigue crack initiation. 2) Crack arrested close to rim. 3) Fatigue crack dimensions not determined.

196

TABLE B5.–CONTINUED

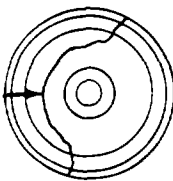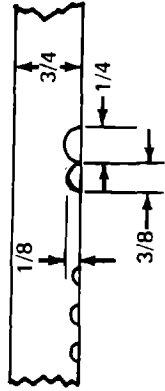| Wheel design	Class	Age (yr)	Rim thickness (in.)	Month failed	Sketch of cracked wheel and initial crack	Calculated failure stress (ksi)	Remarks
28 in (Wr)	U (0.74C, 0.74 Mn)	—	—	—			1) No defects associated with fatigue crack initiation. 2) Crack arrested close to rim. 3) Fatigue crack dimensions not determined.
28 in (Wr) 1W	BR	6	15/16	November	28-1/2 15/16 Multiple nucleation		Multiple nucleation of fatigue cracks in roughly formed surface.

197

Wheel design	Class	Age (yr)	Rim thickness (in.)	Month failed	Sketch of cracked wheel and initial crack	Calculated failure stress (ksi)	Remarks
28 in (Wr) 1W	B (0.67C, 0.72 Mn)	5	1-5/16	November			1) Multiple nucleation in area of entrapped mile scale. 2) Fatigue crack dimensions not reported
33 in (Wr) 2W	CR (0.77C, 0.69 Mn)	5	1-15/16	February		47	1) Fatigue cracks initiated at rear rim fillet and nucleated brittle fracture thru rim. 2) Numerous fatigue cracks were present at front hub fillet, up to 3/4 in. deep, and had nucleated secondary brittle fractures. 3) Fatigue cracks developed in roughly machined or rough as rolled surfaces.

198

TABLE B5.—CONTINUED

Wheel design	Class	Age (yr)	Rim thickness (in.)	Month failed	Sketch of cracked wheel and initial crack	Calculated failure stress (ksi)	Remarks
33 in (Wr) 2W	C	6	—	November	21-3/8 ... 1 ... 1-1/2 ... 1/4 ... 1 ... 3/4	31	1) Multiple crack initiation in rough area. 2) One stage brittle fracture.
33 in (Wr) 2W	CR	7	1-15/16	May	19-1/2 ... 5/16 ... 7/8 ... 3/4	39	1) Crack initiated in slightly rough surface. 2) One stage fracture brittle fracture.

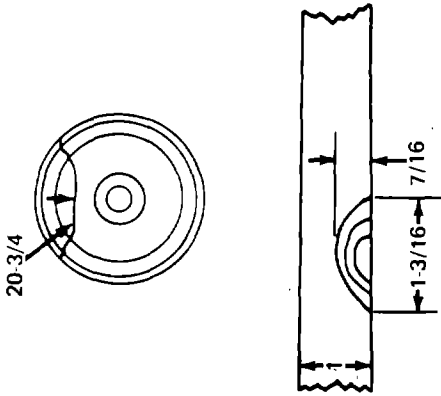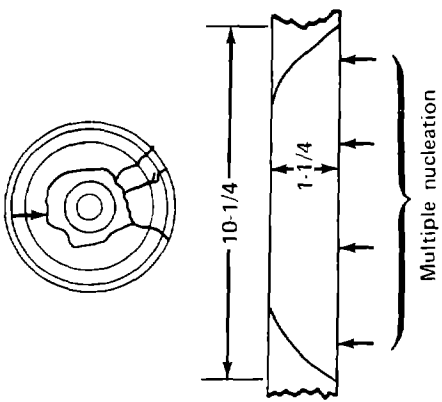| Wheel design	Class	Age (yr)	Rim thickness (in.)	Month failed	Sketch of cracked wheel and initial crack	Calculated failure stress (ksi)	Remarks
33 in (Wr) 2W	CR	8	2	July	20-3/4 7/16 1-3/16	31	1) Crack initiated in slightly rough area of rear rim fillet. 2) One stage brittle fracture.

TABLE B6.—FRACTURES INITIATED AT FRONT RIM FILLET

Wheel design	Class	Age (yr)	Rim thickness (in.)	Month failed	Sketch of cracked wheel and initial crack	Calculated failure stress (ksi)	Remarks
33 in (Wr) MW	B (0.61C, 0.73 Mn)	54	1-1/8	February	10-1/4 1-1/4 Multiple nucleation		Multiple fatigue cracks iniated in deeply corrosion pitted area and extended thru plate thickness.

APPENDIX C

REPORT OF INVENTIONS

After a diligent review of the work performed under this contract, no new innovation, discovery, improvement or invention was made.